universität wien

DISSERTATION / DOCTORAL THESIS

Titel der Dissertation /Title of the Doctoral Thesis

„The interaction of rare earth elements with cadmium: The system Ce-Cd and Nd-Cd“

verfasst von / submitted by

D.I. Barbara Skołyszewska-Kühberger

angestrebter akademischer Grad/ in partial fulfilment of the requirements for the degree of

Doktorin der Naturwissenschaft (Dr. rer. nat.)

Wien, 2016 / Vienna 2016

Studienkennzahl lt. Studienblatt / degree programme code as it appears on the student record sheet:	A 791 419
Dissertationsgebiet lt. Studienblatt / field of study as it appears on the student record sheet:	Chemie
Betreut von / Supervisor:	O. Univie.-Prof. Dr. Herbert Ipser

Acknowledgment

This work was accomplished at the Department of Inorganic Chemistry (Materials Chemistry) from February 2011 to October 2015.

Initially, I would like to express my greatest thank to my supervisor O. Univ.-Prof. Dr. Herbert Ipser for his support in practical and theoretical difficulties as well as for his great patience. Furthermore, I would like to thank him also for his understanding and for giving me motivation during my work.

My thank goes to Prof. Dr. Klaus Richter for employing me at the department after my maternity break and allowing me the opportunity to collect further laboratory experiences.

I am thankful to Dr. Rajesh Ganesan from the Chemistry Group of the Indira Gandhi Centre for Atomic Research in Kalpakkam, India for shearing his knowledge of the isopiestic experiments and his great hospitality during my stay in India.

My thank goes to Prof. Herta Effenberger from the Faculty of Earth Sciences, Geography and Astronomy, University of Vienna for performing the single crystal X-ray diffraction experiments and for the discussions of the results.

In addition, I wish to thank Dr. Stephan Puchegger from the Faculty of Physics of the University of Vienna for his help and suggestions with the SEM measurements.

I wish to thank Dr. Maciej Rumiński and Dr. Tadeusz Pieczonka from the AGH University of Science and Technology, Kraków, Poland for the explanation of microhardness measurement principle and for the execution of dilatometric study.

Financial support by the Austrian Science Fund (FWF) under project No. P 23270-N19 and by the Scientific-Technical Cooperation Austria-India under project No. IN 05/2011 is gratefully acknowledged. I wish to thank the Austrian Agency for International Mobility and Cooperation in Education, Science and Research (OeAD) for the support within the Austrian-Indian Scientific-Technical Cooperation project (No. IN 05/2011).

Special thanks to all colleagues of the Department of Inorganic Chemistry (Materials Chemistry) I met during my employment for providing the nice working atmosphere and for their help in scientific and personal matters. In this respect I would like to thank Dr. Thomas Reichmann for his support as well as Dr. Martin Marker for being the friend. Likewise I want to thank Ms. Olivia Appay for help in preparing some of the isopiestic experiments in the course of an internship and Mr. Mario Ecker for his experimental support.

I want to thank my parents, family and friends for their great support during my studies. Especially thanks to my dear husband, D.I. Dr. Markus Kühberger, for his assistance. Last but not least I express my gratitude to my beloved children for keeping my life in *equilibrium*.

Preface

This thesis is a part of a research project on the interaction of different RE elements (Ce, Pr, Nd and Gd) with Cd. It presents the phase equilibria in the Ce-Cd and Nd-Cd systems as a function of temperature and composition. The existing intermetallic compounds as well as all phase reactions occurring in both systems were investigated. Partial and integral thermodynamic properties of binary Ce-Cd and Nd-Cd alloys, based on Cd vapor pressure measurements with an isopiestic method were provide in this work. Using minor literature data on partial thermodynamic properties of Ce and Nd, integral Gibbs energies of formation could be obtained over a large composition range.

In the binary phase diagram Ce-Cd appears to be reasonably well known. The Nd-Cd binary system was investigated in the past only in the Cd-rich corner and limited information on this system is given in literature. Some authors performed previously short studies concerning thermodynamic properties of these both systems. Most of these investigations were not conclusive and the present work is an attempt to complete missing insufficiencies.

This thesis is written in a cumulative form; it means the Introduction as well as the Experimental and Methods part include particular information where references are pointed out at the end of each chapter. The Results and Discussion part consists of scientific papers, each with its respective bibliography.

Table of contents

Investigated metals

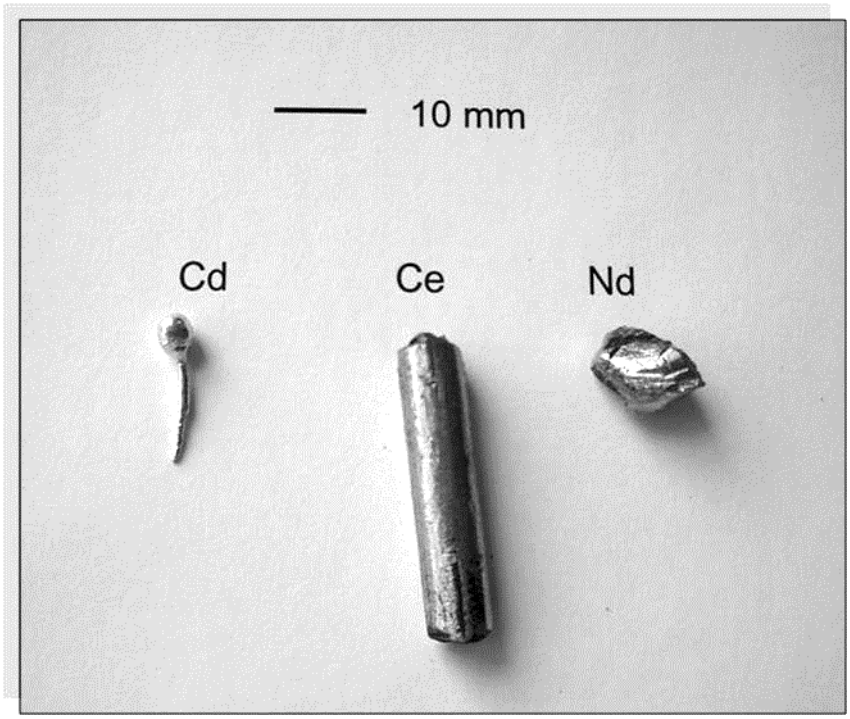

1. Introduction

Energy is a property of a physical system (object) needed to perform work on another object or system [1]. It is transferable among the objects of a system through fundamental interactions, which can be converted in other form but cannot be destroyed. There are several forms of energy such as heat, kinetic or mechanical energy, electromagnetic energy (light), chemical or potential energy, electrical, sound, nuclear energy or others.

On the other hand, energy is essential for human being. It is an important consideration in housekeeping and for all industry branches [2]. Energy is consumed in the industrial sector for a wide range of purposes like processing, assembly, heating and lighting in buildings etc. Therefore, sources of energy are everlastingly an important topic. Energy sources can be classified in two groups: nonrenewable or renewable. Energy explored from the ground in the form of gas, liquid or solid is called nonrenewable resource. Examples include here: oil (petroleum), natural gas, coal and uranium (nuclear). All cannot be replenished or produced again in a short period of time. Oil, natural gas and coal are called “fossil fuels” because they have been formed from the organic remains of prehistoric plants and animals. Renewable energy comes from a source (solar, wind, biomass and hydropower) that is constantly renewed and can be replenished naturally in a short period of time. Currently, it is estimated that about 11 % of world marketed energy consumption comes from renewable energy sources with a projection for 15 % by 2040 [3]. Most of the energy used nowadays in industry comes originally from fossil fuels. On the other hand ecological institutions warn for increasing pollution of the earth due to emission of greenhouse gases and carbon dioxide (CO_2) (as the combustion product of carbon-based fuels).

As it was mentioned above, the nuclear energy can be also applied as the source of power and heat using exothermal nuclear process. A nuclear

power plant produces electricity by heating water to form steam. The steam rotates a turbine connected to a generator, which generates electricity. As the world electricity demands increase, especially in developing countries, the use of the nuclear energy seems to be important. Actually, nuclear energy is being used in more than 31 countries around the world and around 437 nuclear power reactors generate electricity worldwide [4]. Nuclear power plants work basically on the nuclear fission and offer a low carbon power generation method. However, the nuclear fission must be controlled to avoid any failure. Hence there is an ongoing discussion about safety of nuclear power plants. According to the data of the Nuclear Energy Institute (NEI), in 2012 nuclear power plants provided about 12 % of the world's electricity production.

Nuclear fission is a process of splitting an atom with a large nucleus into pieces with excess energy provided in form of photons (γ-ray) and kinetic energy (nuclear fission products). Fission was discovered in 1938 by O. Hahn, L. Meitner and F. Strassmann (Nobel Prize in chemistry 1944). They observed that the uranium atom after bombarding it by neutrons was able to split in two fission products, barium and krypton [5] which can be presented by the following reaction (1):

$$ {}^{1}_{0}n + {}^{235}_{92}U \rightarrow {}^{141}_{56}Ba + {}^{92}_{36}Kr + 3{}^{1}_{0}n \qquad (1) $$

^{235}U is the only nuclide existing in nature (in any appreciable amount) that is fissile with thermal neutrons [6]. Natural uranium consists primarily of two isotopes, 99.284% ^{238}U and 0.711% ^{235}U. For commercial use, uranium has to be enriched in the isotope ^{235}U. Therefore, the low-enriched uranium (so called reactor grade; 3 – 5 % ^{235}U) is applied as fuel for nuclear reactors and the highly enriched uranium containing 90% ^{235}U for weapons manufacturing.

In 1941, the report concerning the 'Use of Uranium as a Source of Power' was presented. E. Fermi's discovery of the nuclear chain reaction (1942) was based on the emission of neutrons in the fission reaction (1) and the possibility of further neutron-activated fission. The science of atomic radiation, atomic change and nuclear fission was developed from 1895 to 1945 [7]. The first use of nuclear fission was during the World War II in 1945 in the form of two

atomic bombs dropped on Hiroshima and Nagasaki (Japan). From 1945, attention was given to harnessing this energy and the man focus was given on applying it for electricity use. The Obninsk Nuclear Power Station in Russia was the first non-military power station in the world. The technological evolution of reliable nuclear power plants started in 1956. They are very costly and cope with a number of problems like production of controlled nuclear fission in reactor and utilization of nuclear waste.

Nowadays there are several international organizations accelerating and enlarging the contribution of atomic energy. One of the most famous is the International Atomic Energy Agency (IAEA) with its headquarters in Vienna, Austria. The structure of this agency is split into three main pillars [8] such as science & technology, safety & security and safeguards & verification. The IAEA provides overviews concerning development of the nuclear energy sector, problems at nuclear power plants and others topics in form of publications, reports and thematic brochures what was used in this work. After the Chernobyl disaster in Ukraine (1986) which was the worst nuclear power plant accident in history, public attention has focused strongly on the nuclear energy safety issue. Again and again it is observed which dangerous influence nuclear radiation has on the biosphere. As an example the UNSCEAR (United Nations Scientific Committee on the Effects of Atomic Radiation) study can be given. It was found that genomic instabilities occurring in the progeny of an irradiated cell can cause chromosome damage and heritable effects that can manifest across generations [9]. Therefore, nuclear power plants have a lot of opponents. In addition, the development of the nuclear power industry is associated with increasing amounts of radioactive waste. The most disputable waste from nuclear power plants is solid spent nuclear fuel. In principle, it contains unconverted uranium and significant quantities of transuranic actinides (mostly plutonium and curium). The deposition of nuclear waste in underground repositories is the acceptable way to removing it from the biosphere to protect the health of human and other living organism. Actually, it is the major challenge for environmental scientists to find a right way.

Nevertheless, the geological insulation is complicated because of the large volume of waste and the political and public issues. It is estimated that the radioactive waste needs to be kept from 10^4 to 10^6 years in stable rock formations [10] until its radioactivity will be below acceptable standards.

The heart of the nuclear power plant is a nuclear reactor. The reactor is a device where a nuclear chain reaction takes place. Heat produced due to nuclear fission is lead to a working fluid (water or gas), and farther on turbines are moved and so electricity can be produced.

Nuclear reactors are classified into several groups and subgroups. As a criterion several aspects were taken into account like:

I. Type of nuclear reaction.
    a. Nuclear fission: all commercial power reactors are based on fission, where uranium is applied as nuclear fuel;
    b. Nuclear fusion: an experimental method using hydrogen as fuel.

II. Type of moderator material.
    a. Graphite moderated reactors are reactors that use carbon as neutron moderator and un-enreached uranium as fuel;
    b. Water moderated reactors:
        - Light water moderated reactors (LWRs) (the most common one) use ordinary water as coolant;
        - Pressurized heavy-water reactors (PHWRs) use heavy water (deuterium oxide, D_2O) to moderate and cool the reactors;
    c. Light-element-moderated reactors using lithium or beryllium as moderator;
    d. Organically moderated reactors (OMR) use biphenyl and terphenyl as moderator and coolant.

III. Type of coolant:

a. Water cooled reactors:
   - Pressurized water reactors (PWRs); the large majority of all nuclear power plants use water that is pumped under high pressure to the reactor core;
   - Boiling water reactors (BWRs); the fuel rods are surrounded by boiling water;
   - Pool-type reactors; the fuel and the control rods are immersed in an open pool of water;

b. Liquid metal cooled reactors are fast reactors where water is used as a moderator and liquid metal (Na, Pb, Bi, Hg) serves as a coolant;

c. Gas cooled reactors; an inert gas (He, N or CO_2) circulates inside the reactor;

d. Molten salt reactor (MSRs); typically the FLiBe eutectic is applied as cooling agent;

IV. Type of phase of fuel:

a. Solid fueled (uranium ore);

b. Fluid fueled
   - Aqueous homogeneous reactors (AHRs); $U(SO_4)_2$ or $UO_2(NO_3)_2$ is dissolved in water;
   - Molten salt reactors (MSRs) where a molten salt mixture is used as fuel material and coolant;

c. Gas fueled (theoretical type);

As it was mentioned above first nuclear research reactors designed for electricity production were activated in 1950–1960. They are called Generation I reactors and are first prototypes of reactors. According to the observation of O. Hahn, L. Meitner and F. Strassmann, uranium was used as fuel material. Through the years four others types of reactors were developed. They are named sequentially Generation II (1970–1980), Generation II+ and Generation

III (1990–present) [11]. In addition, operation of Generation IV reactors is currently being researched and its start is already planned for 2025. The large nuclear reactors of Generation II can be divided into three types: pressurized water reactors (PWRs), boiling water reactors (BWRs), and supercritical water reactors (SCWRs). They used ordinary water as cooling agent and neutron moderator (a medium which reduces the velocity of fast neutrons). They are called light-water reactors (LWRs). The fissile elements are applied in a solid form containing low-enriched uranium (LEU); (3 to 5% ^{235}U). Later the LWRs were modernized where mixed oxide (MOX) or hydride were proposed as an alternative fuel. MOX fuel is commonly a mixture of two oxides (UO_2 and PuO_2) and/or its single phase solid solution $(U,Pu)O_2$. Also hydrides are used in Generation II+ nuclear reactors. Properties of the two-phase hydride $U_{0.3}ZrH_{1.6}$ pertinent to performance as a nuclear fuel for LWRs are reviewed by Olander et al. [12]. Already several countries are in the process of developing the Generation III reactors, mainly based on light water reactor (LWR) design [13]. They are characterized by improved fuel technology and thermal efficiency as well as better safety and maintenance systems.

The nuclear fuel cycle is an industrial process of preparation of a fuel to be used in a reactor and its reprocessing. It consists of several steps (see Fig.1) and can be classified as an open fuel cycle (spent fuel is not reprocessed) or a closed fuel cycle (reprocessed spent fuel). The nuclear fuel cycle includes the ‘front end’, i.e. preparation of the fuel, the ‘service period’ in which fuel is used during reactor operation and the ‘back end’, i.e. the safe management of spent fuel [10].

The cycle starts with the mining of the raw material. Today’s nuclear fuel is uranium. It must be processed through a series of steps to produce an efficient fuel for generating electricity. Uranium is a common metal that occurs naturally in the Earth’s crust. The largest holders of uranium ore are Kazakhstan, Canada and Australia. The mined uranium ore is crushed and chemically treated to separate the uranium. As the result, a yellow powder of uranium oxide (U_3O_8) (so called ‘yellow cake’) is received. Further, it is

converted into gas (UF_6) to prepare it for enrichment. The fission process by which heat energy is released in a nuclear reactor, takes place mainly in the ^{235}U isotope. Therefore, the concentration of this isotope in natural uranium has to be increased to a level of 3-5%. Uranium hexafluoride is introduced in fast-spinning centrifuges, where the heavier isotope ^{238}U is pushed out to the walls and so uranium can be enriched in ^{235}U. UF_6 (in enriched form) is converted afterwards into uranium oxide (UO_2) in form of pellets by sintering at a temperature higher than 1400 °C. For some types of nuclear reactors the enrichment step is not required. Once the nuclear fuel is loaded inside the reactor, controlled fission can occur. The fuel is used for 3-6 years and once a year 25-30 % of it is removed and replaced with fresh one. During the nuclear reaction, the fissile isotopes in nuclear fuel are consumed.

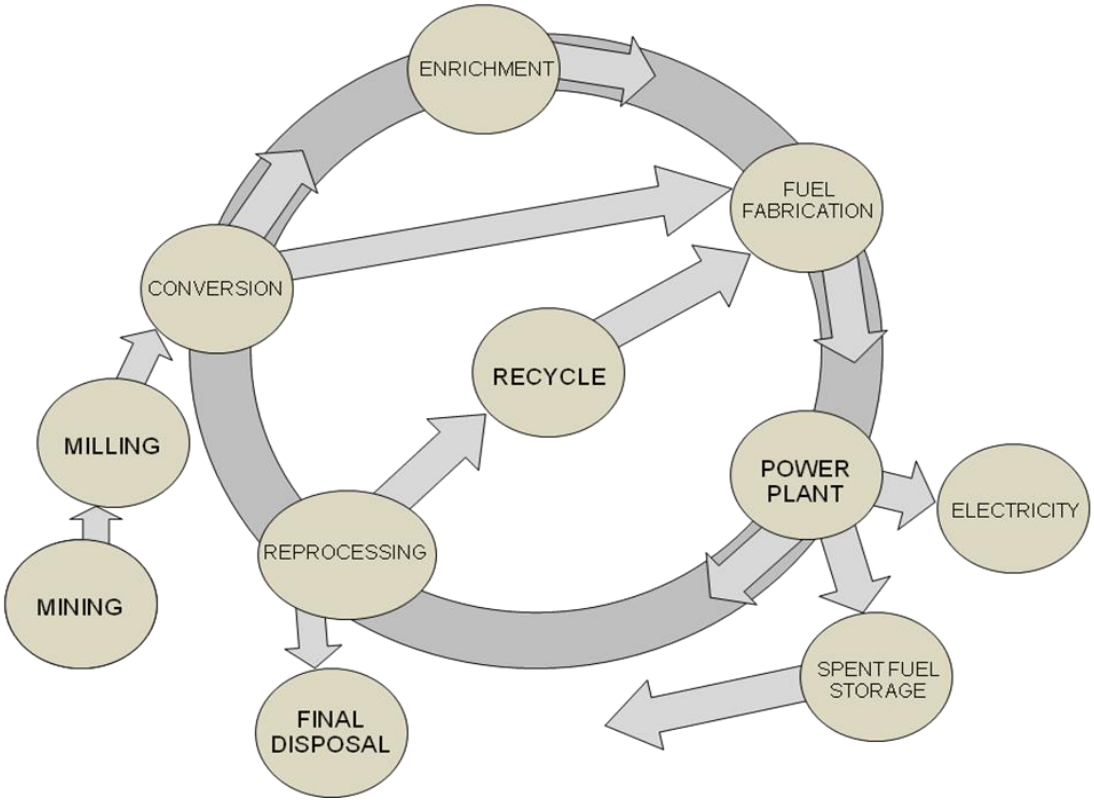

Fig.1. The nuclear fuel cycle scheme.

The spent fuel assemblies discharged from the reactor are very hot and still radioactive. They contain uranium (96%), plutonium (1%) and high level waste (HLW) products (3%). Therefore, the spent nuclear material is stored under water for cooling and radiation shielding. After a few years, spent fuel can be transferred to an interim storage facility. It can be kept in water pools (wet storage) or in casks (dry storage). The heat as well as radioactivity decrease significantly over time. The water storage of spent fuel constitutes an integral pre-reprocessing step to facilitate the decay of some short-lived radioactive isotopes [14]. Spent fuel can also be recycled to produce more power because it still contains fissile ^{235}U (less than 1%) and plutonium. Recovered uranium can be returned to the conversion plant and further enriched. Recovered plutonium mixed with uranium is applied to fabricate mixed oxide fuel (MOX). Spent nuclear fuel can be safety disposed in stable rock formations (e.g. granite). The low-level radioactive waste is already kept in geological repositories. High-level waste (HLW) contains a small amount of long-lived nuclides, mainly minor actinides (MAs) hence the need of its reprocessing before it will be deposited. The first disposal facilities for such waste will be in operation around 2020. Waste will be packed in long-lasting containers and buried deep and stable underground characterized by limited water movement.

The core focus of activities at the back end of the nuclear fuel cycle revolves around reprocessing and waste management [14]. Development of reprocessing technologies, waste treatment and supporting technologies is an extremely important issue over the last 50 years. Nuclear reprocessing reduces only the volume of HLW, but does not reduce its radioactivity. One of the central goals of nuclear sustainable R&D is to enhance the effectiveness of resource utilization and to reduce the volume of long-lived radio-toxicity of HLW. It can be achieved employing partitioning and transmutation of minor actinides.

The advanced reprocessing of high burn-up fuel has to address the following issues:

- minor actinides (MA) separation
- secondary waste minimization
- safety
- security
- sustainability.

At present, reprocessing options include separation of certain elements from the spent fuel. The research of new recovery technologies is constantly required. Mainly uranium and plutonium are recovered but also the minor actinides (MA), especially neptunium (Np), americium (Am) and curium (Cm) as well as certain fission products that can be recycled.

The following separation techniques of spent fuel are already established:

I. Aqueous methods
   a. PUREX
   b. Modifications of PUREX
   c. Electrochemical methods
II. Pyroprocessing

The PUREX (Plutonium and Uranium Recovery by Extraction) is currently the most commonly applied industrial reprocessing method. In this technique, the spent fuel rods are dissolved in hot concentrated nitric acid. Uranium and plutonium are extracted independently of each other and further returned to the input of the fuel cycle. Several modifications of the PUREX process are being considered. The pure plutonium can no longer be recovered because of proliferation reasons. Therefore, the UREX (Uranium Extraction) method was developed where uranium and technetium are extracted [11]. Uranium causes the vast majority of the mass and volume of waste, and after enrichment it can be again used as fuel. After the PUREX process the most troublesome radioisotopes like strontium and cesium are recovered. To separate the

transuranic metals (Am, Cm) from nuclear spend material the TRUEX (Transuranic Extraction) process was invented. Another modification of the PUREX is the SANEX (Selective Actinide Extraction) process which is still under R&D. Here trivalent minor actinides and lanthanides can be removed. The complicated separation of the minor actinides from the lanthanides can be carried out by the TALSPEAK process [11]. Moreover a reprocessing method based on ion exchange in ammonium carbonate solution was proposed by Asanuma et al. [15]. There are also several other aqueous reprocessing techniques differing by the extracting compound. However, these separation processes are mainly replaced by the PUREX method.

The pyroprocessing recovering technology is considered as a promising alternative to traditional aqueous processes of spent nuclear fuel. It was applied for the first time in the Aragonne National Laboratory (US), but still it is not in favor worldwide. The evolution of it began already in the middle 1960s, however the modern pyro-reprocessing technology was expanded in the 1980s [16]. Laidler et al. [16] reported that it is a compact and efficient method for recycling integrated fast reactor (IFR) fuel. Generally, the pyrochemical reprocessing relies on refining in a molten salt bath (e.g. LiCl/KCl eutectic) at high temperature (~500 °C) [13]. The principle of this method is to separate actinide elements from spent rods and recycle them to the reactor as fuel [16]. The pyro-reprocessing consists of electrorefining, distillation and solvent-solvent extraction steps. It can be applied to high burn-up fuel and fuel with short cooling time. The demonstration of the process has been performed on used rods from the Experimental Breeder Reactor (EBR-II) [17]. During the electrorefining step the spent fuel was immersed in a molten LiCl-KCl-UCl_3/liquid cadmium system in a pilot scale electrorefiner (Mark-IV ER). In the view of a large scale development of this process, some successive experimental runs could be carried out so far. Fanghänel et al. [13] described the results of 25 experiments done for Zr-based fuels used in IFR (Generation IV). The goal of R&D on the pyroprocessing process is to find optimal conditions and to provide the sustainability of the process.

The pyroprocessing is a batch-mode process. The irradiated fuel assembly should be first dismantled and individual rods should be removed. The transportation of spent nuclear fuel is described by stringent regulatory requirements given by a local government or appropriate nuclear energy board. The whole procedure is set under IAEA guidelines. Protection of mankind and environment must be ensured. Special casks made of steel or a combination of steel and lead, have been designed [14]. The used rods are placed in casks and so delivered to an electrorefining installation which is the central step of the pyroprocessing. These rods are sent first to a chopper, where they are cut into short segments (6-7 mm) [16]. An electrorefiner consists of an anode and two cathodes as it is presented in Fig.2.

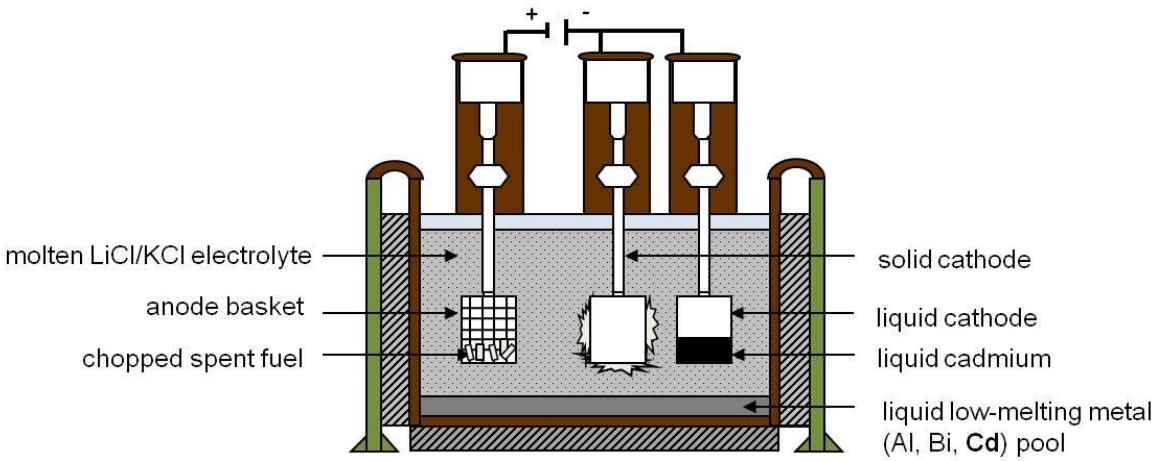

Fig.2. The electrorefiner scheme.

An anode is in form of a basket in which the chopped segments of spent fuel are loaded. Both cathodes are at the same potential relative to the anode. The first cathode is made of stainless steel and the second is filled with liquid cadmium. The molten salt LiCl/KCl is applied as an electrolyte (the LiCl/KCl eutectic temperature is 350 °C). A pool of liquid Cd occupies the bottom of the electrorefiner. The whole unit is produced from steel and is operated

at ~500 °C. Due to electrotransport through a suitable electrolyte, an impure metal placed in the anode will deposit at a cathode and obtain then higher purity. During electrorefining, several other electrochemical processes occur because beside U also Pu, MA and rare earth (RE) elements are electrotrasportable. The chemical similarity of actinides and RE caused that they can be recovered together. Despite this fact, the separation factors of actinides and lanthanides have quite different values [18]; lanthanides have the lower affinity for extraction as actinides.

In the electrorefiner U^{3+} ions are reduced at a solid cathode. Very pure uranium will be deposited on the solid cathode surface in the form of dendrites. A mixture of Pu, Am, Np, Cm and the MA ions will move to the liquid Cd cathode. Here they will also be reduced to metal and automatically dissolve in liquid Cd. Uranium does not form an intermetallic compound with cadmium therefore it is only collected on the first cathode. The other fission products like noble metals or Zr (if it is contained in the spent fuel) will drop in the Cd pool at the bottom of the unit. On the other hand, Cs and alkaline earths (Ba, Sr) as well as the rare-earths fission elements will dissolve in the electrolyte. The distribution of fission products depends on the stability of their chlorides (compare Table 1). Olander [11] explained all electrochemical reactions occurring on the anode and both cathodes. Some experimental observations in a pilot scale electrorefiner were described [17]. The cadmium pool acts as an intermediate electrode during the direct transport process. However, the high vapor pressure and high vaporization rate of Cd at operational temperature (~500 °C) caused problems and finally generated an electrical shorting.

Beside Cd, other low melting metals such as Al [19] and Bi [20] are suggested to be employed in the electrorefiner. However, among the proposed and investigated metals, Cd has the most profitable properties according to its rather high vapor pressure as well as the existence of rather stable RE-Cd intermetallic compounds. Moreover, the presence of reductive Li in the molten

salt (electrolyte) simplifies the extraction of RE elements into the liquid metal pool and further the formation of intermetallic phases. An important issue in the design of a pyrochemical reprocessing is the variation in solubility or activity of solute (actinides and REs) in multi-component system [21]. Therefore, the detailed knowledge of RE-Cd intermetallic compounds as well as their thermodynamic stability is very important issue. This would enrich the deficiencies in the literature concerning some RE-Cd systems and facilitate further development of the pyrometallurgical reprocessing method.

Table 1. Standard free energies of formation of some fission product chlorides at 500 °C. (based on data given in Ref. [16])

Relatively stable (salt phase)		Electrotransportable		Relatively unstable (metal phase)	
chloride	$\Delta G^0_{f,}$ (kJ/mol)	chloride	$\Delta G^0_{f,}$ (kJ/mol)	chloride	$\Delta G^0_{f,}$ (kJ/mol)
CsCl	-367.4	$PuCl_3$	-261.1	$CdCl_2$	-135.1
$SrCl_2$	-354.4	$NpCl_3$	-243.1	$NbCl_5$	-111.7
LiCl	-345.2	UCl_3	-231.0	$MoCl_2$	-70.3
$LaCl_3$	-293.7	$ZrCl_4$	-195.0		
$PrCl_3$	-288.7				
$CeCl_3$	-287.0				
$NdCl_3$	-284.1				

Although several of the RE-Cd phase diagrams appear to be reasonably well studied, there is still missing information, e.g. on the melting behavior of their intermetallic compounds. Regarding thermodynamic data, only a small number of investigations were performed.

The volume of experimental work like determination of phase diagrams, characterization of intermetallic compounds and thermodynamic

measurements of the rare-earth-based alloys increases continuously. Some of the phase diagrams are already well known, but some are only available as an old version or are only partially studied. Many of them were investigated in the early 1950s [22]. Anyhow, an updated and reliable version is needed for several of them. Table 2 shows an overview on the availability of phase diagrams of RE-Cd binary systems. Due to economic reason as well as special conditions of alloying and measurement, only a few RE-Cd systems have been examined yet. However, several intermetallic compounds are actually confirmed (Fig.3, Ref. [23]).

Table 2. Level of phase diagram knowledge for lanthanides-Cd binary systems (o - complete (recent phase diagram), □ - incomplete (no or old version of phase diagram). (based on data given in Ref. [22])

	La	Ce	Pr	Nd	Sm	Eu	Gd	Tb	Dy	Er	Tm	Yb	Lu
Cd	o	□	□	□	o	o	o	□	□	□	□	o	□

The first attempt to establish a general RE-Cd phase diagram was done by Gschneidner and Calderwood [24] (Fig.4). They presented a ‘Mischmetal’ (MM)-Cd diagram where ‘Mischmetal’ (from German: *Mischmetall* - "mixed metal") means an alloy of rare earth elements (approximately 50% cerium and 25% lanthanum, with small amounts of neodymium and praseodymium.). The diagram was featured according to the melting points of pure metals (Cd and MM) as well as the α ↔ β transformation temperature of MM. Six intermetallic phases were pointed out like MMCd, $MMCd_2$, $MMCd_3$, $MM_{13}Cd_{58}$, $MMCd_6$ and $MMCd_{11}$. This diagram can serve as a base to determine the individual RE-Cd phase diagrams.

Regarding the crystal structure investigation and thermodynamic study of the Ce-Cd and Nd-Cd systems, information will be given in the next two sub-chapters, where they are described separately.

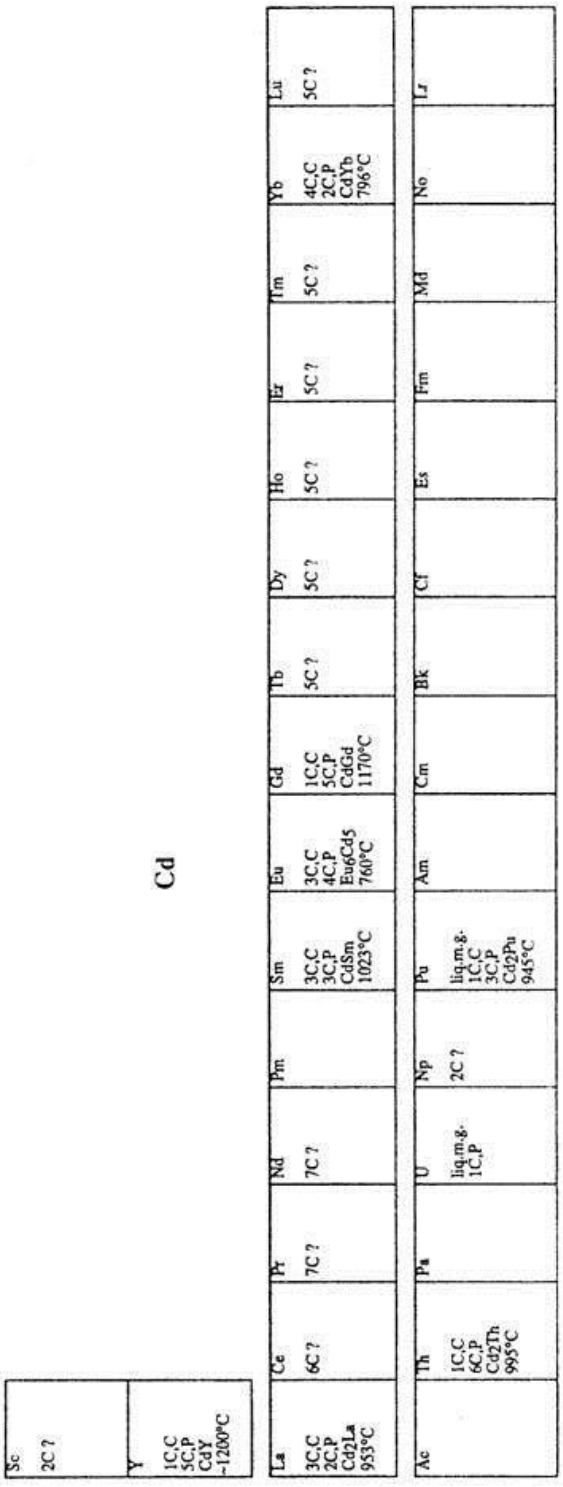

Fig.3. Main features of the phase diagrams of cadmium with rare earths according to Ref. [23].

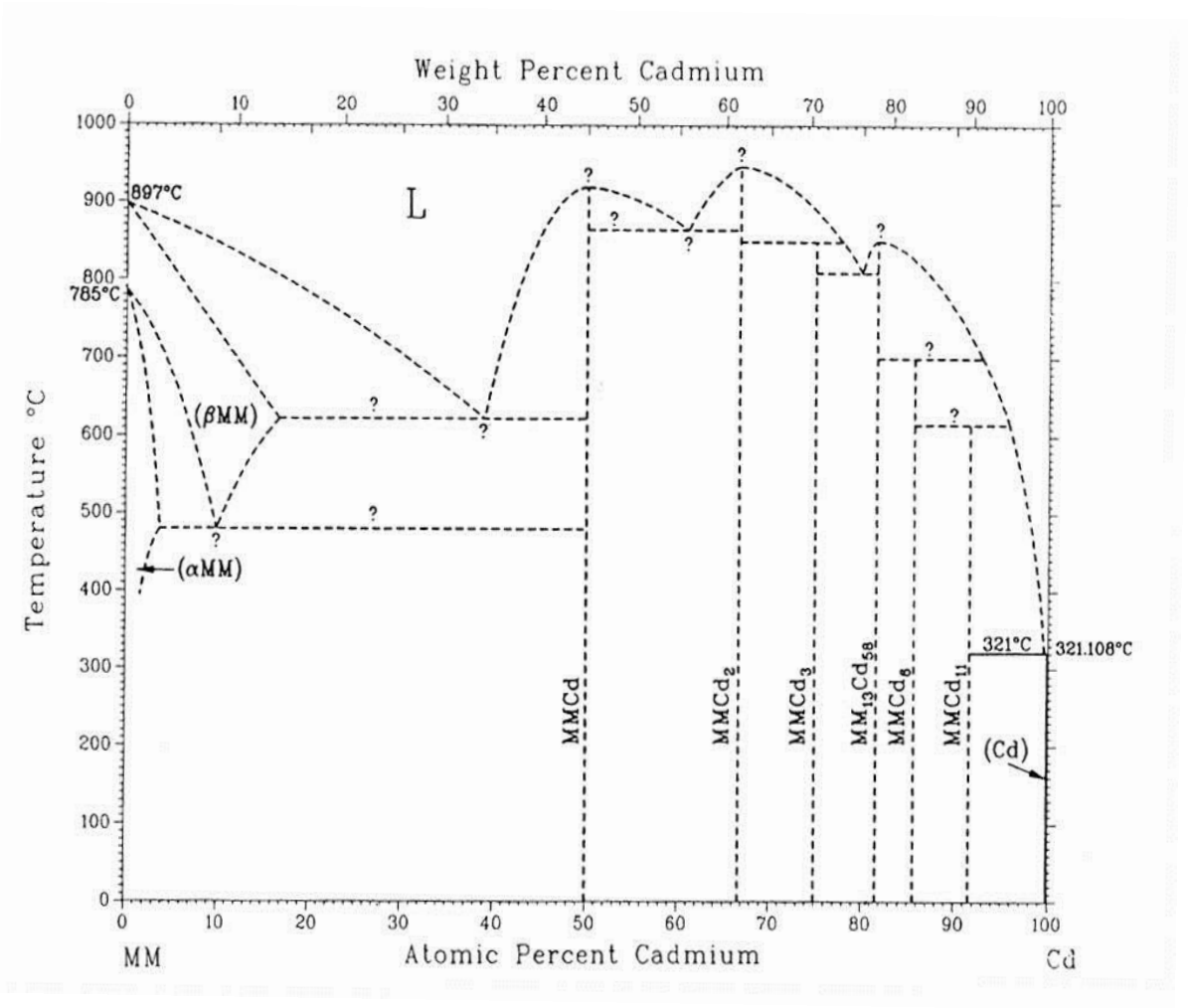

Fig.4. The proposed phase diagram for the MM (Mischmetal)-Cd system presented in Ref. [24].

1.1 The Ce-Cd system

The Ce-Cd phase diagram seems to be well known in the literature. First features were presented by Massalski [25]. This was based on the data given by Gschneidner and Calderwood [24]. The diagram showed only the Cd-rich part (composition range from 0 to 50 % Ce) up to 700 °C. Later on, Johnson et al. [26] investigated the Cd-rich part in more detail. The peritectic decomposition of $CeCd_{11}$ was recorded using differential thermal analysis (DTA). In addition, the liquidus line was drawn up to 7 at.% Cd. In 1985, Canepa et al. [27] experimentally studied the interaction of Ce with Cd, using DTA, XRD and metallography. The results of their investigation allowed featuring the complete version of the Ce-Cd binary phase diagram (Fig.5). The existence of the Ce_2Cd_{17} phase was pointed out [27]. The melting behavior of the Ce-Cd intermetallic compounds was examined. In addition, the temperature of all invariant reactions was determined applying DTA results. However, no information about the homogeneity range of intermetallic compounds was given. Further Okamoto [28] presented an overview of Ce-Cd system data given in the literature. The system is characterized by seven intermetallic compounds, of which three (CeCd, $CeCd_2$, and $Ce_{13}Cd_{58}$) show a congruent melting behavior and the others ($CeCd_3$, $CeCd_6$, Ce_2Cd_{17}, and $CeCd_{11}$) are formed through peritectic reactions.

Iandelli and Ferro [29] described the crystal structures of almost all Ce-Cd compounds, such as CeCd, $CeCd_2$, $CeCd_3$, $Ce_2Cd_{9\sim}$, $CeCd_6$ and $CeCd_{11}$, excepting the Ce_2Cd_{17} intermetallic phase. The stoichiometry of the $Ce_2Cd_{9\sim}$ compound was corrected later on to $Ce_{13}Cd_{58}$. Anyhow, in older literature the $Ce_2Cd_{9\sim}$ formula is commonly used. Recently, a closer study of the crystal structure of the $Ce_{13}Cd_{58}$ intermetallic compound was performed by Piao et al. [30],and a more complex structure was reported than previously observed.

The disorder mechanism was analyzed and a stoichiometry of $Ce_{12.60}Cd_{58.68}$, derived from the crystallographic data [30], was assumed.

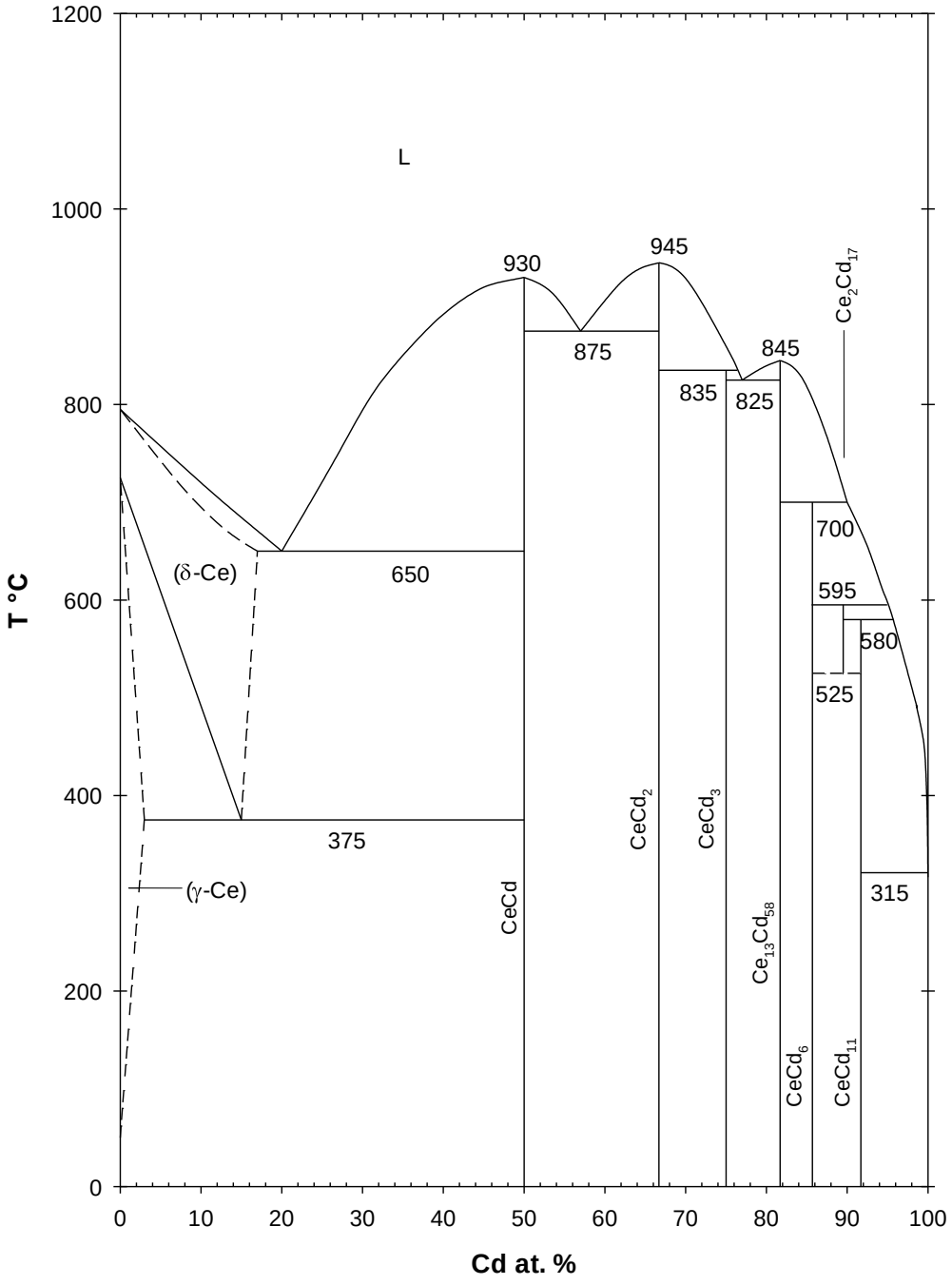

Fig.5. The Ce-Cd phase diagram according to the work of Canepa et al. [27].

Iandelli and Palenzona [31] carried out a systematic study of the structural behavior of the rare earths (RE) in intermetallic compounds with Cd. All Ce-Cd phases, both Ce modification and Cd with their crystal structure are listed in Table 3. Cerium was studied in details by Gschneidner [32]. The γ-Ce modification exists between -10 and 725 °C [32]. It has the face-centered cubic, copper (A1) type structure. A second modification of Ce, occurring in the temperature range 725 to 797 °C, has also cubic structure, i.e. the body-centered, tungsten (A2) type. Cadmium crystallizes in the hexagonal close-packed, magnesium (A3) type.

The richest phase in Ce at a composition of 50 at.% Cd is cubic structured CeCd (CsCl (*B2*)). This phase was described in detail by Iandelli et al. [33]. According to the results of Canepa et al. [27] it melts congruently at 930 °C. $CeCd_2$ (66.7 at.% Cd) crystallizes with the deformed AlB_2 structure with disordered and ordered arrangements of Cd atoms [29]. According to data of Canepa et al. [27] the $CeCd_2$ compound has congruent melting behavior (945 °C). Powder and single crystal methods confirmed that $CeCd_3$ crystallizes with the BiF_3 structure [34] and exists at 75 at.% Cd. It is formed through a peritectic reaction at 835 °C [27]. Further, Bruzzone et al. [34] carried out metallographic and X-ray investigations on the $Ce_{13}Cd_{58}$ phase with composition 81.7 at.% Cd. Based on their results it has $Pu_{13}Zn_{58}$ structure. Moreover, single crystal data for $Ce_{13}Cd_{58}$ indicated the occurrence of different crystal lattices [34]. As it was already mentioned, the exact stoichiometry of the 13:58 phase was discussed previously and the chemical formula $Ce_{12.60}Cd_{58.68}$ was suggested [30]. The phase melts congruently at 845 °C. The existence and lattice constants of the cubic $CeCd_6$ (YCd_6 prototype) intermetallic compound were reported in Refs. [34-35]. It decomposes peritectically at 700 °C [27] at 85.7 at.% Cd. Previously, the study of Johnson et al. [26] did not report about the 2:17 phase. It was found only for the La system although the Ce-Cd system was also examined. The detailed investigation of the Ce-Cd binary phase diagram by Canepa et al. [27] confirmed the existence of the high temperature phase Ce_2Cd_{17}. The phase is

isotypic with Th_2Ni_{17} and is stable in the temperature range from 525 to 595 °C according to Ref. [27]. The most Cd-rich phase is cubic $CeCd_{11}$ (cP36) [29] which decomposes peritectically at 580 °C at a composition of 91.7 at.% Cd.

Only limited thermodynamic information is available for the Ce-Cd binary system in the recent literature. One of the earliest thermodynamic results on the Ce-Cd binary system was given by Elliot and Lemons [36]. They used an isopiestic balance to determine the activity coefficient of Cd over the $CeCd_{\sim 6}$ compound at two selected temperatures. Partial thermodynamic properties of Cd-rich liquid alloys were measured by an electromotive force (emf) method by Bayanov and Serebrennikov [37]. They estimated the activity of Ce in dilute solutions of Ce in Cd in the temperature range 673-823 K. Johnson and Yonco [38] also used a molten salt based emf method to determine the Ce activity in the Cd-rich liquid phase in the temperature range 638-884 K. The free energy of formation of the $CeCd_{11}$ compound was reported [38]. Further, Colinet and Pasturel [39] compared the enthalpies and entropies of formation of $CeCd_{11}$ measured by Bayanov and Serebrennikov [37] and Johnson and Yonko [38]. An electrochemical method was also used by Kurata et al. [40] to measure the activity of Ce in highly diluted liquid Ce-Cd alloys. Later, Kurata and Sakamura [21] estimated values for the Gibbs energy of formation for both the $CeCd_{11}$ and the $CeCd_6$ intermetallic compounds. No thermodynamic data seem to be provided for Ce-richer compositions.

Table 3. The crystal structure data of the Ce-Cd system according to Refs. [28,32].

Phase	Composition (at.% Cd)	Structure type	Pearson symbol	Space group	Ref.
γ-Ce	0	Cu	*cF4*	*Fm$\bar{3}$m*	[32]
δ-Ce	0	W	*cI2*	*Im$\bar{3}$m*	[32]
CeCd	50.0	CsCl	*cP2*	*Pm$\bar{3}$m*	[28]
$CeCd_2$	66.7	$CeCd_2$	*hP3*	*P$\bar{3}$m1*	[28]
$CeCd_3$	75.0	BiF_3	*cF16*	*Fm$\bar{3}$m*	[28]
$Ce_{13}Cd_{58}$	81.7	$Pu_{13}Zn_{58}$	*hP142*	*P6$_3$/mmc*	[28]
$CeCd_6$	85.7	YCd_6	*cI168*	*Im$\bar{3}$*	[28]
Ce_2Cd_{17}	89.5	Th_2Ni_{17}	*hP38*	*P6$_3$/mmc*	[28]
$CeCd_{11}$	91.7	$BaHg_{11}$	*cP36*	*Pm$\bar{3}$m*	[28]
Cd	100	Mg	*hP2*	*P6$_3$/mmc*	[28]

1.2 The Nd-Cd system

A rudimentary phase diagram of the Nd-Cd system can be found in Massalski's handbook [25] (Fig.6), based mainly on the earlier work by Johnson et al. [26,35] and on the assessment of Gschneidner and Calderwood [41]. It shows the peritectic decomposition of $NdCd_{11}$ at 530 °C and the liquidus line in Cd-rich corner (93 to 100 at.% Cd). The liquidus was determined by the chemical analysis of the filtered liquid phase after equilibration time [26]. Seven intermetallic compounds are known in this binary system like NdCd, $NdCd_2$, $Nd_{11}Cd_{45}$, $Nd_{13}Cd_{58}$, $NdCd_6$ and $NdCd_{11}$. The type of melting and the melting points for these phases are presently unknown.

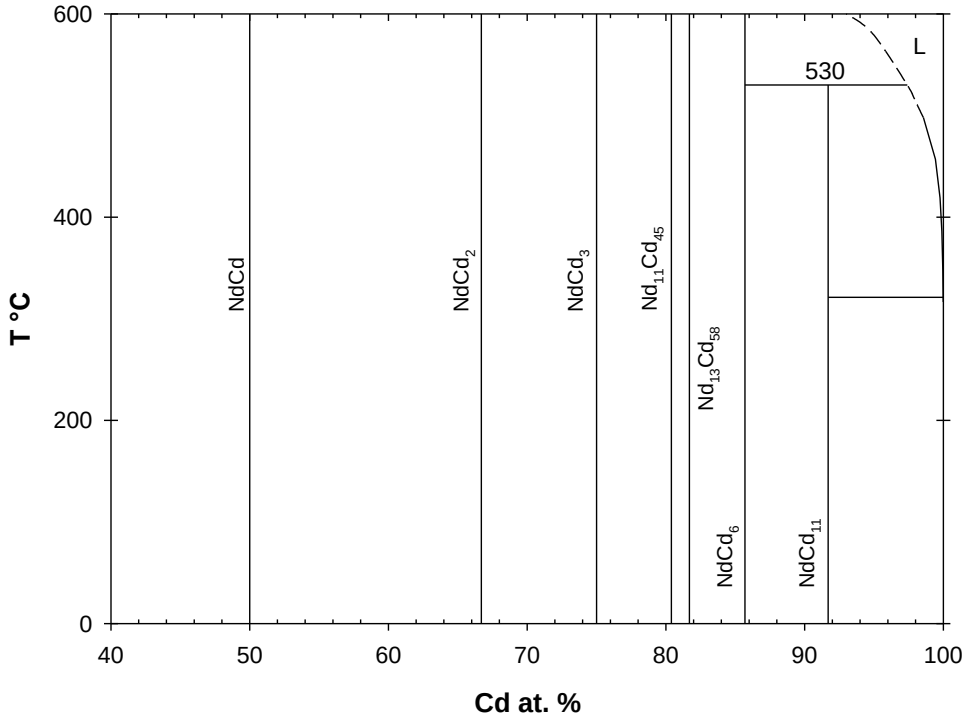

Fig. 6. The Nd-Cd phase diagram according to the work of Massalski (Ref. [25]).

The existence of seven Nd-Cd compounds were also summarized by Colinet and Pasturel [23]. In Table 4, the crystallographic data known for the Nd-Cd phases and two Nd modifications as well as for Cd are collected. In addition, their composition is listed as it is reported in Ref. [25]. Neodymium has the hexagonal (A3') type structure up to 862 °C [32]. The second Nd allotropic modification, β-Nd exists in the temperature range from 862 °C to 1024 °C and, similar to δ-Ce, crystallizes in the cubic tungsten (A2) type. Iandelli [42-43] provided the first more detailed investigation of four intermetallic compounds, i.e. NdCd, $NdCd_2$, $NdCd_3$ and $NdCd_{11}$. The crystal structure determination was performed using X-ray diffraction (XRD). No information on their melting behavior was given. It is to observe that the RE-Cd compounds with the same composition have in general identical crystal structure. The NdCd compound has the CsCl type structure [33] and $NdCd_2$ appears to be similar to $CeCd_2$ (deformed AlB_2 structure) [31]. A small variation in the lattice constants of the $NdCd_2$ phase in samples of different composition was recorded. Therefore, its solid-solubility should be small. Bruzzone et al. [34] discussed the behavior of the following compounds: $NdCd_3$, $Nd_{11}Cd_{45}$, $Nd_{13}Cd_{58}$ and $NdCd_6$. The 1:3 compound crystallizes with the BiF_3 structure as does $CeCd_3$. A detailed investigation of the $Nd_{11}Cd_{45}$ phase (γ-brass type) was carried out applying powder pattern data. X-ray analysis of a single crystal of $Nd_{13}Cd_{58}$ ($Nd_2Cd_{9\sim}$ [34]) revealed the occurrence of different superlattices. Anyhow, the structure was identified to be of the hexagonal $Pu_{13}Zn_{58}$ type. The existence of cubic $RECd_6$ was discussed by Johnson et al. [35], and later on the crystal structure of $NdCd_6$ was determined that shows close relationship with $CeCd_6$ [17]. The crystal structure of the 1:6 intermetallic was investigated by use of metallographic and X-ray methods [34]. It is similar to other $RECd_6$ phases – namely cubic YCd_6 type. In the calculated partial phase diagram by Kurata et al. [21], the peritectic temperature for $NdCd_6$ was shown at 603 °C. It was not marked in Fig.6, because the results from Ref. [21] are more recent than these collected by Massalski [25]. The $NdCd_{11}$ compound decomposes peritectically at 530 °C and crystallizes in the cubic $BaHg_{11}$ structure [25].

Table 4. The crystal structure data of the Nd-Cd system according to Refs. [25,32].

Phase	Composition (at.% Cd)	Structure type	Pearson symbol	Space group	Ref.
α-Nd	0	α-La	*hP4*	*P6$_3$/mmc*	[32]
β-Nd	0	W	*cI2*	*Im$\bar{3}$m*	[32]
NdCd	50.0	CsCl	*cP2*	*Pm$\bar{3}$m*	[25]
$NdCd_2$	66.7	CdI_2	*hP3*	*P$\bar{3}$m1*	[25]
$NdCd_3$	75.0	BiF_3	*cF16*	*Fm$\bar{3}$m*	[25]
$Nd_{11}Cd_{45}$	80.4	γ-brass	*cF448*	*F$\bar{4}$3m*	[25]
$Nd_{13}Cd_{58}$	81.7	$Pu_{13}Zn_{58}$	*hP142*	*P6$_3$/mmc*	[25]
$NdCd_6$	85.7	YCd_6	*cI168*	*Im$\bar{3}$*	[25]
$NdCd_{11}$	91.7	$BaHg_{11}$	*cP36*	*Pm$\bar{3}$m*	[25]
Cd	100	Mg	*hP2*	*P6$_3$/mmc*	[25]

Virtually no thermodynamic data are available for the binary system Nd-Cd in the literature. Only activity coefficients of Nd in liquid Cd in the temperature range between 673 and 773 K were calculated by Kurata et al. [21]. Sakamura et al. [44] evaluated the partial molar enthalpy of mixing and partial molar excess entropy of Nd solutes in Cd.

References

[1] R. Resnick, D. Halliday. Fizyka. vol. 1. 13th ed., Wydawnictwo Naukowe PWN, Warszawa (1998). (in Polish)

[2] W. Bland, T. Laird. Energy. In: An introduction to industrial chemistry. ed.: A. Heaton. 3rd ed. Blackie Academic & Professional (1996).

[3] International Energy Outlook 2013. U.S. Energy Information Administration. Washington, DC (2013). www.eia.gov/ieo

[4] "PRIS (Power Reactor Information System) - Home". (2013) www.iaea.org/pris/

[5] J. Newman. Physics of the Life Sciences. Springer Springer Science & Business Media (2008). p. 652.

[6] OECD Nuclear Energy Agency. Nuclear Development – Nuclear Energy Today. OECD Publishing 2003. p. 25.

[7] World Nuclear Association: www.world-nuclear.org

[8] United Nations Handbook 2008/09. 46th ed. The Ministry of Foreign affairs and Trade. Wellington, New Zealand (2008).

[9] UNSCEAR. UNSCEAR 2006 Report: Effects of ionizing radiation. Vol. II. UN, New York (2009) 3-4.

[10] R.C. Ewing. The design and evaluation of nuclear-waste forms: clues from mineralogy. Can Mineral 39 (2001) 697-715.

[11] D. Olander. Nuclear fuels – Present and future. J Nucl Mater 389 (2009) 1-22.

[12] D. Olander, E. Greenspan, H. D. Garkisch, B. Petrovic. Uranium–zirconium hydride fuel properties. Nucl Eng Design. 239 (2009) 1406-1424.

[13] Th. Fanghänel, J. P. Göatz, J. Somers, F. Wastin. Closing the Nuclear fuel Cycle for Future Sustainable Nuclear Energy. In Nuclear Fuel Cycle I.: H. S. Kamath, T. R. G. Kutty, R. Natarajan, S. D. Misra, D. S. Rana, S. K. Munshi, P. R. Vasudeva Rao (editors), Bhabha Atomic Research Centre Department of Atomic Energy, Trombay, Mumbai, 2009.

[14] S. D. Misra. Back End of Nuclear Fuel Cycle: Indian Scenario. In Nuclear Fuel Cycle II.: H. S. Kamath, T. R. G. Kutty, R. Natarajan, S. D. Misra, D. S. Rana, S. K. Munshi, P. R. Vasudeva Rao (editors), Bhabha Atomic Research Centre Department of Atomic Energy, Trombay, Mumbai, 2009.

[15] N. Asanuma, M. Harada, M. Nogami, K. Suzuki, T. Kikuchi, H. Tomiyasu, Y. Ikeda. Anodic dissolution of UO_2 pellets containing simulated fission products in ammonium carbonate solution. J Nucl Sci Technol 43 (3) (2006) 255-262.

[16] J. J. Laidler, J. E. Battles, W. E. Miller, J. P. Ackerman, E. L. Carls. Development of Pyroprocessing Technology. Progr Nucl Energy 31 (1/2) (1997) 131-140.

[17] S.X. Li, D. Vaden, R. D. Mariani, T. A. Johnson. Experimental observation on the reoles of the cadmium pool in Mark-IV ER. ANS 4th Topical Meeting - DOE Spent Nuclear Fuel and Fissile Material Management, San Diego, CA (US) 2000.

[18] H. Moriyama, S. Seshimo, K. Moritani, Y. Ito, T. Matsugashira. Reductive extraction behavior of actinide and lanthanide elements in molten salt and liquid metal binary phase. J Alloys Comp 213-214 (1994) 354-359.

[19] O. Conocar, N. Douyere, J. Glatz, J. Lacquement, R. Malmbecke, J. Serp. Promising pyrochemical actinide/lanthanide separation processes using aluminum. Nucl Sci Eng 153 (2006) 253-261.

[20] M. Kurata, Y. Sakamura, T. Hijikata, K. Kinoshita. Distribution behavior of uranium, neptunium, rare-earth elements (Y, La, Ce, Nd, Sm, Eu, Gd) and alkaline-rare metals (Sr, Ba) between molten LiCl-KCl eutectic salt and liquid cadmium or bismuth. J Nucl Mater 227 (1995) 110-121.

[21] M. Kurata, Y. Sakamura. Thermodynamic assessment of system of actinide or rare earth with Cd. J Phase Equil 22 (2001) 232-240.

[22] A. Iandelli, A. Palenzona. Crystal chemistry of intermetallic compounds, in: K.A. Gschneidner Jr., L.R. Eyring (Eds.), Handbook on the Physics and Chemistry of Rare Earths – Alloys and Intermetallics, North-Holland Publishing, Amsterdam 1982, pp. 4-13.

[23] C. Colinet, A. Pasturel. Thermodynamic properties of metallic systems, in: K.A. Gschneidner Jr., L.R. Eyring, G.H. Lander, G.R. Choppin (Eds.), Handbook on the Physics and Chemistry of Rare Earths - Lanthanides/Actinides: Physics – II, Elsevier Science B.V., Amsterdam 1994, pp. 479-631.

[24] K. A. Gschneidner Jr., F. W. Calderwood. The cadmium-rare earth systems. Bull Alloy Phase Diag 9 (1988) 16-21.

[25] T. B. Massalski. Binary Alloy Phase Diagrams. 2nd ed.Ohio: ASM International, Materials Park 1990.

[26] I. Johnson, K. E. Anderson, R. A. Blomquist. Partial constitutional diagram for the Cd-La, Cd-Ce, Cd-Pr, Cd-Nd, and Cd-Sm systems. Trans ASM 59 (1966) 352-355.

[27] F. Canepa, G. A. Costa, E. A. Franceschi. The phase diagram of the Ce-Cd system. Lanthanide Actinide Res 1 (1985) 41-47.

[28] H. Okamoto. Cd-Ce (cadmium-cerium). J Phase Equilibria 20 (1999) 636.

[29] A. Iandelli, R. Ferro. Sulle leghe del Cadmio col Lantanio, Cerio e Praeseodimio. Gazz Chim Ital 84 (1954) 463-478.

[30] S. Y. Piao, L. Palatinus, S. Lidin. All the disorder mechanisms in the 13:58 phases come together. Out of the modulated confusion rises the remarkable phase $Ce_{12.60}Cd_{58.68(2)}$. Inorg Chem 47 (2008) 1079-1086.

[31] A. Iandelli, A. Palenzona. On the occurrence of the MX_2 phase of the rare earths with the IB, IIB and IIIB group elements and their crystal structures. J Less-Common Met 15 (1968) 273-284.

[32] K. A. Gschneidner. Rare Earth Alloys. D. van Nostrand Company Ltd, Canada; 1961.

[33] A. Iandelli, A. Palenzona. Atomic size of rare earths in intermetallic compounds. MX compounds of CsCl type. J Less-Common Met 9 (1965) 1-6.

[34] G. Bruzzone, M. L. Fornasini, F. Merlo. Rare earth intermediate phases with cadmium. J Less-Common Met 30 (1973) 361-375.

[35] I. Johnson, R. Schablaske, B. Tani, K. Anderson. $CeCd_6$-type rare earth-cadmium alloy. Trans AIME 230 (1964) 1485-1487.

[36] G. R. B. Elliot, J. F. Lemons. A balanced isopiestic apparatus. Application to $CeCd_{\sim 6}$ solid solution systems. J Phys Chem 64 (1960) 137-145.

[37] A. P. Bayanov, V. V. Serebrennikov. E.M.F. study of the thermodynamic properties of cerium and erbium in some metallic melts. Zhur Fiz Khim 39 (1965) 717-721.

[38] I. Johnson, R. M. Yonco. Thermodynamics of cadmium- and zinc-rich alloys in the Cd-La, Cd-Ce, Cd-Pr, Zn-La, Zn-Ce and Zn-Pr systems. Met Trans 1 (1970) 905-910.

[39] C. Colinet, A. Pasturel. Thermodynamic properties of metallic systems. In: K. A. Gschneidner Jr, L. Eyring, G. H. Lander, G. R. Choppin, editors. Handbook on the Physics and Chemistry of Rare Earths - Lanthanides/Actinides: Physics – II, Amsterdam: Elsevier Science B.V.; 1994, p. 479-631.

[40] M. Kurata, Y. Sakamura. Ts. Matsui. J Alloys Comp 234 (1996) 83.

[41] K. A. Gschneidner Jr., F. W. Calderwood. The Cd-Nd (Cadmium-Neodymium) systems. Bull Alloy Phase Diag 9 (1988) 128.

[42] A. Iandelli, Congr. Intern. Chim. Pure Appl., 16, Paris, Mem. Sect. Chim. Minerale, 1958, 35-40.

[43] A. Iandelli, Atti. Accad. Nazl. Lincei, Rend., Classe Sci. Fis., Mat. e Nat. 29 (1960) 62-69.

[44] Y. Sakamura, T. Inoue, K. Storvick, L. F. Grantham. Proc. 26th Symp. On Molten Salt Chemistry, Saporo, 1994. Japan Molten Salt Chem. Soc., Saporro, p. 101 (in Japanese)

2. Experimental and methods

Inorganic materials can be characterized by use of dynamic and isothermal methods as well as measurement of thermodynamic properties. The characterization of physical feature of a system as a function of a temperature can be carried out by few common dynamic techniques such differential thermal analysis (DTA), differential scanning calorimetry (DSC), thermo gravimetric analysis (TGA), thermo mechanical analysis (TMA) or dilatometry. In this work DTA and dilatometry measurements were performed operating on recording the temperature difference and the size change, respectively. Both were applied to determinate phase reactions occurring in investigated systems. For further experimental determination of a phase diagram the standard techniques were applied as light optical microscopy (LOM), scanning electron microscopy (SEM) and X-ray diffraction (XRD). They were used in combination with the dynamic methods and provided information about the isothermal equilibrium of as-cast as well as quenched samples (at different temperatures and nominal compositions).

Thermodynamic quantities of substances can be achieved through calorimetry, vapour pressure or electromotive force measurements. Due to the high volatility and on the other hand extremely toxicity of cadmium, nothing except experiment in an arrangement separated from lab equipments (in case of unexpected progress) has to be applied. The vapor pressure method based on the equilibration seems to be an ideal opportunity. It enables controlled heating of a closed system and equilibration of samples with a gas phase.

2.1 Sample preparation

For the determination of the Ce-Cd and the Nd-Cd phase diagrams as-cast samples as well as equilibrated alloy samples were used. As-cast sample were prepared in a simple way, where pieces of metals were placed in a crucible and further analyzed (DTA). To achieve homogenized and annealed samples, a certain temperature treatment for a sufficient period of time to reach equilibrium was applied. The annealing temperature was in the range from 250 °C to 850 °C and the heat-treatment time between 3 – 12 weeks. Afterwards the quenched specimens were characterized using LOM, SEM-EDX, XRD, DTA and dilatometry.

To assess a thermodynamical data of both binary systems the ispiestic equilibration experiments were carried out. In this method, rare earth metal (Ce, Nd) was equilibrated using cadmium vapor in a broad temperature range. After quenching the samples were weighed and thermodynamical values could be estimated. Representative samples were analized (SEM, XRD) in order to check their calculated composition.

The high reactivity of RE with water and oxygen [1] as well as the high volatility of Cd restricts the number of materials that can be used for sample preparation. RE metals attack alumina and quartz glass at high temperature preventing their application. Tantalum had been found to be an ideal material. Therefore all samples were prepared in crucibles made of tantalum. Dennison et al. [2-3] estimated the very low solubility of Ta in liquid Nd for high temperatures between 1547 and 2070 °C. In addition, the result of the assessment by Garg et al. [4] indicated a negligible solubility of Ta in liquid Ce as well as Nd. Furthermore, a Ta crucible can be easily closed with a corresponding lid made also from Ta by welding in a standard arc furnace [5] providing sufficient protection of the contained sample.

2.1.1 Phase diagram investigation

The starting materials used to prepare the Ce-Cd and Nd-Cd alloys were Cd shot (United Mineral & Chemical Corporation, U.S.A, and Alfa Aesar, Karlsruhe, Germany; both 99.9999%), Ce (99.9 %) rod (Alfa AESAR, Karlsruhe, Germany) and pieces (smart-elements, Vienna, Austria) as well as Nd (99.9%) in form of foil/rod (Alfa Aesar, Karlsruhe, Germany) and pieces (smart-elements, Vienna, Austria). Due to the high reactivity of rare earth elements the preparation procedure took place in a glove box (mBRAUN labmaster 130) under an Ar atmosphere containing less than 1 ppm O_2 and 5 ppm H_2O. The Ce and Nd pieces were cleaned with a file before use until a shiny surface was obtained. Both metals were cut is small pieces by use of a metal cutter. Cadmium was also introduced into a glove box where it was cut with a scissors. Calculated amounts of Ce, Nd and Cd were weighed on a semi-micro balance with an accuracy of at least 0.5 %. The alloys were prepared in Ta crucibles (Fig.1a) (10 mm O.D., 15 mm height) which were designed in the laboratory. The output Ta sheet was stamped in several steps using a hydraulic punch. After further machining Ta crucibles were cleaned with an acid mixture ($HCl/HNO_3/H_2SO_4$), rinsed with distilled water and ethanol and dried in a laboratory dryer. They were closed by welding with a corresponding lid in a water-cooled arc furnace (Fig.1b) (Johanna Otto GmbH, MAM1) under 0.5 bar of Ar. The mass loss during the whole sample preparation procedure was usually below 0.2% and did not significantly affect the sample composition. The total sample weight was usually 1 g.

The Ta-crucibles were sealed separately in quartz glass tubes (Fig.2a) under 10^{-3} mbar and placed into a muffle furnace for various durations ranging from 3 – 12 weeks. First all samples were heated slowly for at least 3 days above the melting point of Cd for reaction of Cd and RE metal (Ce, Nd). For proper homogenization of the elements samples containing ≤ 70 at.% Cd

a temperature of 1050 °C was selected; above the melting point of pure Ce and Nd, all other samples were kept at 700 °C. Afterwards, different heat treatment steps in the temperature between 250 and 850 °C were applied. After equilibration the crucibles were open in a glove box using of metal cutter (Fig.2b) and the sample was taken out for further characterization. It was observed; some of the samples were sticking to Ta-crucibles and were difficult to remove out of crucible.

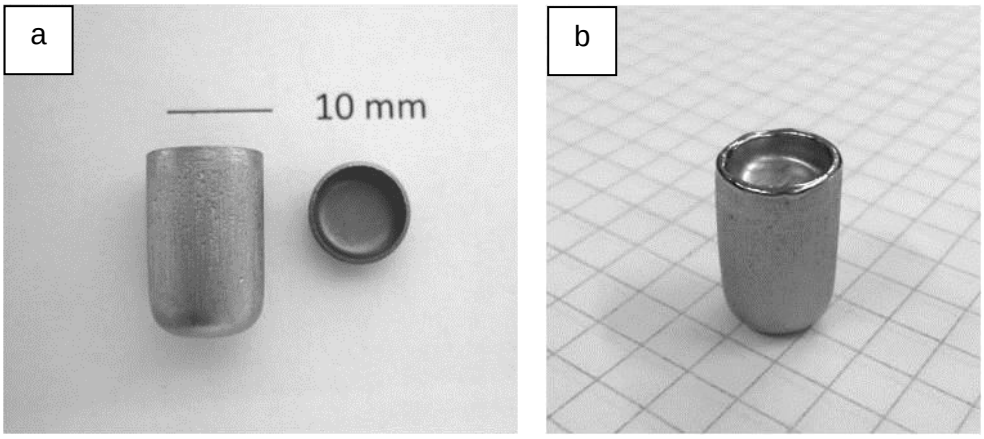

Fig.1. Ta crucible used for sample preparation (a); welded with a corresponding lid (b).

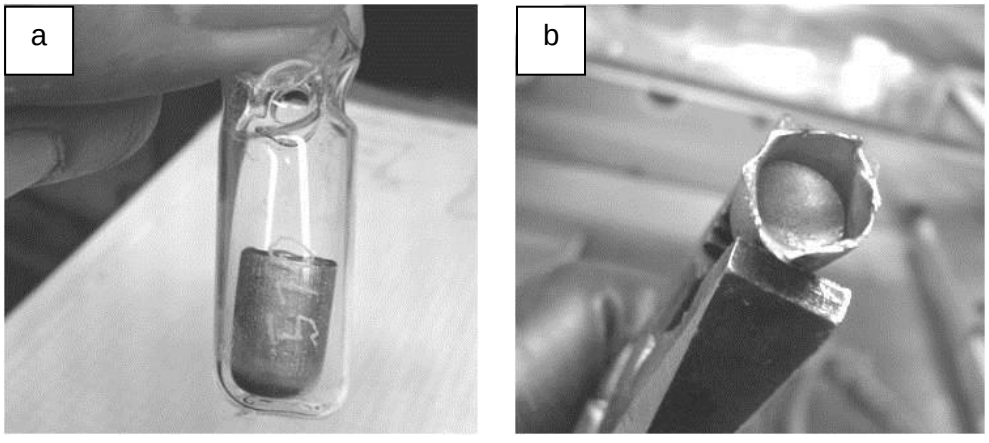

Fig.2. Sealed and evacuated sample in Ta-crucible (a); NdCd sample inside crucible (b).

A sample mass of 100 mg was used for differential thermal analyses. All samples were contained in hermetically closed Ta-crucibles with plane bottom (for better contact with thermocouple of DTA equipment; Fig.3a) which was obtained by using a hydraulic press. As-cast and annealed samples were investigated. In addition, pure Ce and Nd sample were also studied. The pieces of metal were arc melted into a inglot on a water-cooled copper plate under an argon atmosphere of 0.5 bar, using zirconium as a getter material.

Samples containing 1, 2, and 4 at.% Cd were also studied on heating and cooling by dilatometry. The samples (2 g) were prepared in tantalum tubes (Fig.3b) (12 mm O.D., 35 mm long), welded in Ar atmosphere on top and bottom with exactly fitting lids and placed in a muffle furnace at 200 °C. After an equilibration time of 12 weeks, the alloys were cut and precisely machined into the form of cuboids. In order to compare the DTA results with the dilatometric ones, similar experimental conditions like heating and cooling rate as well as an Ar flow were used.

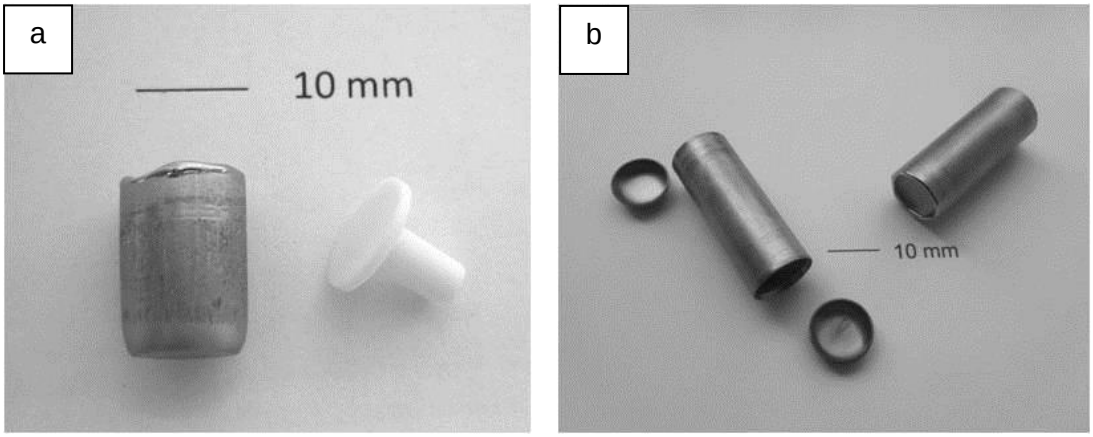

Fig.3. Ta crucible used for DTA investigations (a) and Ta tubes applied for preparation of samples for dilatometric study (b).

During preparation of the samples several technical problems appeared due to high vapor pressure and volatility of cadmium what is presented in Fig.4. Such samples were not analyzed.

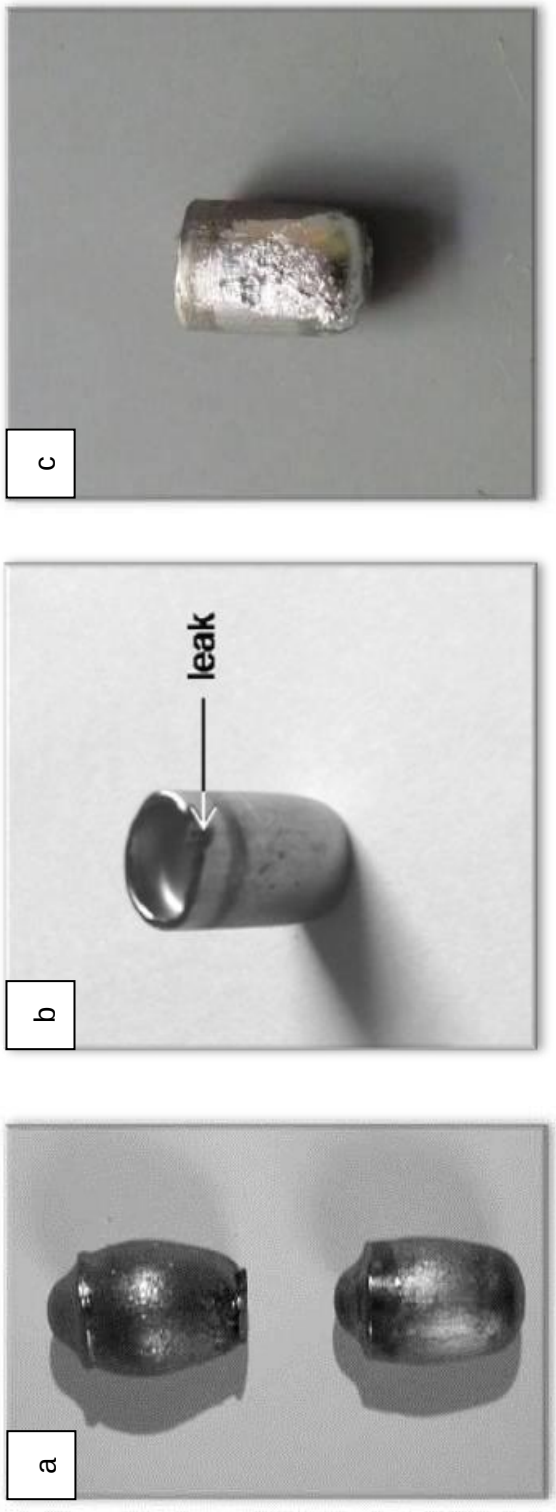

Fig.4. Deformation of Ta crucible after applying to high temperature (a) (author: Dr. Thomas L. Reichmann) and caused by incorrect welding (b) where Cd crept out of the crucible (Cd).

2.1.2 Isopiestic equilibration experiments

The principle and experimental details of the isopiestic method applied in this work were described previously by Ipser et al. [6-7]. A schematic diagram of the particular setup used in the present investigation is shown in Fig.5. The apparatus is essentially made of quartz glass. It consists of an outer tube of 38 mm O.D. with one end closed and the other end fitted with a ground joint which can be connected to a vacuum pump. A quartz glass crucible with 32 mm O.D. is placed at the bottom serving as a reservoir for Cd. On top of the reservoir, a quartz glass spacer of suitable height and a quartz supporting tube (15 mm O.D.) are located where the Ta crucibles (prepared in the similar way as it is written above) containing pure Ce or Nd as samples are inserted. An inner tube of 7 mm O.D. with its upper end widened to 32 mm O.D. is used as a thermocouple well. The apparatus can be sealed under vacuum in its upper part.

Before use the entire apparatus was cleaned with an acid mixture ($HF/HNO_3/H_2O$), rinsed with distilled water and dried. Afterwards the fully assembled setup, including the empty tantalum crucibles (approximately 20), was degassed under vacuum (10^{-3} mbar) at 900°C for 5 h. All preparations for the experiments were then carried out under Ar atmosphere in a glove box. The reservoir was filled with 25 to 35 g of Cd (99.9999 % Alfa AESAR, Karlsruhe, Germany), depending on the experimental reservoir temperature. Between 150 and 200 mg of pure Ce or Nd (both 99.9 % Alfa AESAR, Karlsruhe, Germany and smart-elements, Vienna, Austria) were weighed into each Ta crucible with an accuracy of ±0.1 mg. The assembled apparatus was brought outside the glove box securely closed using a glass stopper. It was connected to the vacuum pump, evacuated and sealed under a dynamic vacuum of better than 10^{-3} mbar.

The isopiestic equilibration experiments were carried out in different temperature gradients, applied by two-zone furnaces, for periods of about 3 to

5 weeks. The temperatures of the samples (T_S) and the reservoir (T_R) were measured periodically by raising a Pt/Pt10%Rh thermocouple inside the thermocouple well. After equilibration, the isopiestic apparatus was quenched in cold water and cut open by a diamond saw. The individual samples (which had become Ce-Cd or Nd-Cd alloys during the equilibration) were weighed again and their compositions were derived from the mass difference which was attributed to the uptake of Cd.

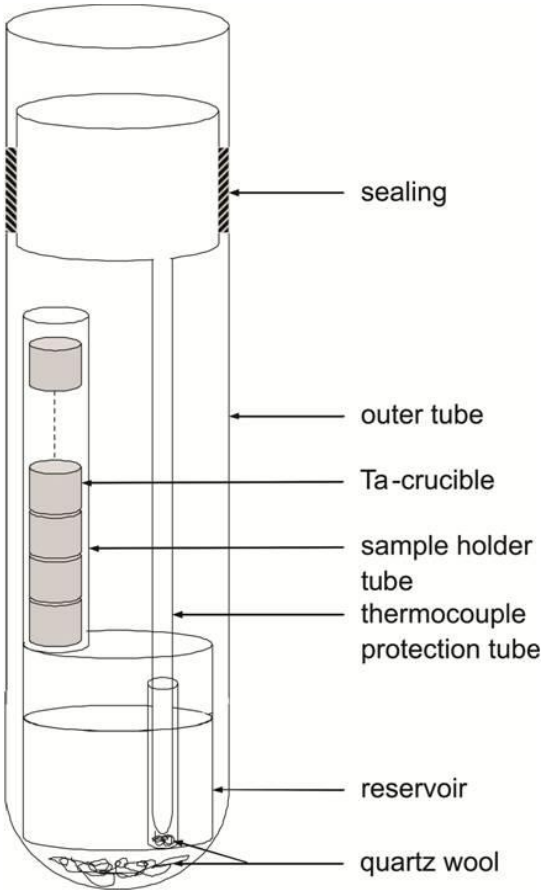

Fig.11. The isopiestic quartz glass apparatus.

For Nd-Cd system a master alloy $Nd_{11}Cd_{45}$ was also prepared. Representative samples were characterized in order to check the calculated compositions.

2.2 Characterization methods

Ce-Cd and Nd-Cd alloys were investigated with different methods like LOM, SEM-EDX, XRD, DTA and dilatometry. In each system series of samples were prepared with varying nominal compositions. As-cast as well as annealed samples were investigated for construction of phase diagrams. All handling of the samples was done with due care to minimize any potential reaction with oxygen and moisture.

For metallographic investigations a representative part of samples were embedded in resin/carbon mixture. It was ground as well as polished and the surface quality was checked in light optical microscope (LOM). Scanning electron microscopy (SEM) with directly coupled EDX detector was used to determine the microstructure and exact phase compositions of specimens. Powdered alloys were used for structure identification with X-ray diffraction (XRD) and single crystal x-ray diffraction was performed to study the crystal structure of the Ce_2Cd_{17} compound. Thermal effects of as-cast and equilibrated alloys were studied by differential thermal analysis (DTA). In addition, the dilatometric study of the Ce/Nd-rich samples was carried out.

2.2.1 Light Optical Microscopy (LOM)

The optical microscope is common investigation equipment in life science as well as material science. It uses visible light and consists of a system of glass lenses which magnifies an image of studied bulky specimen. By use of optical microscope basic information concerning the quality of the sample can be checked like: homogeneity, microstructure, number and dispersion of phases, grain size, porosity etc. LOM gives direct and real colour imaging with no need of sample pre-treatment as well as it is easy to be operated and integrated with digital camera system. On the other hand, the use of light microscope is limited by low resolution due to the light diffraction limit and possibility to see only two dimensional plane of the specimen at a time.

In the current work optical imaging was achieved with a Zeiss Axiotech 100 microscope equipped with a camera and a halogen light source. Several objective magnification (5x, 10x, 20x, 50x and 100x) and four contrasting techniques were applied during observation (bright field (BF), dark field (DF), polarization (PI) and differential interference contrast (DIC)). Representative pieces of alloys were placed into a resin/carbon mixture, heated up to 180 °C and cooled. The surface of the embedded samples were ground and polished in order to remove scratches and cracks. Grounding was performed with silicon carbide abrasive paper using paraffin oil or kerosene as fluid applying different paper mesh size (400, 600, 800, 1000 and 1200). Afterwards the samples were polished with an oil-based diamond suspension and finally cleaned in an ultrasonic bath with n-hexane. With increasing Ce/Nd content the surface oxidation rate increased, hence, the polishing of samples containing more than 50 at.% RE was more laborious and required a rapid transfer into the glove box.

Using the bright field mode, presence of phases can be distinguished due to its different reflectance. In dark field mode (DF) only the light scattered on scratches, cracks and holes or grain boundaries can be observed. Therefore this method is used for verification of the quality of polishing and provides information on grains size. For identification of number and orientation of phases the polarized imaging (PI) mode is used where the embedded sample is rotated. The incident light is polarized and each present phase modifies the plane of polarization according to its own optical properties. Different phases appear in varying colours. Grains of the same phase with different orientations appear also in different colours, but show the same sequence of colours by rotating. In difference interference contrast (DIC) mode, a polarized light source is separated into two polarized orthogonally parts, displaced and recombined before observation. The technique is useful for determining the orientation of phase gradients.

2.2.2 Scanning Electron Microscopy (SEM)

The scanning electron microscope (SEM) is nowadays one of the most useful devices in research. Electron microscope formed greatly magnified images of solid objects by means of electrons [8]. High-energy electrons focused in a beam excite atoms in a sample and provide emission of characteristic spectrum of X-rays. The schema of scanning electron microscope is shown in Fig.6. A beam of electrons is produced at the top of the microscope by an electron gun. The electron beam follows a vertical path through the microscope. The beam passes through electromagnetic fields and lenses, which focus the beam down toward the sample. Once the beam hits the sample, electrons and X-rays are emitted out of the sample. Detectors collect characteristic X-rays, backscattered electrons (BSE), secondary electrons (SE), light (cathode-luminescence), specimen current and transmitted electrons. It is converted into a signal that is sent to an integrated monitor where the final image is produced. Secondary electrons (SE) and backscattered electrons (BSE) are commonly used for imaging samples. SEM provides the information about the sample's surface topography and composition and other properties such as electrical conductivity. Almost all kind of samples, conducting and non-conducting (stain-coating with metals needed), are able to be investigated using SEM. Imaging at all directions (3D) is possible in this method. However it has disadvantages; the samples should be dehydrated and the measurement is carried out in vacuum.

For this study a scanning electron microscope (SEM: Zeiss Supra 55 VP) with directly coupled energy-dispersive X-ray detector (EDX) was applied. The measurements were performed at an acceleration voltage in the range of 15-20 kV. Pure Co acted as a standard to control parameters of the measured beam. Secondary as well as backscattered electrons imaging was used for samples investigation. Using secondary electrons the information on topology of sample can be obtained. Backscattered electrons are most valuable for

illustrating contrasts in composition in multiphase samples. In BSE mode, phases with distinct compositions are distinguishable because of their difference in the average atomic number (Z). Elements or phases containing elements with a high atomic number have a higher backscatter coefficient than light atoms. Therefore a higher atomic number is related to a brighter contrast.

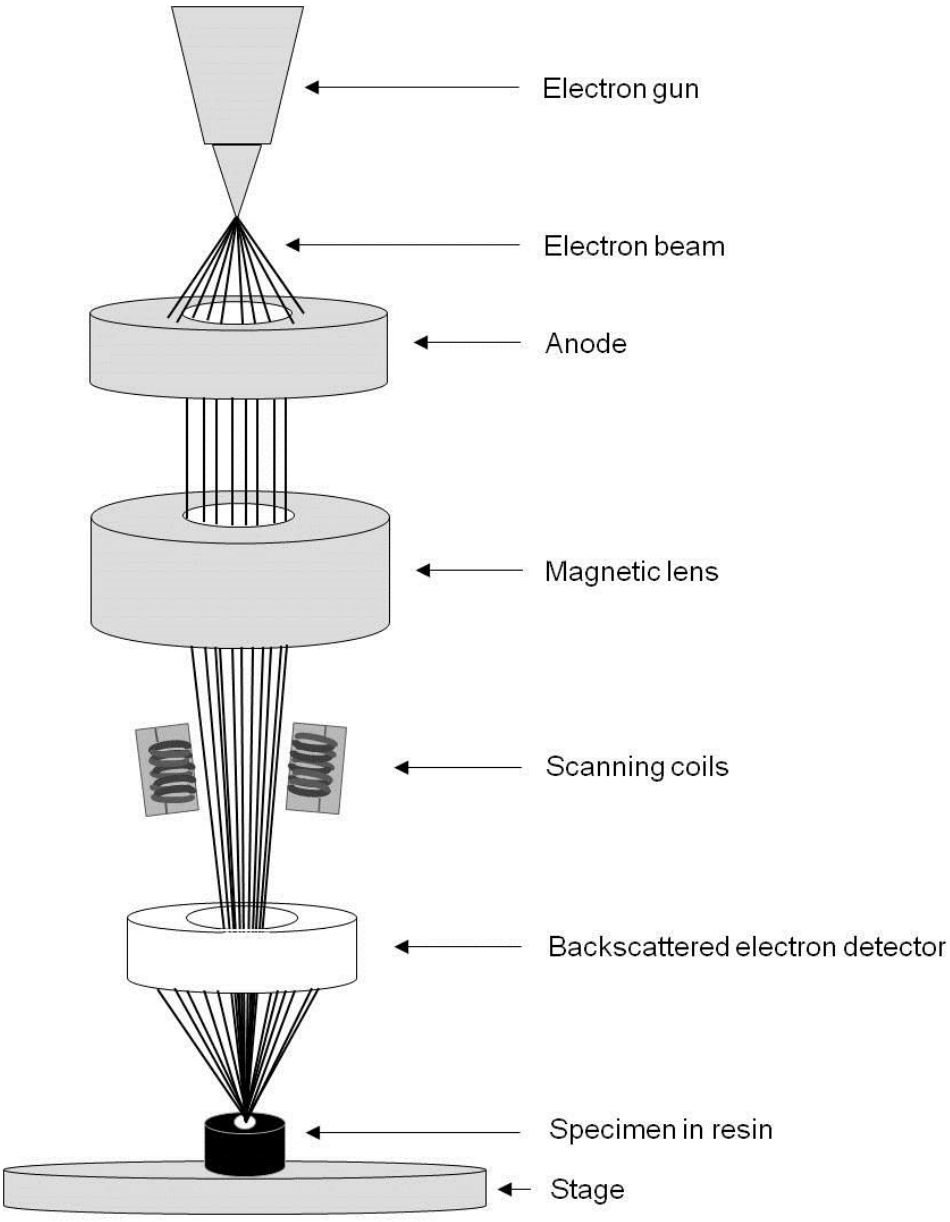

Fig.6. The schema of scanning electron microscope.

2.2.3 X-Ray Diffraction Measurement (XRD)

X-ray diffraction is the most powerful analytical method used for phase identification of crystalline material. Single-crystal samples as well as polycrystalline samples can be considered for this technique. From single-crystal XRD data it is possible to solve and refine the crystalline structure of a new or not entirely known material [9]. X-ray powder diffraction (XRPD) analysis has a wide range of applications. After a fast XRPD measurement, it is simple to distinguish if a solid material is crystalline or amorphous. Full profile analysis like crystal structure determination, structural model refinement, quantitative phase analysis, texture analysis, investigation of domain size, etc. is possible by mean of this method.

The X-rays are generated by a cathode ray tube (usually made of Cu, Fe, Mo, Cr) and directed toward the sample. The diffracted rays are collected, counted and analyzed. The dimension of the unit cell of crystal can be determined using Bragg's law given by following equation:

$$n\lambda = 2d\sin\theta \tag{1}$$

where relation between the wavelength (λ) of radiation and the diffraction angle ($\sin\theta$) as well as lattice spacing (d) is given [10-11]. For this technique a representative piece of a sample must be powdered. It is scanned through a range of 2θ angles – due to the random orientation of the powdered material all possible diffraction directions of the lattice should be attained. Each mineral has a set of unique d-spacing therefore conversion of the diffraction peaks to d-spacing allows identification. The characteristic x-ray diffraction pattern generated in XRD analysis provides a unique signal of each sample. Regarding information that every crystal is built up in layers or planes and the planes correspond to the crystallographic planes (described by the Miller Indices (h k l)) identification of the crystalline form is possible. The standard reference patterns and measurements pattern are therefore compared. Solid

materials which are very ductile or very hard can not be characterized by powder XRD. Peak overlay may also occur as well as fluorescence of contained element can disturb the result.

For single-crystal structure determination, a Nonius four-circle diffractometer equipped with a 300 μm capillary-optics collimator, graphite monochromatized MoKα radiation and a CCD (charge couple device) detector, was used. Unit-cell parameters were obtained by least-square refinements of all 2θ values of the registered reflections. Corrections of Lorentz, polarization and adsorption effects were made using the multi-scan method and complex scattering functions [12]. The final structure refinement was carried out using the software SHELXL-97 [13-14]. Suitable single crystals of investigated phase in form of needle were found under optical microscope in previously powdered sample. To prevent the measured specimen from oxidation during the experiments, it was coated with vaseline and investigated under a dry nitrogen atmosphere.

Phase identification was performed by powder XRD using a Bruker D8 Advance Diffractometer with Bragg-Brentano pseudo-focusing geometry and CuKα radiation. A one-dimentional silicon strip (LynxEye) detector and special sample holders with X-ray transparent lids (for RE-rich samples) as well as normal holders were used for investigation (see Fig.7).

Fig.7. The sample holders used for X-ray powder diffraction (XRD) study.

Pieces of each sample were crushed and powdered in a tungsten carbide mortar inside the glove box and fixed on the sample carrier by the use of Vaseline dissolved in n-hexane. The X-ray powder diffractograms were refined by the Rietveld method [15] using the fundamental parameter approach [16] for peak profile modeling. Analysis and refining of the collected data were done using the TOPAS® 3 software [17] (provided by Bruker). Structural information on phases present in a sample is obtained from literature [18]. The measured diffraction pattern was fitted to the calculated one. Several structural parameters can be refined using TOPAS software like the lattice parameters, crystal size, atomic positions, occupation factors and the atomic displacement factors. Also the peak shape can be described by different mathematical models. In reality peak broadening occurs caused by not perfect crystals or setup of the instrument. Refinement of parameters should be done step by step, where after each step a fitted parameters has to be control in order to get a physically reasonable value. Adjustment and refinement of the parameters mentioned above leads to a final structure with different structural properties compared to the initial structure model.

2.2.4 Differential thermal analysis (DTA)

Differential thermal analysis (DTA) is a method where the thermal behavior of a heated sample can be analyzed. It is a technique where physical and chemical properties of substances can be observed. A reference (a thermally inert material) is applied to compare the thermal effects recorded for a sample occurring during heating and cooling. The study of solid state reactions, thermal decompositions and phase transitions that involve absorption or emission of heat can be performed on DTA equipment [19]. This information is used with combination with additional methods for phase diagram determination. All thermal reactions are connected with the exchange of heat. The principle of DTA is the measurement of difference of the temperature ΔT between the sample (T_S) and a reference (T_R) as a function of temperature. The basic DTA equipment contains a sample holder with two ends (one for a sample and another one for a reference), two crucibles, a furnace, a cooling system, a temperature controller and a recording device (PC). The chamber is flushed continuously with an inert gas to avoid oxidation. The crucible material (alumina, graphite, Ta) is chosen due to the investigated temperature range and the reactivity with the sample. In case of open crucibles, Ti or Mo are placed additionally inside device as getter material. The samples as well as the reference holders are equipped with thermocouples; each measuring the temperature at its end. Depending on the nature of effect the temperature of the sample increases in case of an endothermic reaction (e.g. melting), or decreases in case of an exothermic reaction (e.g. crystallization). Two heating and cooling cycles are usually performed for each sample in order to be sure to get reproducible results.

The example of a DTA-curve interpretation with significant points is shown in Fig.8.The determination of values of reaction temperatures is done by the analysis of the onset, the peak maximum or the step (end of the reaction) for non-invariant reactions and by the extrapolated onset for invariant

reactions. The phenomenon of supercooling during the solidification process can be observed for some samples; i.e. the crystallization temperature is lower than the melting temperature. This effect can be affected by e.g. the sample volume, crystal structure of the solid or cooling rate.

In this work differential thermal analyses were performed on a Netzsch DTA 404 S and DSC 404 F1 Pegasus (Netzsch, Selb, Germany), both equipped with Pt/Pt10%Rh thermocouples. The instruments were calibrated at the melting points of high purity metals: Ag, Cu, Ni and Zn. The mass of the standard metals was usually in the range from 80 and 100 mg. The samples were closed in Ta crucibles with flat bottoms as it is illustrated in chapter 2.1.1. Therefore no getter material was use additionally in DTA chamber. A sample mass of 100 mg was used for the experiments and high-purity γ-Al_2O_3 was employed as reference material. All samples, except pure Cd, were subjected for two heating and cooling cycles using a heating/cooling rate of 2 K min^{-1} (as-cast samples) and 5 K min^{-1} (annealed samples). A constant Ar flow of 50 ml min^{-1} was applied in the DTA furnace chamber. The accuracy of the temperatures determined from the DTA curves is estimated to be than ±2 °C. The evaluation of the resulting data was performed by Proteus® Software for Thermal Analysis (supplied by Netzsch).

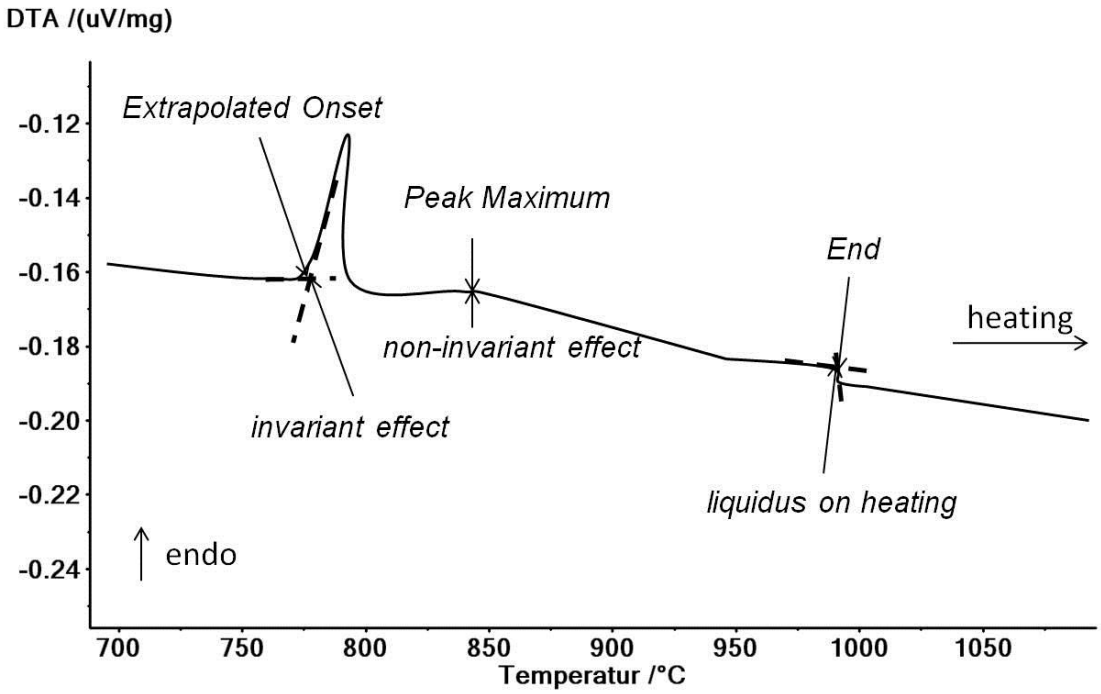

Fig.8. Experimental DTA curve with significant points.

2.2.5 Dilatometry

Dilatometry is a thermoanalytical technique used to measure the expansion or shrinkage of solid specimen under negligible load at a programmed temperature change. The principle of this method is based on the material's coefficient of expansion (α), what express the degree of expansion divided by the change in temperature and is given by following equation:

$$\alpha = \frac{1}{L_0}\frac{(\Delta l)}{(\Delta T)} \tag{3}$$

where:

L_0 : initial sample length

Δl : change in length

ΔT : change in temperature

To perform a dilatometric analysis, a sample is inserted into a special holder within a movable furnace. A pushrod made from alumina is positioned directly against the sample and transmits the length change to a linear variable displacement transducer (LVDT) which is moved [20]. An output signal proportional to the displacement is recorded and the temperature program is controlled by thermocouple placed next to the sample. For dilatometric measurements a plan-parallel sample should be prepared for ideal fitting between its holder and a pushrod.

In this study a horizontal dilatometer Netzsch DIL 402 E (Netzsch, Selb, Germany) with inner tube diameter of 35 mm was used. This model allows easy access for uncomplicated insertion or change of a sample that is precisely machined into the form of cuboids. The sample holder was made out of alumina. For each sample two heating and cooling cycles using a heating/cooling rate of 5 K min^{-1} were conducted. A constant Ar flow of 50 ml min^{-1} was applied in the dilatometer chamber.

References

[1] F.H. Spedding, A.H. Daane, Preparation and properties of rare earth metals, in: Progress in Nuclear Energy, I (5) Metallurgy and Fuels, 1956.

[2] D.H. Dennison, M.J. Tschetter, K.A. Gschneidner Jr., The solubility of Ta in 8 liquid RE metals, J. Less-Comm. Met. 10 (1965) 108-115.

[3] D.H. Dennison, M.J. Tschetter, K.A. Gschneidner Jr., The solubility of Ta and W in liquid RE metals, J. Less-Comm. Met. 11 (1966) 423-435.

[4] S.P. Garg, M. Venkatraman, N. Krishnamurthy, S.J. Vijaykar, The RE-Ta system, J. Phase Equilibria, 19 (4) (1998) 385-394.

[5] Y. Janssen, M. Angst, P.C. Canfield, R.W. McCallum, Small sealed Ta crucibles for thermal analysis of volatile metallic samples, Rev. Sci. Instrum. 77 (2006) 056104_1-056104_3.

[6] H. Ipser, R. Krachler, K. L. Komarek. The isopiestic method and its application to a thermodynamic study to Au-Zn system. In: Brodowsky H, Schaller H-J, editors. Thermochemistry of Alloys, Dordrecht : Kulwer Academic Publisher; 1989,p. 293-306.

[7] H. Ipser. Vapor pressure method: A source of experimental thermodynamic data. Ber Bunsenges Phys Chem 102 (1998) 1217-1223.

[8] J. Goldstein. Scanning electron microscopy and x-ray microanalysis. 3rd ed., Springer, US (2003).

[9] M. Font-Bardia, X. Alcobé. X-ray single crystal and powder diffraction: possibilities and applications. In: Handbook of instrumental techniques for materials, chemical and biosciences research. J. R. Seoane, X. Llovet Ximenes, editors. Centres Científics i Tecnològics, Universitat de Barcelona (2012).

[10] W.L. Bragg, W.H. Bragg. X-rays and crystal structure. G. Bell and Sons, London (1924).

[11] B.D. Cullity, S.R. Stock. Elements of X-Ray Diffraction. Prentice-Hall (2001).

[12] A.J.C. Wilson, editor. International tables for Crystallography, Dordrecht: Kluver Academic Publishers, The Netherlands (1992).

[13] G.M. Sheldrick. SHELXS-97. University of Göttingen, Germany (1997).

[14] G.M. Sheldrick. A short history of SHELX. Acta Crystallographica 64 (2008) 112-122.

[15] L.B. McCusker, R.B. Von Dreele, D.E. Cox, D. Louer, P. Scardi. Rietveld refinement guidelines. Journal of Applied Crystallography 32 (1999) 36-50.

[16] R.W. Cheary, A. Coelho. A Fundamental Parameters Approach to X-Ray Line-Profile Fitting. Journal of Applied Crystallography 25 (1992) 109-121.

[17] A.X.S. BRUKER. TOPAS V3: General profile and structure analyis software

for powder diffraction data, in: Users´s Manual, Bruker AXS, Karlsruhe, Germany (2005).

[18] P. Villars, L.D. Calvert. Pearson´s Handbook of Crystallographic Data for Intermetallic Phases, 2nd ed., ASM International (1991).

[19] B. Wunderlich. Thermal Analysis. Academic Press, Inc. (1990).

[20] Netzsch Product Brochures. Analyzing & Testing: Dilatometry - Method, Instruments, Applications – From -180°C to 2800°C. NETZSCH-Gerätebau GmbH, Selb, Germany; www.netzsch.com/n33623

3. Results and discussion

3.1. Re-investigation of the Cd-Ce phase diagram and structural characterization of the high-temperature phase $Cd_{17+2x}Ce_{2-x}$ (x ~ 0.02)

Barbara Skołyszewska-Kühberger[a], Thomas L. Reichmann[a,c,], Martin Marker[a], Herta S. Effenberger[b], Herbert Ipser[a]*

[a] Department of Inorganic Chemistry (Materials Chemistry),
University of Vienna, Währinger Straße 42, A-1090 Wien Austria
[b] Department of Mineralogy and Crystallography,
University of Vienna, Althanstraße 14, A-1090 Wien Austria
[c] Institute for Applied Materials, Karlsruhe Institute of Technology, D-76344 Eggenstein-Leopoldshafen, Germany

*Corresponding author:
E-mail address: Thomas.Reichmann@kit.edu

Submitted: *Journal of Phase Equilibria and Diffusion,* JPED-15-09-1719

Contributions to this paper:
B.S-K.: sample preparation, analysis and interpretation, wrote the paper
T.L.R: advice in interpretation, structure determination, wrote the paper
M.M.: help in sample preparation
H.S.E.: single crystal XRD measurements, advice in structure determination
H.I.: proofreading, general advice and helpful comments

Contribution of B. Skołyszewska-Kühberger to this article: 75 %

Abstract

The complete Cd-Ce equilibrium phase diagram was investigated with a combination of powder-XRD, SEM and DTA. The presence of seven intermetallic compounds, i.e. CdCe, Cd_2Ce, Cd_3Ce, $Cd_{58}Ce_{13}$, Cd_6Ce, $Cd_{17}Ce_2$ and $Cd_{11}Ce$, reported previously in literature, was confirmed. A polymorphic transformation of Cd_2Ce into a high-temperature modification was indicated to occur at 871 °C at the respective stoichiometric composition. The homogeneity range of both the low (γ) and high-temperature (δ) allotropic modification of Ce could be determined precisely and a limited solubility of 2.5 as well as 17 at.% Cd was derived. In addition, liquidus temperatures and all invariant reactions were examined by thermal analyses. One eutectoid reaction at 421 °C and ~15 at.% Cd as well as four eutectic reactions at ~20 at.% Cd (646 °C), 56 at.% Cd (910 °C), 77.5 at.% Cd (857 °C) and close to 100 at.% Cd (320 °C) were detected. One peritectoid reaction at 852 °C and three peritectic reactions at 730, 610 and 605 °C were recorded. Moreover, single-crystal X-ray diffraction was employed, and a complete description of the structure of $Cd_{17+2x}Ce_{2-x}$ (x ~ 0.02) is given with focus on the correct defect mechanism. It turned out that vacancy formation on one of the Ce sites (Ce1) is compensated by 2 Cd atoms on Cd sites (Cd5) very close by.

Introduction

For an efficient utilization of high burn-up nuclear fuels several reprocessing techniques have been developed. Traditional aqueous methods seem not to be effective enough for an adequate recovery of high-level radioactive waste (HLW). Currently several innovative techniques appear to be more reasonable for application. Among these, a well-proven pyrochemical reprocessing technique is described by Olander [1], which avoids the major disadvantages of conventional aqueous methods. Its central part is an electro-refining cell filled with a molten LiCl-KCl electrolyte where chopped spent fuels are placed into the anode basket. The elements U, Pu, and the so-called minor actinides (MA) are transported to two different cathodes. The rare earth (RE) elements dissolve in the electrolyte and are extracted by a low melting metal such as Bi [2], Cd [2], or Al [3] located at the bottom of the electro-refiner. Of these three metals, Cd seems to be the most promising extracting agent [4] due to its rather high vapor pressure (which means it can be easily distilled off) as well as the existence of rather stable RE-Cd intermetallic phases. For an optimization of the pyrochemical reprocessing of HLW, a detailed knowledge on the existence and stability of the compounds of RE and actinides with Cd is essential. A first overview of the solubility and thermodynamic activity of some RE and actinide elements in liquid Cd was given by Kurata et al. [4]. Thermodynamic assessments for a number of systems of Cd with actinide and RE elements were presented by Kurata and Sakamura [5].

Continuing the study of the interaction of RE elements (La, Ce, Pr, Nd and Gd) with Cd [6-13], a detailed re-investigation of phase equilibria in the system Cd-Ce together with a conclusive determination of the crystal structure of $Cd_{17}Ce_2$ was done in the present study. The corresponding thermodynamic properties of this binary system were already reported earlier by Skołyszewska-Kühberger et al. [7].

First information concerning the Cd-Ce binary system was given by Iandelli and Ferro [14]. They described the crystal structures of at least six Cd-Ce compounds, namely CdCe, Cd_2Ce, Cd_3Ce, Cd_9Ce_2, Cd_6Ce and $Cd_{11}Ce$. In a later review, Gschneidner [15] listed detailed information of Cd-Ce intermetallic phases based on the studies of [14]. Subsequently, Johnson et al. [16] studied the Cd-rich part in more detail. The latter authors used differential thermal analysis (DTA) to determine liquidus temperatures up to 7 at.% Cd as well as defined the peritectic decomposition behavior of $Cd_{11}Ce$.

Afterwards, Canepa et al. [17] carried out a systematic study of Cd-Ce alloys in the whole temperature and composition range. A complete version of the Cd-Ce phase diagram was given comprising all invariant reaction temperatures and a complete reaction scheme. These authors identified a new equilibrium compound with the stoichiometric composition $Cd_{17}Ce_2$ which was indicated to be isotypic with $Ni_{17}Th_2$. Structural analysis was performed both by powder- and single-crystal X-ray diffraction (XRD). The corresponding lattice parameters were calculated by least squares refinement of the angular values of 25 reflections, given as a = 10.012 (1) Å, c = 9.815 (1) Å. Surprisingly, no further crystallographic information was given.

More recently, a detailed study of the crystal structure of $Cd_{17}Ce_2$ was done by Franceschi [18]. The author characterized the phase as $Cd_{17.10}Ce_{1.95}$. Obviously, the atomic arrangement represents a defect $Ni_{17}Th_2$ type with small deviation from stoichiometry. In fact, Franceschi determined minor amounts of vacancies on one of two Ce positions and an additional position occupied by minor amounts of Cd atoms.

According to the given phase diagram by Canepa et al. [17], $Cd_{17}Ce_2$ is only stable in a limited temperature range at elevated temperatures. An analogous phase had also been found in the Cd-La system, where it is stable down to ambient temperature. Moreover, Canepa et al. confirmed all six intermetallic compounds which had previously been found in Ref. [14]. Actually, the stoichiometry of Cd_9Ce_2 was corrected to $Cd_{58}Ce_{13}$.

All intermetallic compounds between Cd and Ce were described to be line-compounds, hence no solid solubility of either Cd or Ce is present. The

compounds richest in Ce are CdCe (CsCl-*B2*-type) and Cd_2Ce. The latter was described in detail by Iandelli and Palenzona [19], together with a large series of REX_2 phases (X = element from group 11 to 13). It crystallizes with the deformed AlB_2 structure, commonly designated as Cd_2Ce prototype [14, 17, 19], with disordered and ordered arrangements of Cd atoms [19]. Moreover, powder-XRD confirmed that the 3:1 compound (Cd_3Ce) has cubic symmetry with the lattice constant *a* in the range from 7.222 to 7.228 Å [15, 17, 19]. Bruzzone et al. [20] performed metallographic and X-ray investigations on the $Cd_{9\sim}Ce_2$ phase and suggested an actual stoichiometry $Cd_{58}Ce_{13}$. Based on the results of isopiestic experiments by the present authors [7], the order composition would be expected at even higher Cd contents, i.e. at about 82.3 at.%. This is in good agreement with the observations by Piao et al. [21] who discussed for the compound $Cd_{58.68}Ce_{12.60}$ a metrically commensurate representative that obviously represents a lock-in phase.

Iandelli and Ferro [14] reported the existence of the 6:1 intermetallic compound, however, without any structural details. The powder-XRD photographs taken by Johnson et al. [22] were indexed based on a cubic unit cell referring to a Cd_6Y prototype. The most Cd-rich phase is cubic $Cd_{11}Ce$ [12]. All Cd-Ce compounds are isotypic or even isomorphous to those found in other Cd-RE systems and are listed in Table 1. In their recent thermodynamic study, Skołyszewska-Kühberger et al. [7] suggested refined phase boundaries for the phases CdCe, Cd_2Ce, $Cd_{58}Ce_{13}$ and Cd_6Ce at 550 °C derived from isopiestic vapor pressure measurements.

Whereas the work of Canepa et al. [17] was not considered in the monograph by Massalski et al. [23] (where still only a partial phase diagram is shown) Okamoto [24] presented an assessment of the full Cd-Ce phase diagram based on all previous data. Systematic trends in the phase diagrams of the Cd-RE systems were discussed in a compilation by Gschneidner and Calderwood [25]. The present study attempts to clarify a number of open questions, for example, accurate temperatures of invariant reactions, homogeneity ranges of the individual phases, stability of the $Cd_{17}Ce_2$ compound, and others.

Experimental

The samples were prepared from Cd shot (United Mineral & Chemical Corporation, U.S.A, and Alfa Aesar, Karlsruhe, Germany; both 99.9999 %), Ce rod (99.9 %, Alfa Aesar, Karlsruhe, Germany) and pieces (99.9 %, smart-elements, Vienna, Austria). The oxide layer was scraped off from the Ce pieces before use. Calculated amounts of the elements were weighed on a semi-micro balance with an accuracy of at least ±0.5 mg. To prevent Ce from oxidation, the whole sample preparation was done in a glove box (MBraun Labmaster 130) under Ar atmosphere (both O_2 and H_2O level: <1 ppm). Ta crucibles (10 mm O.D., 15 mm height) were used for alloying Cd and Ce. An arc-melting furnace (MAM1, Johanna Otto GmbH, Germany) was applied to close the crucibles with a corresponding lid by welding. The total sample weight was usually 1 g and the mass loss during the whole sample preparation procedure was usually below 0.2 mg. The closed Ta crucibles were placed into quartz glass tubes which were evacuated and sealed under a dynamic vacuum of better than 10^{-3} mbar. Due to the high vapor pressure of Cd, different heating procedures were applied. Samples containing less than 70 at.% Cd were pre-heated at 1050 °C; for Cd-rich samples a temperature of 700 °C was used. The samples were slowly (0.5-0.7 K/min) heated up to the selected temperature and kept there for at least 3 days. It turned out that such moderate heat treatment was necessary to prevent rapid increase of the inner pressure of the crucibles, due to the rather low boiling point as well as the relatively high vapor pressure of Cd. After pre-heating, samples were annealed at various temperatures between 300 and 600 °C. Long-term heat treatment usually lasted for about 3 to 12 weeks, and subsequent quenching in cold water was employed to freeze thermodynamic equilibrium at the respective annealing temperatures.

Phase identification was performed by powder-XRD using a Bruker D8 Advance Diffractometer with Bragg-Brentano focusing geometry and CuKα radiation. A LynxEye silicon strip detector and special sample holders with

X-ray transparent lids were used. Pieces of each sample were crushed and powdered in a tungsten carbide mortar inside the glove box and the powders were fixed on the sample carrier by the use of Vaseline dissolved in cyclohexane. Analysis and Rietveld refinement of the collected data was done using the TOPAS 3 software (provided by Bruker). For single-crystal XRD, a Nonius Kappa four-circle diffractometer, equipped with a 300 µm capillary-optics collimator, graphite monochromatized MoKα radiation and a CCD detector, was used. Unit-cell parameters were obtained by least-squares refinements of all 2θ values of registered reflections. Corrections of Lorentz, polarization and absorption effects were performed. The structure solution and refinement was done with the software SHELX-97 [26, 27].

Metallographic and microstructural characterization started by embedding parts of the samples in a hot mounting resin followed by a grinding and polishing (oil-based diamond suspension) procedure. Finally, the specimens were cleaned in an ultrasonic bath and transferred into the glove box. The quality of the polished samples was checked in an optical microscope (Zeiss Axiotech 100). Further examinations were carried out on a Zeiss Supra 55 VP environmental scanning electron microscope (SEM) with a directly coupled energy-dispersive X-ray detector (EDS). The measurements were performed with an acceleration voltage in the range of 15-20 kV. Pure Co was used as a standard material for energy calibration.

Differential thermal analyses were performed on a DTA 404 S and a DSC 404 F1 Pegasus (Netzsch, Selb, Germany), both equipped with Pt/Pt10%Rh thermocouples. The instruments were calibrated at the melting points of high purity metals: Ag, Cu, Sn and Zn. The samples were enclosed in Ta crucibles with flat bottoms. A sample mass of about 100 mg was usually used for the experiments and empty Ta crucibles employed as reference material. All samples were subjected to two heating and cooling cycles using a heating/cooling rate of 2 K min^{-1} (as-cast samples) and 5 K min^{-1} (annealed samples). A constant Ar flow of 50 ml·min^{-1} was applied in the DTA furnace chamber. The accuracy of the temperatures determined from the DTA curves is estimated to be better than ±2 °C.

Results and discussion

Both equilibrated as well as as-cast samples were considered to specify homogeneity ranges of the intermetallic compounds and their crystallization behavior. A total number of 34 samples were examined with isothermal methods. A compilation of representative samples are listed in Table 2 together with the corresponding annealing temperatures and the results of powder-XRD and SEM; details are discussed in chapter *Isothermal methods for phase diagram investigation*. In addition, the crystal structure of the high-temperature intermetallic compound $Cd_{17}Ce_2$ was characterized by means of single-crystal XRD. The respective crystal structure is extensively described in chapter *The atomic arrangement in the $Cd_{17+2x}Ce_{2-x}$ (x~0.02).* The phase boundaries of all Cd-Ce compounds as well as solid solutions were determined and are listed in Table 3. Results of thermal analyses are discussed in *Dynamic methods for phase diagram investigation* and the thermal effects recorded for all relevant samples are listed in Table 4 and 5, respectively. The complete Cd-Ce binary phase diagram, established from the combination of all results from isothermal and thermal analysis, is shown in Fig.1.

Isothermal methods for phase diagram investigation

All seven intermetallic compounds reported previously in literature (Tab. 1) were confirmed by powder-XRD as well as by SEM: CdCe, Cd_2Ce, Cd_3Ce, $Cd_{58}Ce_{13}$, Cd_6Ce, $Cd_{17}Ce_2$ and $Cd_{11}Ce$. The presence of an extended solid solubility of Cd in the low- and high-temperature modification of Ce, i.e. γ-Ce and δ-Ce, was also confirmed. Experimental phase compositions and lattice parameters of equilibrium phases in selected Cd-Ce samples are given in Table 2. All lattice parameters measured by powder-XRD agree well with the

literature data. Unfortunately, some of the samples could not be examined by powder-XRD, due to their ductility and corresponding problems during powder preparation. This is in line with the results of Canepa et al. [17] who performed microhardness tests. They found relatively small hardness values in the Ce-rich part of the system, i.e. for the $Cd_{15}Ce_{85}$ eutectoid sample and the compound CdCe, which explains the powdering problems encountered here for samples up to 50 at.% Cd.

The existence of a solid solution of Cd in γ-Ce could be clearly identified in a single-phase sample (No. 27, Table 2) and also in two-phase samples with CdCe and δ-Ce (Nos. 25 and 26, Table 2). Attempts to synthesize a pure single-phase alloy of δ-Ce were not successful. However, this phase was detected in several two-phase samples. The microstructure of the sample Cd_4Ce_{96}, annealed at 500 °C for 8 weeks (Fig. 2a), shows the co-existence of the two solid solutions γ-Ce and δ-Ce (Table 2). Due to very limited amount of δ-Ce in this sample and the fact that the alloy was cooled down from its melt to the respective annealing temperature, the remaining δ-Ce matrix was very fine structured (Fig. 2a). Hence, a reliable determination of the phase composition of the matrix phase was not possible (Table 2). The extrapolation of the phase boundaries from DTA and EDS data indicated that γ-Ce dissolves up to 2.5 at.% Cd at 421 °C and δ-Ce even up to 17 at.% Cd at 646 °C; compare Fig. 1.

The compound richest in Ce crystallizes with the CsCl structure type and has the ideal stoichiometry CdCe. According to EDS investigations, CdCe shows the widest homogeneity range of all the equilibrium compounds in this system (47.9-50.3 at.% Cd at 600 °C) which compares quite well with the values found previously by Skołyszewska-Kühberger et al. [7] (48.0-50.9 at 550°C), see Table 3. According to the present phase diagram (Fig. 1), CdCe is in equilibrium with Cd_2Ce. From the results of Ref. [7], a homogeneity range of 65.5-66.4 at.% Cd was estimated for Cd_2Ce at a temperature of 550°C which is in reasonable agreement with the present results.

From the XRD powder patterns, the crystal structure of Cd_3Ce was confirmed as reported in the literature ($AlFe_3$-type) [17, 20, 28]. Powder-XRD

data collected for $Cd_{58}Ce_{13}$ were also comparable with previous studies [17, 20]. The next intermediate phase is Cd_6Ce; its phase boundary was investigated, and the homogeneity range appears to be shifted slightly to the Cd-rich side (see Table 3), as it was already mentioned earlier in Ref. [7].

It was possible to obtain a homogenous single-phase sample of the high-temperature phase $Cd_{17}Ce_2$ (No. 4, Table 2). It was prepared by quickly lowering the temperature from the melt to 550 °C. After annealing for 4 weeks, a single-phase sample could be obtained. This procedure was taken from Canepa et al. [17]. All efforts to prepare two-phase samples like Cd_6Ce+$Cd_{17}Ce_2$ or $Cd_{17}Ce_2$+$Cd_{11}Ce$ were unsuccessful. It was even remarked in [17] that annealing of $Cd_{17}Ce_2$ at 500 °C for only one hour caused its decomposition into Cd_6Ce and $Cd_{11}Ce$ through a eutectoid reaction. The microstructure of the sample $Cd_{90}Ce_{10}$, annealed at 500 °C for 6 weeks, is shown in Fig. 2b. EDS analysis identified Cd_6Ce and $Cd_{11}Ce$ in agreement with the results of Canepa et al.

Single-crystal XRD results and structure determination of $Cd_{17}Ce_2$ are described in 3.2. An initial powder-XRD pattern of this sample was indexed based on structural data of Th_2Ni_{17} (a = 10.0213(1) Å, c = 9.8119(1) Å, Tab. 2) and the values agree with those given in Ref. [17]. The respective pattern is presented in Fig. 3 together with the calculated pattern of $Cd_{17}Ce_2$ and the difference curve. All reflections were explained and a low R_{wp} (R-weighted profile) value of 1.87 was determined. Considering the uncertainty of sample weighing and the EDS error, one can explain the difference between the nominal sample composition (89.0 at.%) and the stoichiometric composition of the $Cd_{17}Ce_2$ compound at 89.5 at.% Cd. EDS results were in the range from 89.2 to 89.9 at.%, thus confirming the correct stoichiometry $Cd_{17}Ce_2$.

For $Cd_{11}Ce$, no significant change of homogeneity and lattice parameters could be detected, therefore it is treated as a line-compound with its stoichiometric composition 91.7 at.% Cd. The microstructure of sample $Cd_{92}Ce_8$, annealed at 300 °C for 10 weeks, can be seen in Fig. 4. It shows grains of $Cd_{11}Ce$ with a size of 5-25 μm and precipitated Cd located at the

grain boundaries. The corresponding powder-XRD results are listed in Table 2.

The homogeneity ranges for all Cd-Ce phases, determined by SEM (see Table 2) and obtained in Ref. [7] are listed in Table 3. As can be seen, both results agree quite well with each other.

The atomic arrangement in $Cd_{17+2x}Ce_{2-x}$ (x ~ 0.02)

During the present work we were interested to verify the variability in the composition of $Cd_{17}Ce_2$, which in fact is characterized by minor amounts of vacancies at one of two Ce positions but an additional position occupied again by minor amounts of Cd atoms. A detailed study of the crystal structure of $Cd_{17}Ce_2$ was already done by Franceschi [18] who characterized the phase as $Cd_{17.10}Ce_{1.95}$. Franceschi's crystals were annealed at 550°C and quenched to room temperature from a melt consisting of 89.7 at.% Cd, *i.e.*, an excess of Cd as compared to the Cd:Ce = 17:2 ratio. The present sample (No. 4, Table 2) was prepared by quickly cooling an alloy with the nominal composition $Cd_{89}Ce_{11}$ from the liquid state. EDS investigations of the respective phase-pure alloy (Fig.3) showed $Cd_{89.5}Ce_{10.5}$ as the average composition. Hence the present crystals show less excess of Cd compared to those of Franceschi.

The crystal structure was refined starting from the atomic coordinates of the ideal $Ni_{17}Th_2$ structure type [29]. After a few cycles of least-squares refinements it became evident that, in accordance with Franceschi [18], one of the sites (atom Ce1) exhibits a lower scattering power but the difference Fourier summation showed clearly a significant electron density at (0, 0, 0.400). Consideration of these changes improved the reliability indices and reduced the residual electron density. From the atomic radii and bond distances, the allocation of Cd atoms on this additional site is absolutely certain. The structural formula of the investigated sample is $Cd_{17.04}Ce_{1.98}$. Details of data collection, structure refinements, atomic coordinates and interatomic bond distances are given in Tables 6, 7 and 8, respectively.

The parent structure $Ni_{17}Th_2$ [29] is characterized by six crystallographic distinct sites. Two of them fit for atoms with relatively large radii like REE. Four sites are characteristically occupied by atoms with much smaller atomic radii as Mg, Al, Si or first row transition elements like Cr, Mn, Fe, Co, Ni, or Zn. The ratio of metal atoms at these sites is 2:17. The structure type is frequently verified in binary compounds. In ternary compounds, the distinct sites allow ordering of different kind of atoms, but mixed occupations occur often. Many of the compounds are of interest with respect to their physical properties; their magnetic behaviour was studied extensively. Occupation of interstitial sites is generally rare although the inclusion of hydrogen was observed in various $RE_2Fe_{17}H_x$ compounds [30].

The structure type $Ni_{17}Th_2$ is characterized by a three-dimensional network of the coordination polyhedra $Ce2Cd_{20}$. The coordination polyhedron with $\bar{6}m2$ symmetry consists of a slightly distorted hexagonal prism formed by Cd2 and Cd4 atoms; all prism faces are capped by a Cd3 atom whereas the top and bottom faces are capped by a Cd1 atom. The polyhedra are corner connected *via* the Cd2 atoms (Fig. 5a). The network forms channels in [00*z*] which host the Ce1 atoms. These are coordinated by 18 Cd atoms, again forming slightly distorted hexagonal prisms (Cd4 atoms) with $\bar{6}m2$ symmetry, but only the faces of the prisms are capped by a Cd atom (Cd3). The $Ce1Cd_{18}$ polyhedra share their top and basal trigon faces, respectively, forming $CeCd_{15}$ rows along [001]. The Cd3 and Cd4 atoms link the $Ce2Cd_{20}$ and $Ce1Cd_{18}$ polyhedra.

In the $CaCu_5$ structure type [31], $CaCu_{18}$ coordination polyhedra are a comparable structure motive. The changed space-group symmetry 6/*mmm* cause ideal hexagonal prisms with capped prism faces. The connection *via* two opposite hexagon faces result in $CaCu_{12}$ rows running in [001]. However, these rows are connected already among each other sharing faces formed by four ligands.

The Ce1 site exhibits vacancies whereas an additional site is occupied by minor amounts of Cd atoms (Cd5) resulting in the chemical formula $Cd_{17.04}Ce_{1.98}$. Similarly, Franceschi [18] found a chemical formula of

$Cd_{17.09}Ce_{1.96}$ from structure refinements. Both structure refinements agree with the substitution mechanism $Cd_{17+2x}Ce_{2-x}$. The coupled exchange is evident from the crystal structure (*cf*. Fig. 5b). A simultaneous full occupation of the Ce1 and Cd5 sites is impossible due to distances that are too short. In analogy, also neighbouring Cd5 sites cannot be simultaneously occupied. However, a vacancy at the Ce1 site allows the occupation of both neighbouring Cd5 positions. This mechanism allows a substitution of a maximum of 50 % of the Ce1 positions by two Cd5 atoms ($x \leq 0.25$); it changes the coordination polyhedron from $Ce1Cd_{18}$ to $Ce1Cd_{19}$ or even $Ce1Cd_{20}$; the latter corresponds to the $Ce2Cd_{20}$ polyhedron.

An analogous substitution for the $Ni_{17}Th_2$ structure type was found for $Ag_{7.4}Al_{9.78}Ce_{1.61} = (Ag,Al)_{17+0.18}Ce_{2-0.39}$ [32]. The number of vacancies at the Ce1 site is significantly larger as compared to the title compound and exceeds the limit for a coupled substitution according to 1 Ce ↔ 2 (Ag,Al). Only parts of the possible positions at 4(*e*) are occupied by Ag atoms whereas the other sites 4(*f*), 6(*g*), 12(*j*) and 12(*k*) are mixed occupied by (Ag,Al) atoms but in variable ratios. However, Cordier et al. [33] described a somewhat Al-richer compound $Ag_{6.4}Al_{10.6}Ce_{1.8} = (Ag,Al)_{17}Ce_{1.8}$ with vacancies at the 2(*b*) site but the authors did not mention any occupations at 4(*e*).

Dynamic method for phase diagram investigation

All reactions occurring in the Cd-Ce binary equilibrium diagram were examined by DTA. The corresponding alloy compositions and the observed thermal effects from heating and cooling curves are given in Table 4. Both as-cast and equilibrated samples were analyzed using heating rates of 2 K min^{-1} and 5 K min^{-1}, respectively. It was found that both types of sample preparation procedures for DTA samples delivered comparable temperature effects. Liquidus values were evaluated both from heating and from cooling curves. However, due to the strong tendency to supercool, as observed especially for Cd-rich samples (see Table 4), the liquidus line corresponds to the mean

values obtained from the heating curves. In the case of all other reactions, the temperature was determined only from the first heating curve. All transition reactions observed in the present study are listed in Table 5; reaction temperatures are given as the average values from several independent measurements together with estimated error limits.

The γ↔δ transformation and the melting point for a pure Ce sample were observed at 730 and 800 °C, respectively. This agrees well with the temperatures reported by Gschneidner [15], i.e. 725 and 797 °C. For the phase diagram construction in Fig. 1, the values of the melting and transformation temperature recorded in the present work were used. A eutectic is formed between δ-Ce and the CdCe phase

$$L \rightleftarrows \delta\text{-Ce} + CdCe$$

at 646 °C and ~20 at.% Cd. The eutectic point was fixed based on the liquidus temperatures of several samples in the corresponding part of the phase diagram and agrees well with literature data [17]. Strangely enough, Gschneidner and Calderwood [25] reported the temperature of the eutectic reaction at 417 °C based on an earlier report by Veleckis and Van Deventer [34]. This temperature is clearly too low and, most probably, confused with the eutectoid temperature (see below).

The eutectoid reaction

$$\delta\text{-Ce} \rightleftarrows \gamma\text{-Ce} + CdCe$$

takes place at 421 °C and ~15 at.% Cd. A representative DTA curve, showing both the eutectic and the eutectoid reaction in the Ce-rich part, is shown in Fig. 6a. The corresponding sample $Cd_{25}Ce_{75}$ was annealed at 300 °C for 10 weeks (Table 4). In contrast to Canepa et al. [17], the limiting solubility of Cd in γ-Ce was determined to be significantly higher (about 2.5 at.% Cd instead of less than 0.5 at.% Cd) and the eutectoid reaction temperature was evaluated at a considerably higher temperature (421 °C) than in Ref. [17] (375 °C). For the sample $Cd_{45}Ce_{55}$ the eutectoid reaction at 421 °C could not be recorded in the heating and cooling curves, probably due to an insignificant amount of γ-Ce in this sample.

The phases richest in Ce are CdCe and Cd_2Ce. Both are congruently melting with their melting points at 960 and 990 °C, respectively. Cd_2Ce exhibits the highest melting point of all Cd-Ce intermetallic compounds. A polymorphic transformation of Cd_2Ce into a high-temperature modification (indicated as ht-Cd_2Ce in Table 5) was assumed to occur, based on an additional DTA effect at 871 °C of a sample at the ideal stoichiometry (*cf.* Table 4). The respective heat effect is considered in Fig. 1. It has to be mentioned that a series of minor effects, probably dedicated to a more complex reaction scheme in the solid state phase fields around Cd_2Ce, were observed in the DTA curves of a few samples close to the stoichiometry of the latter compound. However, all attempts to synthesize the potential ht-Cd_2Ce phase by annealing and quenching proved unsuccessful. Further studies are going on to clarify phase relations in this part of the phase diagram. An analogous high temperature modification of the type Cd_2RE was also observed in the Cd-Nd [8], Cd-Pr [10], and Cd-Gd phase diagrams [35]. The phase CdCe forms a eutectic with the high-temperature modification of Cd_2Ce at 910±2 °C and 56 at.% Cd

$$L \rightleftarrows CdCe + Cd_2Ce.$$

Rather symmetric liquidus branches arise from the eutectic point. A symmetric shape (with respect to the composition) of the respective Gibbs energy curve of the liquid phase is thus indicated, at least in the range between the two stoichiometric compositions of CdCe and Cd_2Ce. Actually, regular solution behavior in the liquid is expected in the vicinity range of equimolar mixture especially at the respective elevated temperature. If this is the case here, the eutectic point has to be shifted towards CdCe because the congruent melting point of Cd_2Ce is significantly higher. In fact, the eutectic point lies at 56 at.% Cd, a composition closer to the stoichiometry of CdCe.

The phase Cd_3Ce is formed through the peritectoid reaction

$$Cd_2Ce + Cd_{58}Ce_{13} \rightleftarrows Cd_3Ce$$

at 852 °C. Slightly above this temperature, a eutectic reaction

$$L \rightleftarrows Cd_2Ce + Cd_{58}Ce_{13}$$

is observed at 857 °C and 77.5 at.% Cd. Both the peritectoid and eutectic reaction could be clearly observed in the DTA curves of samples with nominal compositions between 70 and 80 at.% Cd, see Table 4. The corresponding peak intensities of both reactions were certainly higher in the DTA curves of samples between 74 and 78 at.% Cd. Actually, one would expect the highest heat exchange during thermal analysis in samples showing major amounts of the decomposing compound Cd_3Ce (peritectoid) as well as liquid phase forming through the eutectic reaction. Hence, the two invariant effects could not be separated in the DTA curve of sample $Cd_{76}Ce_{24}$ (Table 4), whose composition lies in between the stoichiometry of Cd_3Ce and the eutectic point (77.5 at.% Cd, Table 5).

Concerning the melting temperatures of the two samples $Cd_{80}Ce_{20}$ and $Cd_{82}Ce_{18}$ (*cf*. Tab. 4), a congruent melting point of about 873 °C was estimated for the intermetallic compound $Cd_{58}Ce_{13}$. From the latter stoichiometry, the liquidus curve decreases continuously with increasing Cd content. All following intermediate compounds, i.e. Cd_6Ce, $Cd_{17}Ce_2$ and $Cd_{11}Ce$ are formed by peritectic reactions at 730, 610 and 605 °C, respectively. The value of the peritectic temperature of Cd_6Ce fits excellently with the earlier data by Johnson et al. [16], taking into account our experimental error of ±5 °C or less.

The high-temperature phase $Cd_{17}Ce_2$ (89.5 at% Cd) is stable between about 610 and 530 °C and is formed by the peritectic reaction

$$L + Cd_6Ce \rightleftarrows Cd_{17}Ce_2.$$

Slightly beneath the isothermal reaction temperature of this reaction, another peritectic occurs forming $Cd_{11}Ce$:

$$L + Cd_{17}Ce_2 \rightleftarrows Cd_{11}Ce.$$

Samples with Cd contents between 87 and 93 at.% showed only one invariant thermal effect on heating at 605±3 °C (see Fig. 6b). Neither the formation nor the decomposition of the high-temperature compound $Cd_{17}Ce_2$ was seen in any DTA curves. Therefore, additional DTA experiments were performed to clarify the situation: a single-phase sample $Cd_{11}Ce$ was measured in DTA against pure $Cd_{17}Ce_2$ as the reference material. It was assumed that both

sample and reference position are symmetrical within the furnace. The corresponding DTA-curve is shown in Fig. 7. It can be seen, that first an endothermic effect appears around 605 °C which is followed by an “exothermic” effect at around 610 °C. From this it must be concluded that the phase $Cd_{11}Ce$ (the sample material) starts to decompose at the first temperature whereas the second (exothermic) effect is due to the peritectic decomposition of the high-temperature phase $Cd_{17}Ce_2$. The corresponding DTA measurement was reproduced putting $Cd_{17}Ce_2$ onto the sample position while $Cd_{11}Ce$ served as the reference material. An exactly inverse DTA curve confirmed the assumed reaction sequence. Consequently, the two peritectic reactions are shown at 610 °C ($Cd_{17}Ce_2$) and 605 °C ($Cd_{11}Ce$) in Fig. 1, somewhat higher than reported by Canepa et al. [17]. Although the two samples with 87 and 89 at.% Cd showed also the thermal effect at about 605 °C it is assumed that this is due to the decomposition of non-equilibrium $Cd_{11}Ce$ since not all of it is transformed into $Cd_{17}Ce_2$ during heating in the DTA. Therefore, the corresponding effects are shown in parentheses in Table 4.

Canepa et al. [17] reported the eutectoid reaction

$$Cd_{17}Ce_2 \rightleftarrows Cd_6Ce + Cd_{11}Ce$$

at 525 °C based on effects that were observed on cooling only. Although we also found a rather strong effect at about 530 °C on cooling in the two samples with 90 and 91 at.% Cd (but nothing on heating, see Fig. 6b), we tend to conclude that these are non-equilibrium effects and not necessarily due to the eutectoid reaction. Sample 4 with 89 at.% Cd, annealed at 550 °C, resulted in single-phase $Cd_{17}Ce_2$ which proves that the phase is stable at this temperature. On the other hand, sample no. 5 with 88 at.% Cd, annealed at 400°C showed the two phases Cd_6Ce and $Cd_{11}Ce$. In addition, powder-XRD analysis of the single-phase $Cd_{17}Ce_2$ sample after DTA showed that grains of $Cd_{17}Ce_2$ were still remaining, however, together with the phases Cd_6Ce and $Cd_{11}Ce$. From this observation it must be concluded that $Cd_{17}Ce_2$ is not stable at room temperature but decomposes in a eutectoid reaction somewhere between 400 and 550°C.

For compositions containing more than 90 at.% Cd (Table 4) a strong tendency to supercooling was observed (as already earlier in Refs. [8, 17, 36]). Anyway, the entire liquidus curve in the Cd-Ce diagram (Fig. 1) corresponds to the values registered on heating. A degenerate eutectic reaction occurs between $Cd_{11}Ce$ and pure Cd at 320 °C:

$$L \rightleftarrows Cd_{11}Ce + Cd$$

This temperature is very close to the melting point of pure Cd; that is why the exact eutectic point could not be determined. However, it can be assumed to be around 0.01 at.% Ce using the equation given by Johnson et al. [16]. The latter authors determined the solubility of Ce in liquid Cd by chemical analysis of filtered samples. From an empirical fit of their solubility data the present authors calculated that 4.3 at.% Ce are soluble in liquid Cd at 605 °C (peritectic formation temperature of $Cd_{11}Ce$, Table 5). This fits perfectly with liquidus data determined in the present study (sample $Cd_{95}Ce_5$, Table 4). Hence, the liquidus between 100 and 95.7 at.% Cd was drawn from a combination of the present DTA data and the results given by [16].

Generally, the temperatures of all invariant reactions recorded in the present work appear to be slightly higher than those reported earlier by Canepa et al. [17] where no information about the evaluation of DTA curves was given. All invariant reactions in the binary Cd-Ce system derived from the present results are collected in Table 5.

Conclusions

The current work presents results for the Cd-Ce phase diagram over the entire composition range. The equilibrium phase diagram was constructed by the use of SEM-EDS, powder-XRD and DTA (Fig. 1). Seven intermetallic compounds, reported previously in literature, were confirmed. The corresponding phase boundaries were determined precisely. Additionally, the solubility of Cd in γ-Ce and δ-Ce was determined. The melting and decomposition temperatures of the Cd-Ce phases as well as all invariant reactions and the liquidus temperatures were determined by means of DTA. A congruent melting was observed for CdCe, Cd_2Ce and $Cd_{58}Ce_{13}$ whereas Cd_3Ce, Cd_6Ce, $Cd_{17}Ce_2$ and $Cd_{11}Ce$ show incongruent melting behavior. The existence of the high-temperature phase $Cd_{17}Ce_2$ was confirmed and its crystal structure was investigated by powder and single-crystal XRD, respectively. The powder patterns could be indexed based on a hexagonal cell of the Th_2Ni_{17}-type. All intensities were very close to the calculated values, and the cell parameters agreed well with values given by Canepa et al. [17].

Based on the single-crystal data, a complete description of the $Cd_{17+2x}Ce_{2-x}$ (x ~ 0.02) structure is given with focus on the correct defect mechanism. The investigated crystal showed slight differences in composition compared to the one measured previously by Franceschi [18]. However, both structure refinements agree well with the present substitution mechanism $Cd_{17+2x}Ce_{2-x}$.

Acknowledgements

Financial support from the Austrian Science Fund (FWF) under Project No. P 23270-N19 and from the OeAD (Scientific-Technical Cooperation Austria-India) under Project No. IN 05/2011 is gratefully acknowledged. The authors express special gratitude to Dr. Stephan Puchegger (Department of Physics / University of Vienna) for his help with the SEM investigations. Thanks also to Mr. Alexander Beutl for sample preparation and Ms. Olivia Appay for technical assistance during an internship.

Tables

Table 1. Crystal structure data of phases in the Cd-Ce system and Cd(l).

Phase	Composition (at.% Cd)	Structure type	Pearson symbol	Space group	Ref.
γ-Ce	0-2.5 [a]	Cu	*cF4*	*Fm-3m*	[15,37-38]
δ-Ce	0-17.0 [a]	W	*cI2*	*Im-3m*	[15,39]
CdCe	50.0 [b]	ClCs	*cP2*	*Pm-3m*	[18,28,40]
Cd_2Ce	66.7 [b]	Cd_2Ce	*hP3*	*P-3m1*	[14,17]
Cd_3Ce	75.0 [b]	$AlFe_3$	*cF16*	*Fm-3m*	[17,28]
$Cd_{58}Ce_{13}$	81.7 [b]	$Pu_{13}Zn_{58}$	*hP142*	*P6$_3$/mmc*	[17,20]
Cd_6Ce	85.7 [b]	Cd_6Y	*cI168*	*Im-3*	[14,17]
$Cd_{17}Ce_2$	89.5 [a]	$Ni_{17}Th_2$	*hP38*	*P6$_3$/mmc*	[17]
$Cd_{11}Ce$	91.7 [b]	$BaHg_{11}$	*cP36*	*Pm-3m*	[14,17]

[a] according to Canepa et al. [17]
[b] given by Massalski et al. [23]

Table 2. Experimental phase compositions and lattice parameters of equilibrium phases in representative Cd-Ce samples.

No.	Nominal composition (at.%)	Annealing temperature (°C)	Phase analysis		EDS	
			Phases	Lattice parameters (Å)	Cd (at.%)	Ce (at.%)
1	$Cd_{98}Ce_2$	300	Cd	a = 2.9795(3), c = 5.6195(4)	100	0.0
			$Cd_{11}Ce$	a = 9.3194(2)	91.7	8.3
2	$Cd_{92}Ce_8$	300	Cd	a = 2.9796(2), c = 5.6198(1)	100	0.0
			$Cd_{11}Ce$	a = 9.3189(3)	91.8	8.2
3	$Cd_{90}Ce_{10}$	500	$Cd_{11}Ce$	a = 9.3190(4)	91.9	8.1
			Cd_6Ce	a = 15.7839(2)	86.1	13.9
4	$Cd_{89}Ce_{11}$	550	$Cd_{17}Ce_2$	a = 10.0213(1), c = 9.8119(1)	89.5	10.5
5	$Cd_{88}Ce_{12}$	400	$Cd_{11}Ce$	a = 9.3026(7)	91.6	8.4
			Cd_6Ce	a = 15.7841(3)	85.6	14.4
6	$Cd_{85.8}Ce_{14.2}$	300	Cd_6Ce	a = 15.7998(2)	86.5	13.5
7	$Cd_{84}Ce_{16}$	700	Cd_6Ce	a = 15.7778(5)	85.7	14.3
			$Cd_{58}Ce_{13}$	a = 15.7307(2), c = 15.5485(4)	82.0	18.0
8	$Cd_{84}Ce_{16}$	600	Cd_6Ce	a = 15.7961(4)	86.2	13.8
			$Cd_{58}Ce_{13}$	a = 15.7652(2), c = 15.5812(2)	-[a]	-[a]
9	$Cd_{83}Ce_{17}$	500	Cd_6Ce	a = 15.8032(1)	85.8	14.2
			$Cd_{58}Ce_{13}$	a = 15.7721(4), c = 15.5764(3)	-[a]	-[a]
10	$Cd_{82}Ce_{18}$	700	$Cd_{58}Ce_{13}$	a = 15.7574(6), c = 15.5662(3)	[b]	

11	$Cd_{80}Ce_{20}$	700	$Cd_{58}Ce_{13}$	a = 15.7528(3), c = 15.5131(5)		[b]	
			Cd_3Ce	a = 7.2244(4)			
12	$Cd_{81.7}Ce_{18.3}$	600	$Cd_{58}Ce_{13}$	a = 15.7806(2), c = 15.5776(1)	81.6		18.4
13	$Cd_{78}Ce_{22}$	600	$Cd_{58}Ce_{13}$	a = 15.7745(3), c = 15.5649(4)	81.6		18.4
			Cd_3Ce	a = 7.2287(4)	75.1		24.9
14	$Cd_{78}Ce_{22}$	700	$Cd_{58}Ce_{13}$	a = 15.7519(7), c = 15.5149(1)	81.5		18.5
			Cd_3Ce	a = 7.2239(5)	76.4		23.6
15	$Cd_{76}Ce_{24}$	700	Cd_3Ce	a = 7.22292(3)		[b]	
			Cd_2Ce	a = 5.0806(1), c = 3.4325(1)			
16	$Cd_{75}Ce_{25}$	600	Cd_3Ce	a = 7.2252(0)	75.6		24.4
17	$Cd_{74}Ce_{26}$	700	Cd_3Ce	a = 7.2297(5)		[b]	
			Cd_2Ce	a = 5.0822(4), c = 3.4383(5)			
18	$Cd_{72}Ce_{28}$	700	Cd_3Ce	a = 7.2296(3)		[b]	
			Cd_2Ce	a = 5.0731(3), c = 3.4407(3)			
19	$Cd_{70}Ce_{30}$	600	Cd_3Ce	a = 7.2247(2)	74.5		25.5
			Cd_2Ce	a = 5.0754(2), c = 3.4671(3)	66.4		33.6
20	$Cd_{70}Ce_{30}$	700	Cd_3Ce	a = 7.2307(4)		[b]	
			Cd_2Ce	a = 5.0737(2), c = 3.4415(3)			
21	$Cd_{66.7}Ce_{33.3}$	600	Cd_2Ce	a = 5.0791(1), c = 3.4655(2)	66.5		33.5
22	$Cd_{58}Ce_{42}$	600	Cd_2Ce	a = 5.0749(5), c = 3.4574(4)	66.2		33.8
			CdCe	a = 3.8581(3)	50.3		49.7

23	$Cd_{50}Ce_{50}$	600	CdCe	a = 3.8625(1)	50.1	49.9
24	$Cd_{40}Ce_{60}$	600	CdCe	too ductile	47.9	52.1
			δ-Ce	too ductile	16.6	83.4
25	$Cd_{25}Ce_{75}$	300	CdCe	too ductile	48.1	51.9
			γ-Ce	too ductile	1.5	98.5
26	Cd_4Ce_{96}	500	δ-Ce	too ductile	- [a]	- [a]
			γ-Ce	too ductile	1.9	98.1
27	Cd_1Ce_{99}	300	γ-Ce	too ductile	1.2	98.8

[a] The microstructure of the respective phase was too fine for an accurate measurement by EDS
[b] EDS was not performed of this sample

Table 3. Comparison of phase boundaries of all Cd-Ce compounds at different temperatures derived from EDS analyses and isopiestic vapor pressure measurements [7] (according to Table 2 and Ref. [7]).

Phase	Temperature (°C)	Phase boundary / at.% Cd	
		EDS	Isopiestic [7]
CdCe	300	48.1-	
	550	48.0-50.9 [7]	48.0 – 50.0
	600	47.9-50.3	
Cd_2Ce	550	65.5-66.4 [7]	65.4 – 66.4
	600	66.2-66.4	
Cd_3Ce	550		75.0
	600	74.5-75.1	
	700	-76.4	
$Cd_{58}Ce_{13}$	550	80.6-81.7 [7]	80.6 – 81.7
	700	81.5-82.0	
Cd_6Ce	400	-85.6	
	500	85.8-86.1	
	550	85.8-86.3 [7]	85.1 – 85.7
	700	85.7-	
$Cd_{11}Ce$	300	-91.7	
	500	91.9-	

Table 4. Experimental results of DTA from representative Cd-Ce samples.

Sample comp. (at.%)	Anneal. temp. (°C) / t (weeks)	Heating (°C)				Cooling (°C)	
		Invariant reactions		Phase boundary	Liquidus	Liquidus
pure Ce	-			730	800	799
Cd_2Ce_{98}	250/12			330 683	780	779
Cd_5Ce_{95}	300/10	420		632	771	770
$Cd_{10}Ce_{90}$	as-cast	417		519 n-o	726	725
$Cd_{10}Ce_{90}$	300/10	423			725	724
$Cd_{16}Ce_{84}$	as-cast	418		575	687	686
$Cd_{16}Ce_{84}$	300/10	425		651	681	680 n-o
$Cd_{25}Ce_{75}$	as-cast	422	648		730	
$Cd_{25}Ce_{75}$	300/10	423	648		729	714
$Cd_{35}Ce_{65}$	as-cast	419	648		883	876
$Cd_{35}Ce_{65}$	300/10	425 n-o	645		869	868
$Cd_{45}Ce_{55}$	as-cast	644			948	946
$Cd_{50}Ce_{50}$	600/4				960	954
$Cd_{54}Ce_{46}$	600/4	900 n-o	909		934	927
$Cd_{60}Ce_{40}$	600/4	908			963	962
$Cd_{66.7}Ce_{33.3}$	600/4	871			990	983
$Cd_{70}Ce_{30}$	700/6	851	856		965	956
$Cd_{72}Ce_{28}$	700/6	852	857		948	946
$Cd_{74}Ce_{26}$	700/6	852	857 a		914 n-o	907
$Cd_{76}Ce_{24}$	700/6	853				870
$Cd_{78}Ce_{22}$	700/6	852	857		858	854
$Cd_{80}Ce_{20}$	700/6	853	856		874	854
$Cd_{82}Ce_{18}$	700/6				873	854
$Cd_{84}Ce_{16}$	700/6		728		845	834
$Cd_{87}Ce_{13}$	as-cast		(604) 731		810	803

$Cd_{89}Ce_{11}$	as-cast		(603)	728	n-o		761
$Cd_{90}Ce_{10}$	as-cast	531[ec]	606	734	745		740
$Cd_{91}Ce_9$	as-cast	528[ec]	608		733		710[sc]
$Cd_{93}Ce_7$	250/12	319	605		684		654[sc]
$Cd_{95}Ce_5$	250/12	319			599		n-o
$Cd_{98}Ce_2$	as-cast	322			n-o		530

[a] no meaningful evaluation of the eutectic (L ⇄ Cd_2Ce + $Cd_{58}Ce_{13}$, Tab. 5) possible due to strongly overlapping effects
[n-o] not observed, [sc] supercooled effect, [ec] effect recorded only on cooling.

Table 5. Invariant reactions in the binary Cd-Ce system derived from the present results.

Reaction	*T*/ °C	Phase compositions/ at.% Cd			Reaction type
L ⇄ $Cd_{11}Ce$ + Cd	320±2	~100	91.7	~100	Degenerate eutectic
L + $Cd_{17}Ce_2$ ⇄ $Cd_{11}Ce$	605±3	95.7	89.5	91.7	Peritectic
L + Cd_6Ce ⇄ $Cd_{17}Ce_2$	~610	94.9	86.3	89.5	Peritectic
L + $Cd_{58}Ce_{13}$ ⇄ Cd_6Ce	730±5	91.2	81.7	86.0	Peritectic
L ⇄ $Cd_{58}Ce_{13}$	873		81.7		Congruent melting
L ⇄ Cd_2Ce + $Cd_{58}Ce_{13}$	857±2	77.5	66.6	81.7	Eutectic
Cd_2Ce + $Cd_{58}Ce_{13}$ ⇄ Cd_3Ce	852±2	66.6	81.7	75.0	Peritectoid
Cd_2Ce ⇄ ht-Cd_2Ce*	871		66.5		Polymorphic transformation
L ⇄Cd_2Ce	990		66.7		Congruent melting
L ⇄ CdCe +Cd_2Ce	910±2	56.0	50.4	66.2	Eutectic
L ⇄ CdCe	960		50.0		Congruent melting
L ⇄ δ-Ce + CdCe	646±2	20.0	17.0	48.0	Eutectic
δ-Ce ⇄ γ-Ce + CdCe	421±4	15.0	2.5	48.2	Eutectoid

* Polymorphic transformation of Cd_2Ce is assumed according to an effect (DTA) detected in sample $Cd_{66.6}Ce_{33.3}$ (Tab. 4)

Table 6. Collected Single-crystal X-ray data and structure refinements for $Cd_{17+2x}Ce_{2-x}$, x ~ 0.02.

Single-crystal data	
a [Å]	10.0255(7)
c [Å]	9.8162(7)
space group	$P6_3/mmc$
V [Å³]	854.4
Z	2 {$Cd_{17+2x}Ce_{2-x}$, x ~ 0.02}
ρ_{calc} [g cm^{-3}] / μ(Mo$K\alpha$) [mm^{-1}]	8.52 / 25.8
crystal dimensions (μm)	30×45×55
Measurement data	
range of data collection ($\pm h \pm k \pm l$) [°]	$3 < 2\vartheta < 70$
number of images / rotation angle per image [°]	509 / 2
scan mode (at 10 distinct ω-angles)	φ-scans
scan time [s/°] / frame size (binned mode)	150 / 621×576 pixels
detector-to-sample distance [mm]	30
measured reflections	12,985
Refinement	
unique reflections (n) / reflections with $F_o > 4\sigma(F_o)$	743 / 682
$R_{int} = \Sigma \lvert F_o^2 - F_o^2(\text{mean}) \rvert / \Sigma F_o^2$	0.063
extinction parameter k:	0.00137(7)
$F_c^* = F_c \cdot k[1+0.001 \cdot F_c^2 \lambda^3/\sin(2\vartheta)]^{-1/4}$	
$R1 = \Sigma(\lvert \lvert F_o \rvert - \lvert F_c \rvert \rvert) / \Sigma F_o$ (2,551 / 2,283 reflections)	0.019 / 0.022
$wR2 = [\Sigma w(F_o^2 - F_c^2)^2 / \Sigma \lvert wF_o^4]^{1/2}$	0.039
GooF = $\{\Sigma[w(F_o^2 - F_c^2)^2] / (n-p)\}^{0.5}$	1.17
max Δ/σ; number of variable parameters (p)	< 0.001; 30
final difference Fourier map [eÅ^{-3}]	-1.33 to +1.18

$w = 1 / \{ \sigma^2(F_o^2) + [0.013 \times P]^2 + 2.17 \times P \}$; $P = ([\max(0, F_o^2)] + 2 \times F_c^2) / 3]$

Table 7. Fractional atomic coordinates and displacement parameters for $Cd_{17+2x}Ce_{2-x}$, x ~ 0.02; the anisotropic displacement parameters are defined as: $\exp[-2\pi^2 \Sigma^3_{i=1} \Sigma^3_{j=1} U_{ij}\ a^*_i\ a^*_j\ h_i\ h_j]$.

Atomic pos.	*occ.*	Wykoff letter	Site symm.	x	y	z	U_{equiv} / U_{iso}	U_{11}	U_{22}	U_{33}	U_{23}	U_{13}	U_{12}
Cd1	1.0	4(*f*)	3*m*.	⅓	⅔	0.09897(5)	0.01717(10)	0.01772(14)	= U_{11}	0.0161(2)	0	0	= ½ U_{11}
Cd2	1.0	6(*g*)	.2/*m*.	½	0	0	0.01757(9)	0.01481(12)	0.02645(19)	0.01533(16)	0.00434(13)	= ½ U_{23}	= ½ U_{22}
Cd3	1.0	12(*j*)	*m*..	0.03664(4)	0.36428(4)	¼	0.01719(8)	0.02259(14)	0.02194(14)	0.01203(12)	0	0	0.01488(11)
Cd4	1.0	12(*k*)	.*m*.	0.160837(17)	= 2*x*	-0.02567(3)	0.01985(8)	0.01511(10)	0.02794(15)	0.02079(14)	-0.00365(10)	= ½ U_{23}	= ½ U_{22}
Cd5	0.020(2)	4(**e**)	3*m*.	0	0	0.400(2)	0.013(6)	0.011(7)	= U_{11}	0.017(10)	0	0	= ½ U_{11}
Ce1	0.976(3)	2(*b*)	$\bar{6}m2$	0	0	¼	0.01257(14) 0.01101(16)	= U_{11}	0.0157(2)	0	0	= ½ U_{11}	Ce1
Ce2	1.0	2(*d*)	$\bar{6}m2$	⅓	⅔	¾	0.01162(10) 0.01210(13)	= U_{11}	0.01065(19)	0	0	= ½ U_{11}	Ce2

Table 8. Interatomic bond lengths (Å) in $Cd_{17+2x}Ce_{2-x}$, $x \sim 0.02$.

Interatomic bond	Length (Å)	Interatomic bond	Length (Å)	Interatomic bond	Length (Å)
Cd1—Cd1	2.9651(10)	Cd4—Cd4	2.8379(4) 2H	Ce1···Cd5	1.48(3) 2H
Cd1—Cd2	3.0527(3) 3H	Cd4—Cd5	2.886(6)	Ce1—Cd5	3.43(2) 2H
Cd1—Cd4	3.2354(4) 3H	Cd4—Cd2	2.9567(3) 2H	Ce1—Cd3	3.4827(4) 6H
Cd1—Cd3	3.3493(4) 6H	Cd4—Cd3	2.9817(3) 2H	Ce1—Cd4	3.5565(3) 6H
Cd1—Ce2	3.4255(6)	Cd4—Cd5	3.052(9)	Ce1—Cd4	3.8887(4) 6H
		Cd4—Cd3	3.0963(3) 2H		
Cd2—Cd3	2.9170(2) 4H	Cd4—Cd1	3.2354(4)	Ce2—Cd1	3.4255(6) 2H
Cd2—Cd4	2.9567(3) 4H	Cd4—Ce1	3.5565(3)	Ce2—Cd3	3.5641(4) 6H
Cd2—Cd1	3.0527(3) 2H	Cd4—Ce2	3.7176(4)	Ce2—Cd4	3.7176(4) 6H
Cd2—Ce2	3.7944(2) 2H	Cd4—Ce1	3.8887(4)	Ce2—Cd2	3.7944(2) 6H
Cd3—Cd2	2.9169(2) 3H	Cd5···Ce1	1.48(2)		
Cd3—Cd4	2.9817(3) 2H	Cd5···Cd5	1.96(4)		
Cd3—Cd3	3.0886(6) 3H	Cd5—Cd4	2.886(6) 3H		
Cd3—Cd1	3.3494(4) 2H	Cd5—Cd5	2.95(4)		
Cd3—Ce1	3.4828(4)	Cd5—Cd4	3.052(9) 3H		
Cd3—Ce2	3.5642(4)	Cd5—Ce1	3.43(2)		
Cd3—Cd5	3.782(9) 2H	Cd5—Cd3	3.782(9) 6H		

Figures

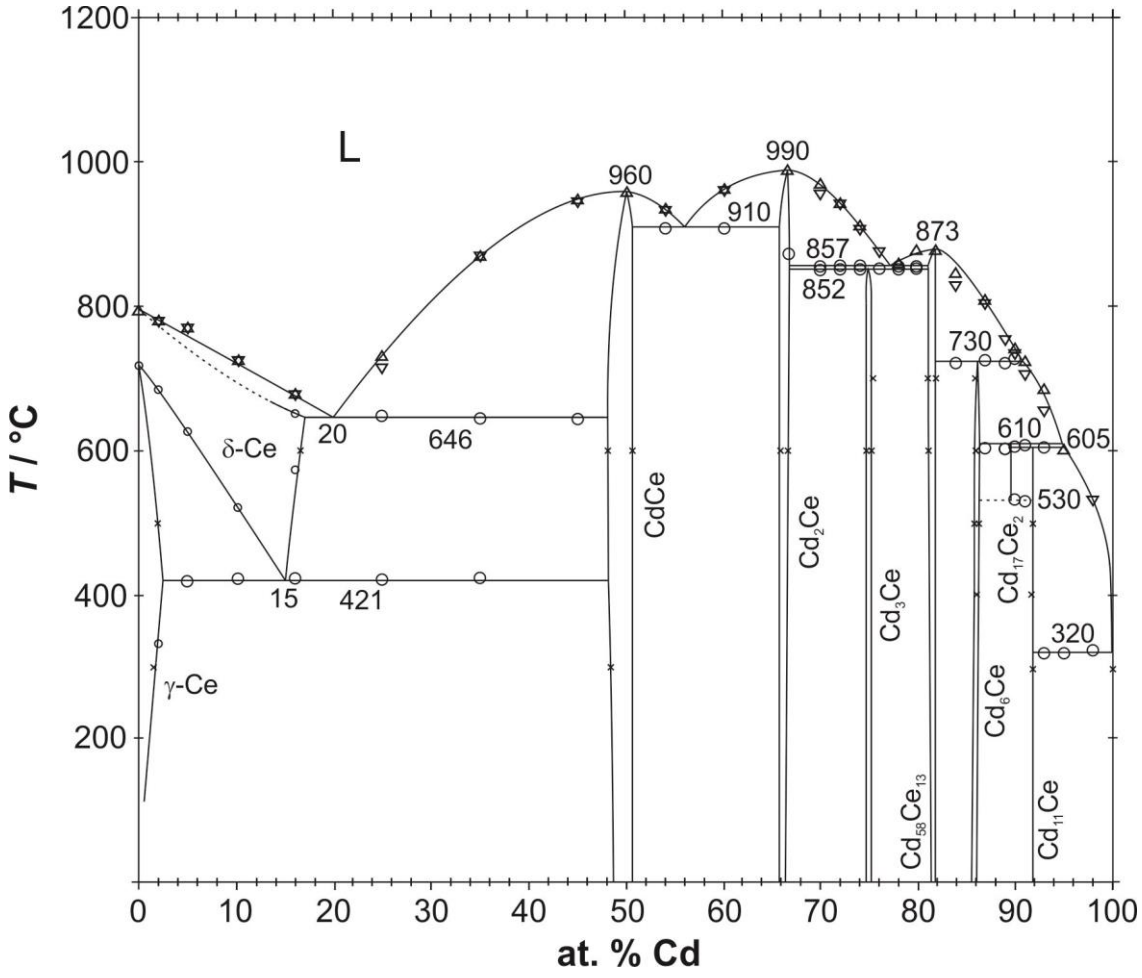

Fig. 1. The Cd-Ce phase diagram according to the present results. Large circles: invariant thermal effects from DTA. Small circles: non-invariant effects. Triangles up and down: liquidus on heating and cooling. X mark: phase composition derived from EDS. The solubility of Ce in liquid Cd between 96.5–99.98 at.% Cd was taken from Johnson et al. [16].

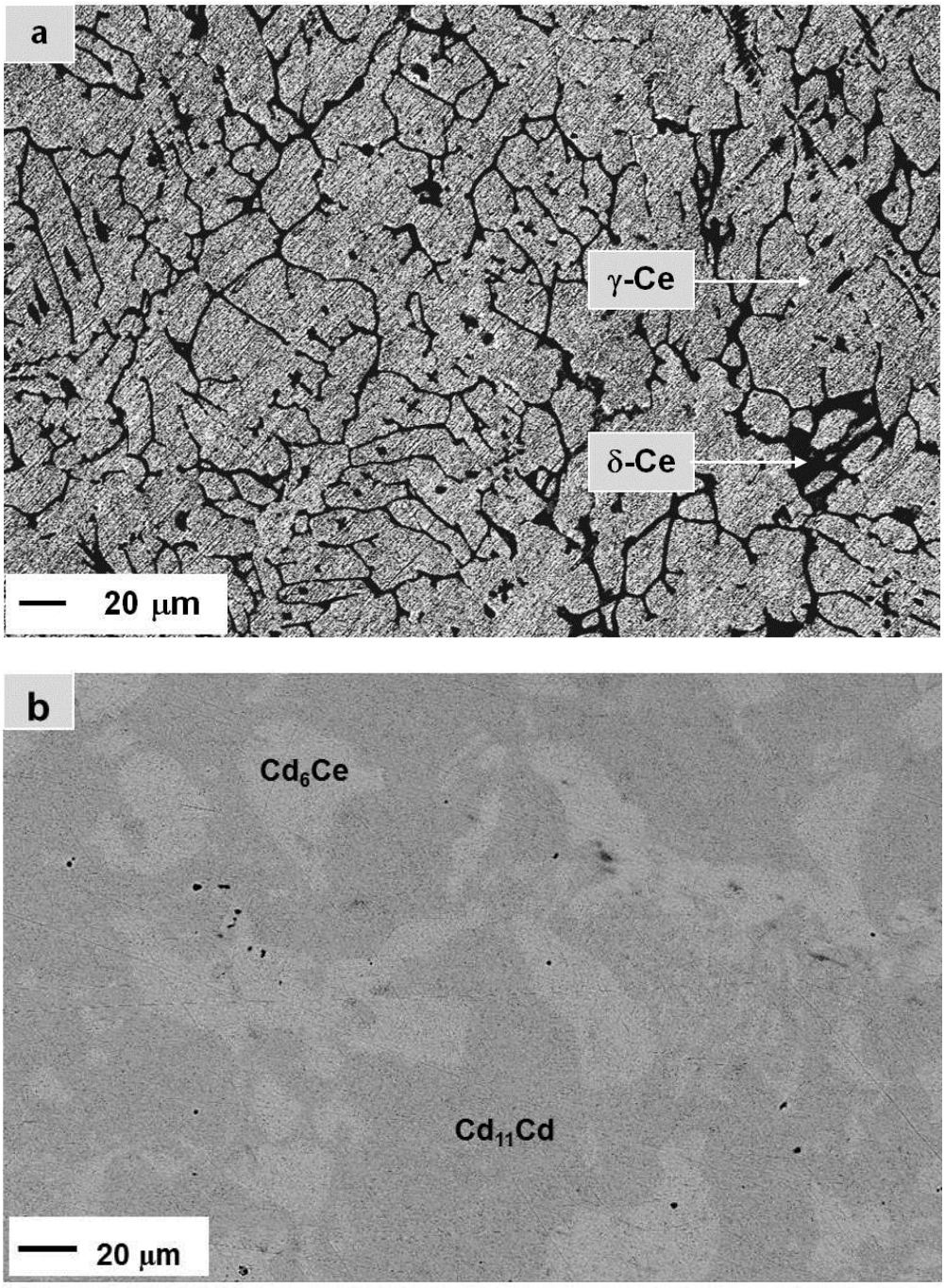

Fig. 2. (**a**) Microstructure of a sample (No. 26, Table 2) with the nominal composition Cd_4Ce_{96} annealed at 500 °C for 8 weeks and (**b**) of a sample (No. 3, Table 2) with the nominal composition $Cd_{90}Ce_{10}$ annealed at 550 °C for 6 weeks.

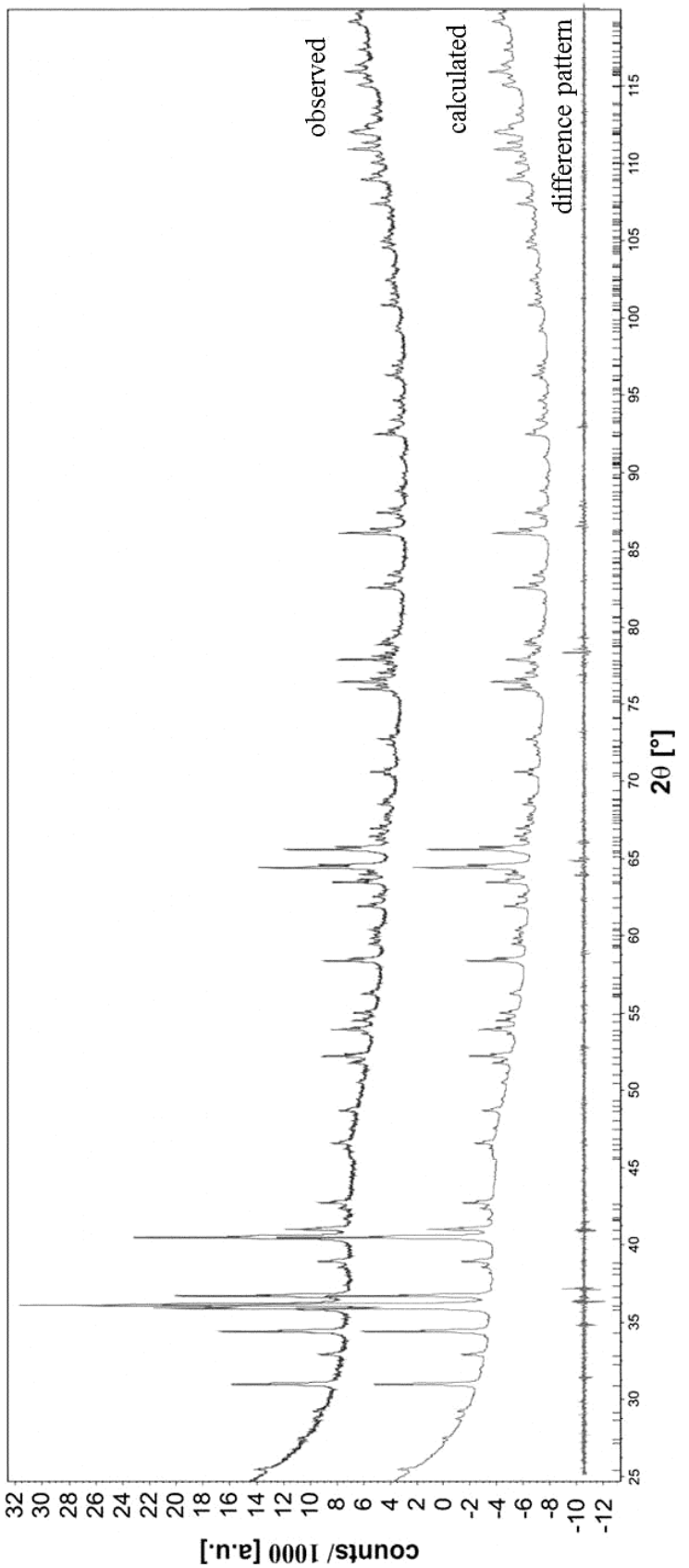

Fig. 3. Powder-XRD pattern of the $Cd_{89}Ce_{11}$ sample (No. 4, Table 2) annealed at 550°C for 4 weeks showing the $Cd_{17}Ce_2$ phase (Rwp = 1.87). The calculated pattern of $Cd_{17}Ce_2$ and the difference curve are shown in the bottom of the graph.

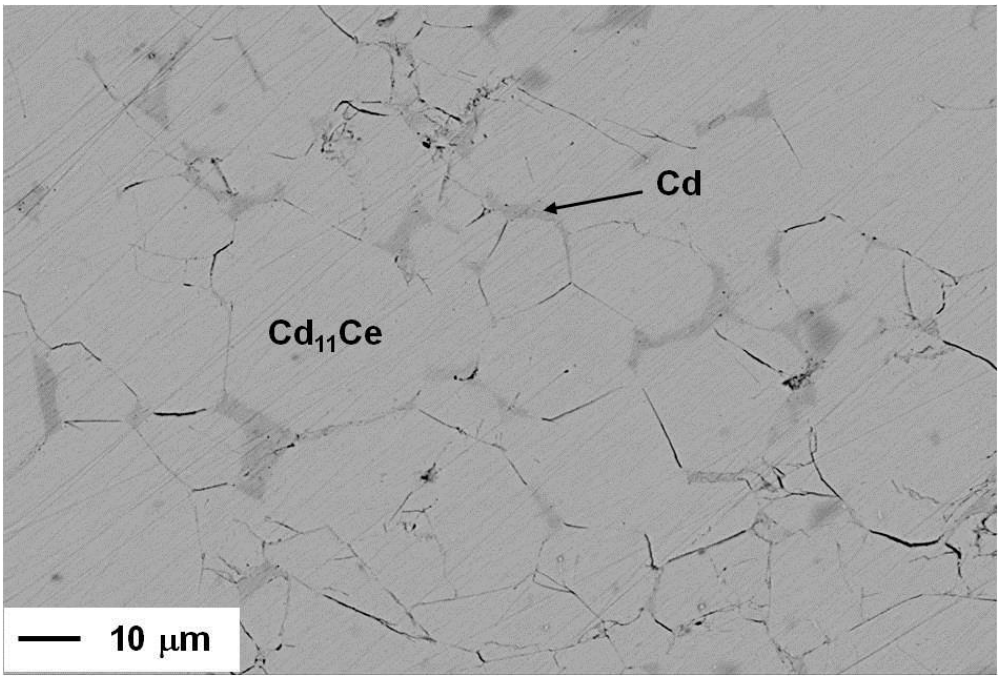

Fig. 4. Microstructure of the sample $Cd_{92}Ce_8$ annealed at 300 °C for 10 weeks.

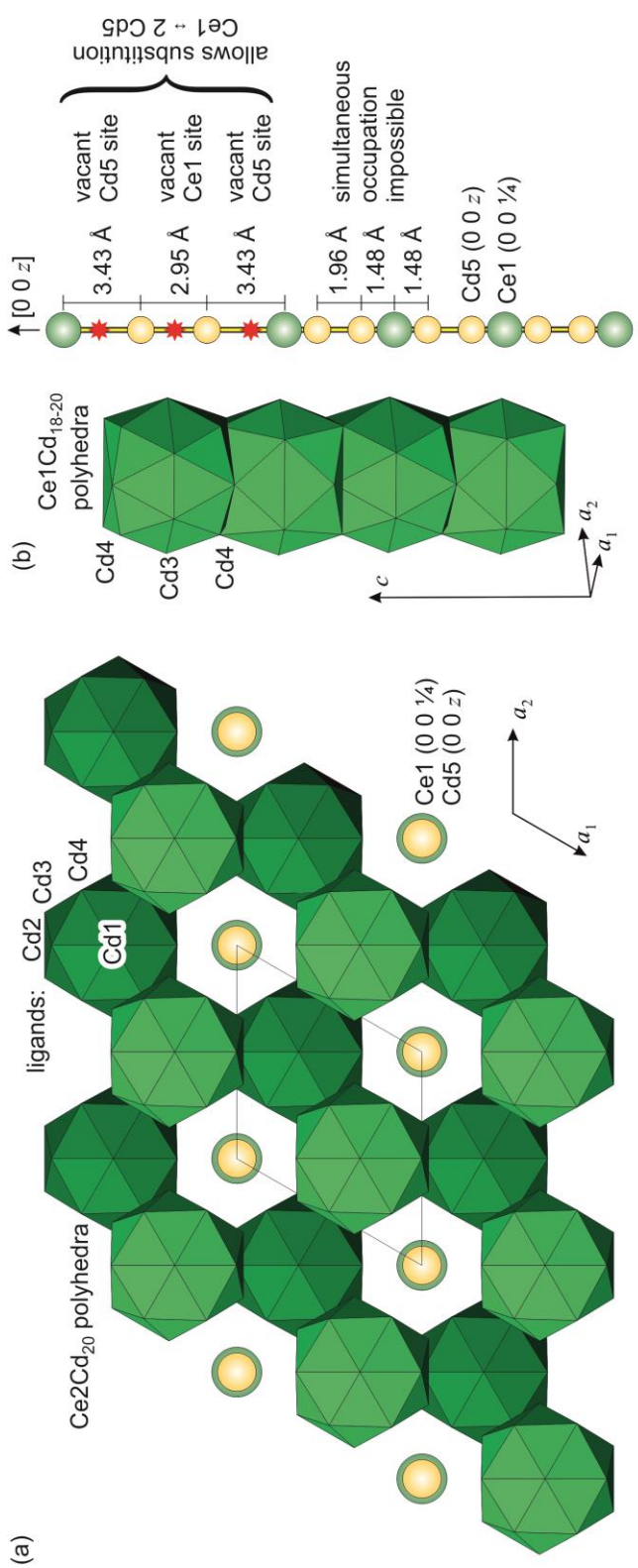

Fig. 5. The crystal structure of $Cd_{17+2x}Ce_{2-x}$ (*x* ~ 0.02): (**a**) The connection of the $Ce2Cd_{20}$ coordination polyhedra forming channels along [001] hosting the Ce1 and Cd5 atoms. (**b**) The connection of $Ce1Cd_{18}$ coordination polyhedra to rows along [001] and the substitution mechanism Ce1 ↔ 2 Cd5; the required vacancies are marked by red stars.

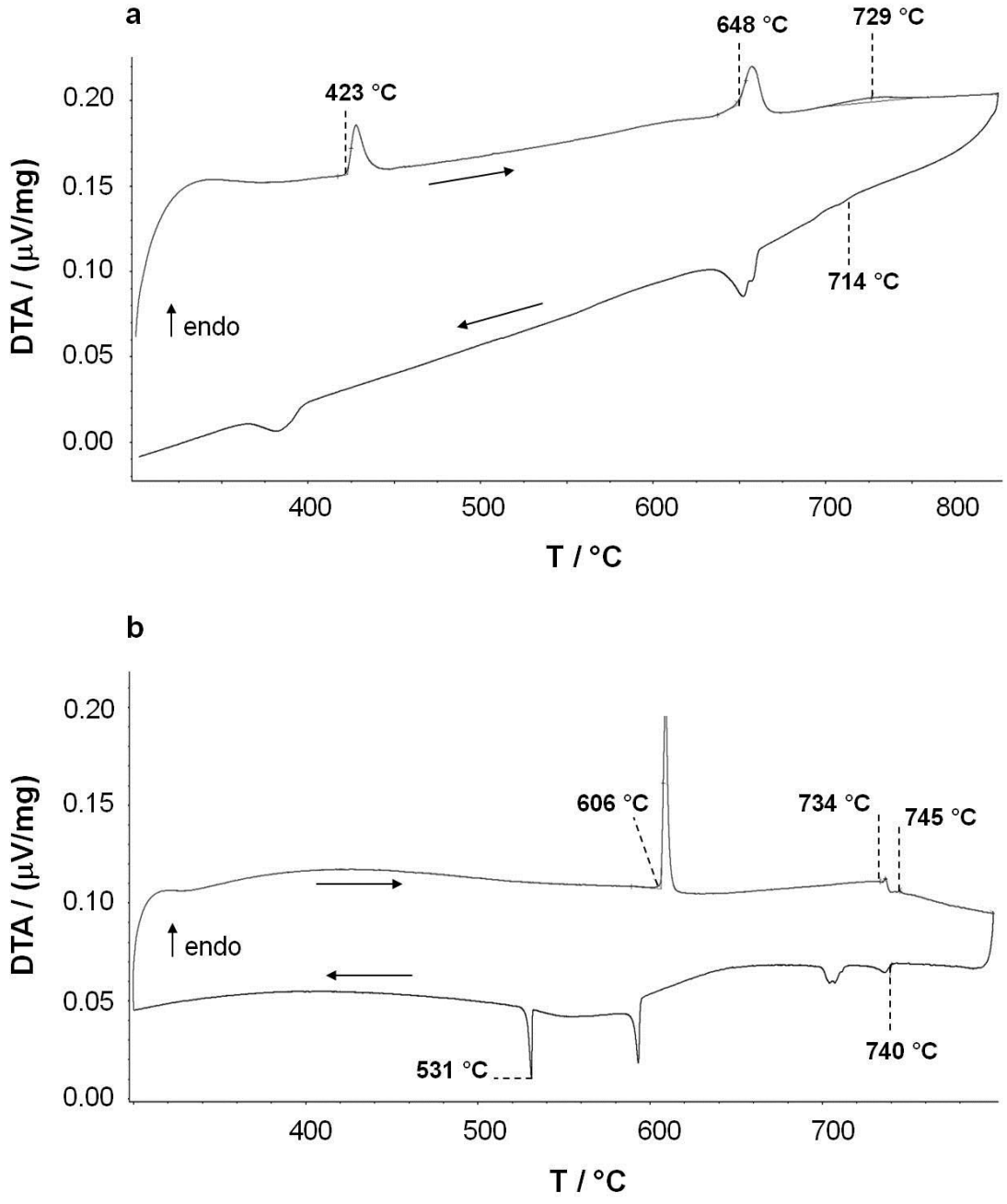

Fig. 6. DTA curves of (**a**) $Cd_{25}Ce_{75}$ (No.25, Table 2) annealed at 300 °C for 10 weeks, measured upon heating and cooling with 5 K min^{-1}, and (**b**) $Cd_{90}Ce_{10}$ (as-cast state) measured upon heating and cooling with 2 K min^{-1}.

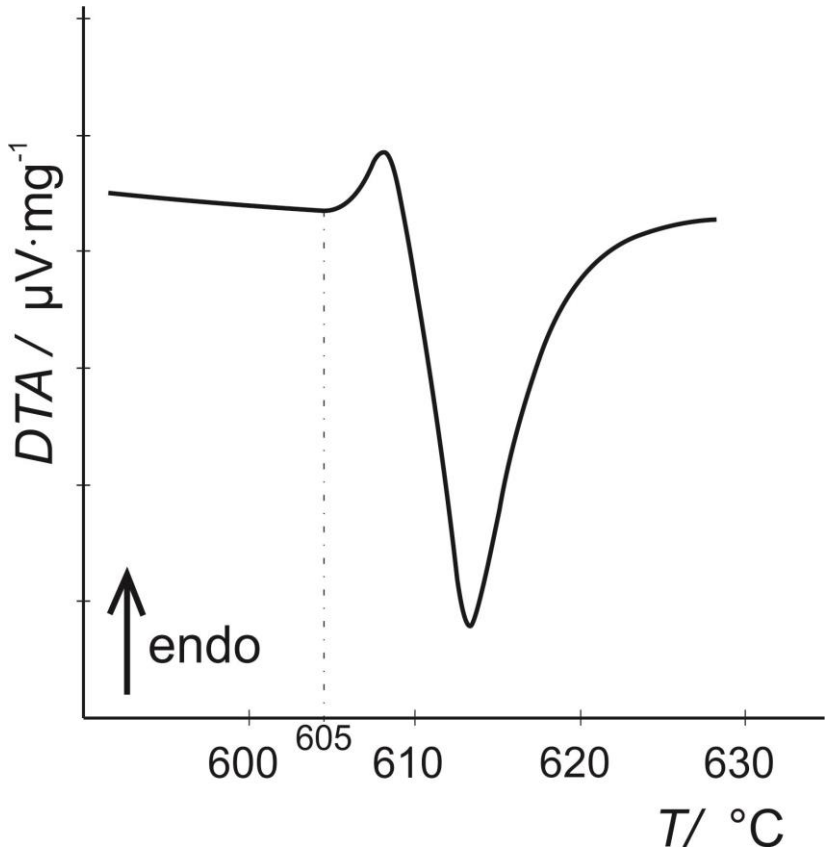

Fig. 7. DTA curves of the single-phase sample $Cd_{17}Ce_2$ (No. 4, Table 2) measured against pure $Cd_{11}Ce$ as the reference material (heating and cooling rate: 5 K min^{-1}).

References

[1] Olander D. Nuclear fuels - Present and future. J Nucl Mater 2009;389:1-22.

[2] Kurata M, Sakamura Y, Hijikata T, Kinoshita K. Distribution behavior of uranium, neptunium, rare-earth elements (Y, La, Ce, Nd, Sm, Eu, Gd) and alkaline-rare metals (Sr, Ba) between molten LiCl-KCl eutectic salt and liquid cadmium or bismuth. J Nucl Mater 1995;227:110-121.

[3] Conocar O, Douyere N, Glatz J, Lacquement J, Malmbecke R, Serp J. Promising pyrochemical actinide/lanthanide separation processes using aluminum. Nucl Sci Eng 2006;153:253-261.

[4] Kurata M, Sakamura Y, Matsui T. Thermodanymic quantities of actinides and rare earth elements in liquid bismuth and cadmium. J Alloys Comp 1996;234:83-92.

[5] Kurata M, Sakamura Y. Thermodynamic assessment of system of actinide or rare earth with Cd. J Phase Equilibria 2001;22:232-240.

[6] Richter KW, Besana S, Borzone G, Ipser H. Thermodynamic investigations in the lanthanum-cadmium system. J Alloys Comp 2004;365:181-187.

[7] Skołyszewska-Kühberger B, Reichmann TL, Ganesan R, Ipser H. Thermodynamic study of the cerium-cadmium system. CALPHAD 2014;44:14-20.

[8] Skołyszewska-Kühberger B, Reichmann TL, Ipser H. Phase equilibria in the neodymium-cadmium binary system. J of Alloys and Comp 2014;606: 242-248.

[9] Reichmann TL, Ipser H. Thermochemical investigations in the system cadmium-praseodymium relevant for pyro-metallurgical fuel reprocessing; Metall. Mater. Trans. A. 2014;45:1171-1180.

[10] Reichmann TL, Effenberger HS, Ipser H. Experimental investigation of the Cd-Pr phase diagram. PLOS ONE 2014;9/4:1-14.

[11] Reichmann TL, Richter KW, Delsante S, Borzone G, Ipser H. Enthalpies of formation of Cd-Pr intermetallic compounds and thermodynamic assessment of the Cd-Pr system; CALPHAD 2014 47: 56-62.

[12] Reichmann TL, Ganesan R, Ipser H. Thermochemical investigations in the system Cd-Gd; J Alloys Comp 2014 610: 676-683.

[13] Reichmann TL, Ipser H. Reinvestigation of the Cd-Gd phase diagram; J Alloys Comp 2014 617: 292-301.

[14] Iandelli A, Ferro R. Sulle leghe del Cadmio col Lantanio, Cerio e Praeseodimio. Gazz Chim Ital 1954;84:463-478.

[15] Gschneidner KA. Rare Earth Alloys. D. van Nostrand Company Ltd, Canada; 1961.

[16] Johnson I, Anderson KE, Blomquist RA. Partial constitutional diagram for the Cd-La, Cd-Ce, Cd-Pr, Cd-Nd, and Cd-Sm systems. Trans ASM 1966;59:352-355.

[17] Canepa F, Costa GA, Franceschi EA. The phase diagram of the Ce-Cd system. Lanthanide Actinide Res 1985;1:41-47.

[18] Franceschi EA. The crystal structure of the $CeCd_{8.73}$ phase. Lanthanide Actinide Re 1988; 2: 181-186.

[19] Iandelli A, Palenzona A. J Less-Common Met 1968;15:273.

[20] Bruzzone G, Fornasini ML, Merlo F. Rare earth intermediate phases with cadmium. J Less-Common Met 1973;30:361-375.

[21] Piao SY, Palatinus L, Lidin S. All the disorder mechanisms in the 13:58 phases come together. Out of the modulated confusion rises the remarkable phase $Ce_{12.60}Cd_{58.68(2)}$. Inorg Chem 2008;47:1079-1086.

[22] Johnson I, Schablaske R, Tani B, Anderson K. $CeCd_6$-type rare earth-cadmium alloy. Trans AIME 1964;230:1485-1487.

[23] Massalski TB. Binary Alloy Phase Diagrams. 2nd ed.Ohio: ASM International, Materials Park; 1990:971-972.

[24] Okamoto H. Cd-Ce (cadmium-cerium). J Phase Equilibria 1999;20:636.

[25] Gschneidner Jr KA, Calderwood FW. The cadmium-rare earth systems. Bull Alloy Phase Diagrams1988;9:16-21.

[26] Sheldrick, G.M. (1997b): SHELXL-97, a program for crystal structure refinement. University of Göttingen, Germany.

[27] Sheldrick, G.M. (2008): A short history of SHELX. Acta Crystallographica; A64: 112-122.

[28] Tang J, Gschneidner KA. Searching for new heavy fermion materials in cerium intermetallic compounds. J Less-Common Met 1989;149:341-347.

[29] Cirafici S, Palenzona A. (1990). Alloying behaviour of thorium with Fe, Co and Ni. Thermochimica Acta 1990;162:117-125.

[30] Tereshina IS, Nikitin SA, Skokov KP, Palewski T, Zubenko VV, Telegina IV, Verbetsky VN, Salamova AA. Magnetocrystalline anisotropy of $R_2Fe_{17}H_x$ (x = 0, 3) single crystals. J. All. Comp. 2003;350: 264-270.

[31] Yang Z, Shi D, Wen B, Melnik R. Structural, elastic, electronic properties and heats of formation of Ca–Zn intermetallics from first principles calculations. J. All. Comp. 2012;524: 53-58.

[32] Denysyuk OV, Stel'makhovich BM, Kuz'ma YB. Crystal structure of new compounds in the RE-Ag-Al systems. J. Solid State Chem. 1994;109:172-174.

[33] Cordier G, Doersam G, Henseleit R, Mehner A, Thies S, Geibel C. Neue ternaere RE-Silber-Aluminide (RE ≡ La, Ce, Pr, Yb) mit gewellten Silber-Aluminium Kagomè Netzen. J. All. Comp. 1992;186:161-175.

[34] Veleckis E, Van Deventer E. Eutectic temperatures in the LnCd-Ln fields of the lanthanon-cadmium systems.ANL-6925, Semi-Annual Report, Jul-Dec 1964, Argonne National Laboratorium, Argonne, IL; 1965.

[35] Bruzzone G, Fornasini ML, Merlo F. The Gadolinium-Cadmium System. J. Less-Com Met. 1975:25:295-301.

[36] Iandelli A. Congr Intern Chim Pure Appl. 16 Paris. Mem Sect Chim Minerale 1958:35-40.

[37] Spedding FH, Daane AH, Herrmann W. The Crystal Structures and Lattice Parameters of High-Purity Scandium, Yttrium and the Rare Earth Metals, Acta Cryst 1956;9:559-563.

[38] Speight JD, Harris IR, Raynor GV. Alloys of cerium with neodymium, samarium and terbium, and of praseodymium with terbium. J Less-Comm Metals 1961;3:110-124.

[39] Spedding FH, Hanak JJ, Daane AH. High temperature allotropy and thermal expansion of the rare-earth metals. J Less-Comm Metals 1961;3:110-124.

[40] Iandelli A. Atti Accad Nazl Lincei. Rend Classe Sci Fis. Mat e Nat 1960;29:62-69.

3.2. Thermodynamic study of the cerium-cadmium system

Barbara Skołyszewska-Kühberger[a], Thomas L. Reichmann[a], Rajesh Ganesan[b], Herbert Ipser[a]*

[a] Department of Inorganic Chemistry/Materials Chemistry,
University of Vienna, A-1090 Wien, Austria
[b] Indira Gandhi Center for Atomic Research, Kalpakkam, Tamilnadu, India

*Corresponding author:
E-mail address: Barbara.kuehberger@univie.ac.at

Published: *Calphad* 44 (2014) 14-20

Contributions to this paper:
B.S-K.: sample preparation, calculation and analysis, wrote the paper
T.L.R: advice in calculation and analysis
R. G.: advice in performing the experiments, wrote the paper
H.I.: proofreading, advice in interpretation and helpful comments

Contribution of B. Skołyszewska-Kühberger to this article: 80%

Abstract

Cadmium vapor pressures were determined over Ce-Cd samples by an isopiestic method. The measurements were carried out in the temperature range from 690 to 1080 K and over a composition range of 48 to 85 at.% Cd. From the vapor pressures thermodynamic activities of Cd were derived for all samples at their respective sample temperatures, and partial molar enthalpies of Cd were obtained from the temperature dependence of the activities. With these partial molar enthalpies the Cd activities were converted to a common temperature of 823 K. By means of a Gibbs-Duhem integration Ce activities were calculated, using a corresponding literature value for the two-phase field ($CeCd_{11}$+L) as integration constant. Finally integral Gibbs energies were calculated for the composition range 48 to 100 at.% Cd with a minimum value of -37 $kJ \cdot g\text{-}atom^{-1}$ at 823 K in the phase CeCd. Phase boundaries of the intermetallic compounds CeCd, $CeCd_2$, $Ce_{13}Cd_{58}$, and $CeCd_{11}$ were estimated from the vapor pressure measurements and from SEM analyses.

Introduction

The nuclear waste disposal is one of the key issues for future use of nuclear energy. Currently several different reprocessing techniques do exist. During traditional aqueous methods some restrictions occur like limited solubility of fuel materials in acidic aqueous solutions and poor radiation stability of the organic solvents employed in the extraction process [1]. The pyrochemical separation techniques seem to be more effective methods for reprocessing of spent high burn-up fuels. The central step in these non-aqueous methods is the electro-refining process where in an electro transportable cell chopped fuel rods are reprocessed [2]. This electro transportable cell consists of a steel anode in form of a basket, where spent fuels are inserted, and two cathodes: a stainless steel cathode for the recovery of U and a liquid metal cathode (using Al [1], Bi [3] or Cd [3]) for the selective recovery of Pu and minor actinides (MA). The entire cell is completely filled with molten LiCl-KCl electrolyte with an additional liquid metal pool occupying its bottom. A variety of liquid metals (Me = Al [1], Bi [3] or Cd [3]) have been explored to extract the rare earth (RE) elements (light rare earth elements between La and Gd with the exception of Pm), which are partially oxidized, from the electrolyte. The extraction behavior is primarily affected by the formation of intermetallic compounds, and thus a thorough knowledge on the existence and stability of intermetallic compounds in the various binary phase diagrams RE-Me are important. Moreover, thermodynamic properties such as the stability of the intermetallic compounds are of high interest, both for a thermodynamic assessment of the binary system based on the CALPHAD[1] method [4], but also for an optimization of the extraction process itself.

This was the starting point for the present study which wants to provide partial and integral thermodynamic properties of binary Ce-Cd alloys, mainly based on Cd vapor pressure measurements with an isopiestic method [5, 6]. Using limited literature information on partial thermodynamic properties of Ce,

[1] CALPHAD = CALculation of PHAse Diagrams

integral Gibbs energies of formation could be obtained over a large composition range. Together with calorimetric measurements to determine enthalpies of formation of several intermetallic compounds and a careful experimental phase diagram reinvestigation (both currently under way) this will serve as input for a CALPHAD optimization of the binary Ce-Cd system.

Literature review

Phase diagram

The Ce-Cd phase diagram appears to be reasonably well known. Johnson et al [7] determined a partial phase diagram in the Cd-rich part, i.e. they established the liquidus line in the composition range up to about 1 at.% Ce by measuring the solubility of Ce in liquid Cd by chemical analysis; they also examined the peritectic decomposition temperature of $CeCd_{11}$ by differential thermal analysis (DTA). Iandelli and Ferro [8] who applied micrography and X-ray diffraction (XRD), reported the existence of the six compounds CeCd, $CeCd_2$, $CeCd_3$, Ce_2Cd_9, $CeCd_6$ and $CeCd_{11}$. The complete phase diagram was experimentally investigated by Canepa et al [9] applying DTA, XRD and metallography. They found one additional high-temperature phase (Ce_2Cd_{17}). Their phase diagram version was the basis for the compilation by Okamoto [10] whereas Massalski et al. [11] still showed only a partial phase diagram. Systematic trends in the phase diagrams of the RE-Cd systems were discussed in a compilation by Gschneidner and Calderwood [12].

According to Okamoto [10] the system is characterized by seven intermetallic compounds, of which three (CeCd, $CeCd_2$, and $Ce_{13}Cd_{58}$) show a congruent melting behavior and the others ($CeCd_3$, $CeCd_6$, Ce_2Cd_{17}, and $CeCd_{11}$) are formed through peritectic reactions. All compounds are shown as line compounds without any significant homogeneity range. Only very recently Piao et al [13] discussed in detail the crystal structure of the compound $Ce_{13}Cd_{58}$ and its complicated disorder mechanism.

Thermochemical data

One of the earliest results on this system was given by Elliot and Lemons [14]. They used an isopiestic balance to determine the activity coefficient of Cd

over the $CeCd_{\sim 6}$ compound at two selected temperatures: 847 and 912 K. Bayanov and Serebrennikov [15] measured the activity of Ce in dilute solutions of Ce in Cd by a molten salt based emf technique in the temperature range 673-823 K and calculated the excess thermochemical properties. Johnson and Yonco[16] also used a molten salt based emf method to determine the Ce activity in the Cd-rich liquid phase in the temperature range 638-884 K and derived the molar Gibbs energy of formation of $CeCd_{11}$, using the solubility values of Ce in Cd reported by Johnson et al [7]. Colinet and Pasturel [17] compared the enthalpies and entropies of formation of $CeCd_{11}$measured by Bayanov and Serebrennikov[15] and Johnson and Yonko [16]. More recently Kurata and Sakamura [18] presented a thermodynamic assessment of RE-Cd systems although only limited information was provided for the Ce-Cd system.

Experimental

The principle and experimental details of the isopiestic method applied in this work were described previously by Ipser et al [5, 6]. A schematic diagram of the particular setup used in the present investigation is shown in Fig. 1. The apparatus is essentially made of quartz glass. It consists of an outer tube of 38 mm O.D. with one end closed and the other end fitted with a ground joint which can be connected to a vacuum pump. A quartz glass crucible with 32 mm O.D. is placed at the bottom serving as a reservoir for Cd. On top of the reservoir, a quartz glass spacer of suitable height and a quartz supporting tube (15 mm O.D.) are located where the tantalum crucibles containing pure Ce as samples are inserted. An inner tube of 7 mm O.D. with its upper end widened to 32 mm O.D. is used as a thermocouple well. The apparatus can be sealed under vacuum in its upper part.

Before use the entire apparatus was cleaned with an acid mixture ($HF/HNO_3/H_2O$), rinsed with distilled water and dried. Afterwards the fully assembled setup, including the empty tantalum crucibles (approximately 20), was degassed under vacuum (10^{-3} mbar) at 900°C for 5 h. All preparations for the experiments were then carried out under Ar atmosphere in a glove box. The reservoir was filled with 25 to 35 g of Cd (99.9999 % Alfa AESAR, Karlsruhe, Germany), depending on the experimental reservoir temperature. Between 150 and 200 mg of pure Ce (99.9 % Alfa AESAR, Karlsruhe, Germany, and smart-elements, Vienna, Austria) were weighed into each Ta crucible with an accuracy of ±0.1 mg. The assembled apparatus was brought outside the glove box securely closed using a glass stopper. It was connected to the vacuum pump, evacuated and sealed under a dynamic vacuum of better than 10^{-3} mbar.

The isopiestic equilibration experiments were carried out in different temperature gradients, applied by two-zone furnaces, for periods of about 3 to 5 weeks. The temperatures of the samples (T_S) and the reservoir (T_R) were measured periodically by raising a Pt/Pt10%Rh thermocouple inside the

thermocouple well. After equilibration, the isopiestic apparatus was quenched in cold water and cut open by a diamond saw. The individual samples (which had become Ce-Cd alloys during the equilibration) were weighed again and their compositions were derived from the mass difference which was attributed to the uptake of Cd.

Representative samples were characterized by XRD with Cu Kα radiation on a Bruker D8 Advance Diffractometer with Bragg-Brentano geometry. The XRD patterns were analyzed and refined by means of the TOPAS 3 software (provided by Bruker), applying the fundamental parameter approach for peak profile modeling. In order to check the calculated compositions selected samples were analyzed by scanning electron microscopy (SEM; Zeiss Supra 55 VP) using energy dispersive X-ray spectroscopy (EDS).

Results and discussion

Isopiestic measurements

Eight successful isopiestic experiments were carried out for the Ce-Cd system, with reservoir temperatures between 673 and 851 K corresponding to total vapor pressures of Cd between about 2 and 76 mbar, respectively. The corresponding sample temperatures were between 690 and 1080 K. Since the vapor pressure of Ce is several orders of magnitude lower compared to that of Cd it can be neglected, and it can be assumed that the total pressure in the system is due to Cd maintained at a constant temperature in the reservoir. When the final equilibrium is reached in an isopiestic experiment the partial pressure of Cd over each sample at its sample temperature T_S, $p_{Cd}(T_S)$, is equal to the vapor pressure of pure Cd at the reservoir temperature T_R, $p^0_{Cd}(T_R)$:

$$p_{\mathrm{Cd}}(T_{\mathrm{S}}) = p^0_{\mathrm{Cd}}(T_{\mathrm{R}}) \tag{1}$$

Under these circumstances the Cd activity in the samples can be calculated by the following equation:

$$a_{\mathrm{Cd}}(T_{\mathrm{S}}) = \frac{p_{\mathrm{Cd}}(T_{\mathrm{S}})}{p^0_{\mathrm{Cd}}(T_{\mathrm{S}})} = \frac{p^0_{\mathrm{Cd}}(T_{\mathrm{R}})}{p^0_{\mathrm{Cd}}(T_{\mathrm{S}})} \tag{2}$$

The vapor pressure of pure Cd as a function of temperature was taken from Binnewies and Milke [[1]9]:

$$\log\left(\frac{p^0_{\mathrm{Cd}}}{\mathrm{bar}}\right) = 8.7 - 5690 \cdot \frac{\mathrm{K}}{T} - 1.07 \cdot \log\frac{T}{\mathrm{K}} \tag{3}$$

The experimental results, i.e. sample temperature, sample composition and thermodynamic activity of Cd for each sample, are listed in Table 1. In Fig. 2 sample temperatures are plotted against sample compositions for all experimental runs (the so-called equilibrium curves) and superimposed on the phase diagram. In order to check the compositions calculated from the weight

change, selected samples were analyzed by scanning electron microscopy using energy dispersive X-ray spectroscopy (EDS). In general, the compositions agreed within 0.5 at.% and the temperatures are assumed to be accurate within ±2 K. As can be seen from Fig. 2, the equilibrium samples obtained in the experimental runs cover the concentration range between about 48 and 85 at.% Cd. The majority of the samples were single phase, namely CeCd, $CeCd_2$, $Ce_{13}Cd_{58}$ and $CeCd_6$. Interestingly, single phase samples of $CeCd_3$ could not be obtained in any of the runs suggesting that $CeCd_3$ is only slightly more stable than a two-phase mixture of its neighboring compounds. Thus the activities of Cd in the adjacent two-phase fields $CeCd_2$+$CeCd_3$ and $CeCd_3$+$Ce_{13}Cd_{58}$ are only slightly different (cf. Fig. 7). Moreover it was found that a majority of data points fall into the composition range of the phase $Ce_{13}Cd_{58}$indicating that this must be one of the most stable compounds in the Ce-Cd system, in agreement with its congruent formation from the liquid [10].

Some of the samples were obtained in various two-phase fields after equilibration, i.e. $CeCd_6$+$Ce_{13}Cd_{58}$, $Ce_{13}Cd_{58}$+$CeCd_3$, $CeCd_3$+$CeCd_2$ and $CeCd_2$+CeCd. This was probably caused by slight variations in the sample temperatures. SEM investigations of some respective two-phase samples were used to define phase boundaries and homogeneity ranges of the compounds $CeCd_6$, $Ce_{13}Cd_{58}$, $CeCd_2$ and CeCd (see Table 2).

Partial enthalpy of mixing of Cd

From the Cd vapor pressures measured over the samples in the four two-phase fields (see above) the corresponding activity values were calculated. They are plotted as ln a_{Cd} versus reciprocal temperature in Fig. 3. Assuming straight phase boundaries, i.e. no variation of the solubilities with temperature for the different compounds, one can apply an adapted Gibbs-Helmholtz equation to estimate partial molar enthalpies of mixing of Cd in these two-phase fields:

$$\frac{\partial \ln a_{\mathrm{Cd}}}{\partial(1/T)} = \frac{\Delta\overline{H}_{\mathrm{Cd}}}{R} \qquad (4)$$

Although it is obvious that the phase boundaries are not temperature independent in the investigated temperature range this procedure gives at least a good estimate of the corresponding $\Delta\overline{H}_{\mathrm{Cd}}$ values which are also included in Table 1. By comparing the slopes in Fig. 3 it can be concluded that with decreasing Cd concentration the partial molar enthalpy of mixing of Cd becomes more negative. This indicates a clearly exothermic behavior in the Ce-Cd system in the investigated composition range.

To derive partial molar enthalpies of mixing of Cd in the phase $Ce_{13}Cd_{58}$, sample temperatures for selected compositions were obtained by interpolation from the equilibrium curves in Fig. 2; the activities for these hypothetical samples were calculated according to Eq. (2), and they were plotted as a function of the reciprocal temperature (see Fig. 4). Straight lines were obtained for the selected compositions by linear regression, corresponding to the Gibbs-Helmholtz equation (4). The calculated partial molar enthalpy values of Cd over the entire homogeneity range of $Ce_{13}Cd_{58}$are shown in Fig. 5. The estimated error in the partial enthalpy values is in the range between ±1 and ±3 kJ·g-atom^{-1}. As can be seen the values vary from close to zero at the Cd-rich end to rather negative values at the Ce-rich end of the homogeneity range, indicating once more that $Ce_{13}Cd_{58}$ is a relatively stable phase. An analogous procedure was applied to estimate $\Delta\overline{H}_{\mathrm{Cd}}$ values for the phase $CeCd_2$ whereas not enough data points were available to allow such an evaluation for the two other phases $CeCd_6$and CeCd. Therefore it was assumed that $\Delta\overline{H}_{\mathrm{Cd}}$ in CeCd varies linearly between the corresponding values in the neighboring two-phase fields whereas a value of -3.1 kJ·g-atom^{-1} was assumed for the Ce-rich end of $CeCd_6$ (the same value as in the neighboring two-phase field $CeCd_6$+$Ce_{13}Cd_{58}$). All partial enthalpy values are included in Table 1.

Thermodynamic activity of Cd

The partial enthalpy values in Fig. 5 (and Table 1) were used to convert the Cd activities in $Ce_{13}Cd_{58}$ to a common temperature of 823 K (which represents an average of all experimental sample temperatures) applying an integrated form of the Gibbs-Helmholtz equation:

$$\ln a_{\mathrm{Cd}}(T_2) - \ln a_{\mathrm{Cd}}(T_1) = \frac{\Delta\overline{H}_{\mathrm{Cd}}}{R} \cdot \left(\frac{1}{T_2} - \frac{1}{T_1} \right) \qquad (5)$$

The normalized activity values are shown in Fig. 6. Once more the drastic change of the Cd activities indicates a relatively high stability of $Ce_{13}Cd_{58}$. Using the partial enthalpy values from Table 1, the activities in all other compounds as well as in all the two-phase fields were converted to the same common temperature of 823 K. The uncertainty of the ln a_{Cd} (823 K) values is less than 10 %. All these values are listed in Table 1, a corresponding plot of ln a_{Cd} over the entire composition range between 40 and 100 at.% Cd is shown in Fig. 7.

Elliott and Lemons determined Cd activities in the phase $CeCd_6$ also by means of an isopiestic method. According to their results ln a_{Cd} in this phase varies between -0.458 and -0.119 at 847 K and between -0.343 and -0.098 at 912 K. If the present results are converted to the same temperatures one obtains values between about -0.47 and -0.05 at 847 K and between about -0.44 and -0.02 at 912 K. Obviously, the agreement is quite good.

Activity of Ce and Integral Gibbs energy

The Ce activity in the two-phase field $CeCd_{11}$+L was determined by Johnson and Yonco [16] in the temperature range 638–884 K. They calculated partial excess Gibbs energies of Ce based on data for the ($CeCd_{11}$+L)/L phase boundary from an earlier investigation of the Cd-rich part of the Ce-Cd phase diagram by Johnson et al. [7], and presented the following equation:

$$\Delta\overline{G}_{Ce}^{xs} = x_{Cd}^2(-179950 + 79.20 \cdot T - 95600 \cdot x_{Ce}) \quad (6)$$

with T in K and $\Delta\overline{G}_{Ce}^{xs}$ in J·mol^{-1}. With the Ce solubility in liquid Cd and their measured Ce activities Johnson and Yonco used the Gibbs-Duhem relationship to derive Cd activities as well as integral Gibbs energies of formation in the corresponding temperature range. From this they obtained the integral Gibbs energy of formation for the compound $CeCd_{11}$ at 823 K, $\Delta_f G(CeCd_{11})$ = -11.8 kJ·g-atom^{-1}.

From Eq. (6) ln a_{Ce} = -20.45 was calculated for the boundary of the liquid phase at 823 K, and this was applied as an integration constant for a Gibbs-Duhem integration based on the present data of ln a_{Cd}. Thermodynamic activities of Ce were calculated in the composition range 48-85 at.% Cd using the so-called □-function as described by Darken and Gurry [20], and are included in Fig. 7. Having activity values both for Ce and Cd, the integral Gibbs energy of formation could be calculated at 823 K for the same composition range. It is shown as a function of composition in Fig. 8.

Homogeneity ranges of intermetallic compounds

As can be seen from Fig. 2, the kinks in the so-called equilibrium curves provide some information on the phase boundaries of some of the intermetallic compounds. It is striking that the homogeneity ranges of $CeCd_6$, $Ce_{13}Cd_{58}$, $CeCd_2$, and CeCd appear to be shifted to the Ce-rich side of the nominal stoichiometry. For example, the ln a_{Cd}-curve in $Ce_{13}Cd_{58}$ shows an inflection point at about 80.9 at.% Cd (cf. Fig. 6) although it would be expected at about 81.7 at.% Cd according to its 13/58 stoichiometry. Considering the stoichiometry of $Ce_{12.60}Cd_{58.68}$, derived from the crystallographic study by Piao et al. [13], the order composition would be expected at even higher Cd contents, i.e. at about 82.3 at.%.

Table 2 shows a comparison of the phase boundaries estimated from the isopiestic vapor pressure measurements (Fig. 2) and those derived from the SEM analyses. As can be seen, the agreement is very good for the phases $CeCd_2$ and $Ce_{13}Cd_{58}$ whereas there are some discrepancies for CeCd and $CeCd_6$. Since the number of isopiestic data points in the latter two phases is rather limited the phase boundaries from SEM should be considered being more reliable. However, this leaves still the question why the homogeneity ranges appear in general shifted to the Ce-rich side. The reason for this is not clear at the moment but may have to do with the actual crystal structures.

Summary

Thermodynamic activities of Cd were determined for the Ce-Cd system in the temperature range between 690 and 1080 K and the composition range between 48 and 85 at.% Cd based on an isopiestic vapor pressure method. The activity values were converted to a common temperature of 823 K and are given for the composition range 48 to 100 at.% Cd. Using a literature value of ln a_{Ce} as integration constant, it was possible to calculate Ce activities and integral Gibbs energies of formation for the same temperature and composition range. A minimum of ΔG_{Cd} = -37 kJ·g-atom^{-1} was obtained in the phase CeCd.

The results of the isopiestic measurements were used to obtain phase boundaries for the four intermetallic phases CeCd, $CeCd_2$, $Ce_{13}Cd_{58}$, and $CeCd_6$. These are compared with phase boundaries obtained from SEM measurements, and the agreement is found to be good for $CeCd_2$ and $Ce_{13}Cd_{58}$, whereas some discrepancies are found for the other two compounds.

Acknowledgements

Financial support by the Austrian Science Fund (FWF) under project No. P 23270-N19 and by the Scientific-Technical Cooperation Austria-India under project No. IN 05/2011 is gratefully acknowledged. In addition, the authors wish to thank Dr. Stephan Puchegger of the Faculty of Physics of the University of Vienna for his help and suggestions with the SEM measurements; likewise they want to thank Ms. Olivia Appay for help in preparing some of the isopiestic experiments in the course of an internship.

Tables

Table 1. Isopiestic experimental results; standard state: Cd (liquid).

Sample No.	Cd (at.%)	T_S (K)	$\ln a_{Cd}$ (T_S)	Phases	$\Delta\overline{H}_{Cd}$ (kJ·g-atom^{-1})	$\ln a_{Cd}$ (823 K)
Run 1	*T_R: 785 K. 37 days*					
1	81.0	850	-1.19	$Ce_{13}Cd_{58}$	-8.5	-1.23
2	81.1	861	-1.37	$Ce_{13}Cd_{58}$	-5.1	-1.41
3	68.7	873	-1.56	$CeCd_3$ + $CeCd_2$	-30.3	-1.82
4	65.6	884	-1.75	$CeCd_2$	-48.3	-2.24
5	65.8	896	-1.93	$CeCd_2$	-45.3	-2.47
6	65.4	909	-2.12	$CeCd_2$	-53.0	-2.85
7	65.9	933	-2.46	$CeCd_2$	-41.5	-3.17
8	66.0	958	-2.79	$CeCd_2$	-40.3	-3.62
9	65.3	976	-3.03	$CeCd_2$ + CeCd	-53.5	-4.25
10	64.2	994	-3.26	$CeCd_2$ + CeCd	-53.5	-4.60
11	49.1	1012	-3.47	CeCd	-57.6	-5.04
12	48.9	1036	-3.74	CeCd	-57.9	-5.48
13	49.0	1056	-3.97	CeCd	-57.8	-5.83
14	48.8	1081	-4.23	CeCd	-58.3	-6.27
Run 2	*T_R: 747 K. 42 days*					
1	85.2	758	-0.24	$CeCd_6$	-3.1	-0.20
2	85.1	767	-0.43	$CeCd_6$	-3.1	-0.40
3	81.1	777	-0.64	$Ce_{13}Cd_{58}$	-4.4	-0.60
4	80.9	788	-0.86	$Ce_{13}Cd_{58}$	-11.8	-0.78
5	80.7	808	-1.24	$Ce_{13}Cd_{58}$	-23.9	-1.18
6	80.6	823	-1.52	$Ce_{13}Cd_{58}$	-35.6	-1.52
7	77.8	842	-1.85	$Ce_{13}Cd_{58}$ + $CeCd_3$	-29.8	-1.95
Run 3	*T_R: 851 K. 29 days*					
1	85.4	870	-0.31	$CeCd_6$	-3.1	-0.34
2	81.4	877	-0.42	$Ce_{13}Cd_{58}$	-2.8	-0.45
3	81.4	884	-0.53	$Ce_{13}Cd_{58}$	-2.6	-0.56
4	81.4	890	-0.63	$Ce_{13}Cd_{58}$	-2.6	-0.66
5	81.1	896	-0.72	$Ce_{13}Cd_{58}$	-4.1	-0.77
6	81.2	900	-0.78	$Ce_{13}Cd_{58}$	-3.1	-0.82
7	81.0	904	-0.84	$Ce_{13}Cd_{58}$	-8.6	-0.95
8	80.9	909	-0.91	$Ce_{13}Cd_{58}$	-12.1	-1.08
9	80.8	917	-1.03	$Ce_{13}Cd_{58}$	-19.3	-1.32
10	80.8	921	-1.09	$Ce_{13}Cd_{58}$	-17.9	-1.36
11	80.9	924	-1.13	$Ce_{13}Cd_{58}$	-13.1	-1.34
12	80.9	929	-1.20	$Ce_{13}Cd_{58}$	-13.7	-1.43
13	80.0	931	-1.23	$Ce_{13}Cd_{58}$ + $CeCd_3$	-29.8	-1.73

14	79.8	934	-1.27	$Ce_{13}Cd_{58}$ + $CeCd_3$	-29.8	-1.79
15	79.6	937	-1.31	$Ce_{13}Cd_{58}$ + $CeCd_3$	-29.8	-1.84
16	78.4	940	-1.35	$Ce_{13}Cd_{58}$ + $CeCd_3$	-29.8	-1.89
17	71.6	944	-1.41	$CeCd_3$ + $CeCd_2$	-30.3	-1.97
Run 4	*T_R: 771 K. 32 days*					
1	85.5	782	-0.22	$CeCd_6$	-3.1	-0.20
2	85.2	788	-0.34	$CeCd_6$	-3.1	-0.32
3	85.1	796	-0.50	$CeCd_6$	-3.1	-0.48
4	81.0	806	-0.69	$Ce_{13}Cd_{58}$	-7.2	-0.67
5	80.9	818	-0.91	$Ce_{13}Cd_{58}$	-11.6	-0.90
6	80.9	832	-1.16	$Ce_{13}Cd_{58}$	-10.7	-1.18
Run 5	*T_R: 719 K. 25 days*					
1	81.5	738	-0.44	$Ce_{13}Cd_{58}$	-3.4	-0.38
2	81.3	746	-0.62	$Ce_{13}Cd_{58}$	-2.7	-0.58
3	81.1	755	-0.82	$Ce_{13}Cd_{58}$	-4.1	-0.76
4	81.1	765	-1.03	$Ce_{13}Cd_{58}$	-4.8	-0.98
5	81.0	774	-1.22	$Ce_{13}Cd_{58}$	-9.0	-1.13
6	80.9	783	-1.40	$Ce_{13}Cd_{58}$	-12.6	-1.30
7	81.0	792	-1.58	$Ce_{13}Cd_{58}$	-9.0	-1.52
8	80.7	802	-1.77	$Ce_{13}Cd_{58}$	-22.3	-1.68
9	66.5	812	-1.96	$CeCd_3$ + $CeCd_2$	-30.3	-1.90
Run 6	*T_R: 673 K. 25 days*					
1	83.9	691	-0.48	$CeCd_6$ +$Ce_{13}Cd_{58}$	-3.1	-0.39
2	81.3	700	-0.71	$Ce_{13}Cd_{58}$	-2.6	-0.64
3	81.0	709	-0.93	$Ce_{13}Cd_{58}$	-6.3	-0.78
4	80.9	719	-1.17	$Ce_{13}Cd_{58}$	-13.1	-0.90
5	80.9	730	-1.43	$Ce_{13}Cd_{58}$	-10.7	-1.23
6	80.9	741	-1.68	$Ce_{13}Cd_{58}$	-14.2	-1.45
7	80.9	753	-1.95	$Ce_{13}Cd_{58}$	-13.1	-1.77
8	80.9	764	-2.18	$Ce_{13}Cd_{58}$	-13.1	-2.03
9	67.3	775	-2.41	$CeCd_3$ + $CeCd_2$	-30.3	-2.14
10	65.9	787	-2.65	$CeCd_2$	-42.6	-2.37
11	65.7	798	-2.87	$CeCd_2$	-47.5	-2.65
12	65.8	809	-3.08	$CeCd_2$	-44.5	-2.96
13	65.9	821	-3.30	$CeCd_2$	-42.9	-3.28
14	65.8	832	-3.49	$CeCd_2$	-44.5	-3.56
15	65.8	844	-3.70	$CeCd_2$	-43.6	-3.86
16	65.8	856	-3.90	$CeCd_2$	-44.7	-4.16
17	65.8	869	-4.12	$CeCd_2$	-44.2	-4.46
18	49.2	881	-4.31	CeCd	-57.4	-4.86
19	49.0	895	-4.52	CeCd	-57.8	-5.20
20	48.9	909	-4.73	CeCd	-58.0	-5.54
21	48.6	924	-4.95	CeCd	-58.8	-5.89
22	48.1	940	-5.17	CeCd	-59.7	-6.26

Run 7	*T_R: 740 K. 25 days*					
1	81.6	764	-0.52	$Ce_{13}Cd_{58}$	-4.5	-0.47
2	81.3	775	-0.75	$Ce_{13}Cd_{58}$	-2.7	-0.73
3	81.0	786	-0.97	$Ce_{13}Cd_{58}$	-7.9	-0.92
4	80.9	797	-1.19	$Ce_{13}Cd_{58}$	-12.6	-1.13
5	80.9	808	-1.40	$Ce_{13}Cd_{58}$	-13.1	-1.36
6	80.7	819	-1.60	$Ce_{13}Cd_{58}$	-28.3	-1.58
7	80.7	830	-1.80	$Ce_{13}Cd_{58}$	-27.4	-1.83
Run 8	*T_R: 795 K. 21 days*					
1	85.5	799	-0.08	$CeCd_6$	-3.1	-0.06
2	85.1	809	-0.27	$CeCd_6$	-3.1	-0.26
3	81.5	820	-0.47	$Ce_{13}Cd_{58}$	-3.5	-0.47
4	81.2	834	-0.72	$Ce_{13}Cd_{58}$	-3.9	-0.73
5	81.0	851	-1.01	$Ce_{13}Cd_{58}$	-6.9	-1.04
6	80.9	867	-1.28	$Ce_{13}Cd_{58}$	-12.1	-1.37
7	80.7	884	-1.55	$Ce_{13}Cd_{58}$	-22.3	-1.77
8	66.3	913	-1.98	$CeCd_2$	-32.2	-2.49
9	66.0	926	-2.17	$CeCd_2$	-40.1	-2.92
10	65.9	938	-2.34	$CeCd_2$	-42.4	-3.19
11	65.7	949	-2.48	$CeCd_2$	-46.1	-3.44
12	65.8	968	-2.73	$CeCd_2$	-44.2	-3.70
13	65.6	977	-2.85	$CeCd_2$	-48.2	-3.96

Table 2. Phase boundaries at 823 K from isopiestic vapor pressure measurements (Fig. 2) and from SEM analyses.

	Phase boundaries (at.% Cd)	
Phase	***from isopiestic***	***from SEM***
CeCd	48.0 – 50.0	48.0 – 50.9
$CeCd_2$	65.4 – 66.4	65.5 – 66.4
$Ce_{13}Cd_{58}$	80.6 – 81.7	80.6 – 81.7
$CeCd_6$	85.1 – 85.7	85.8 – 86.3

Figures

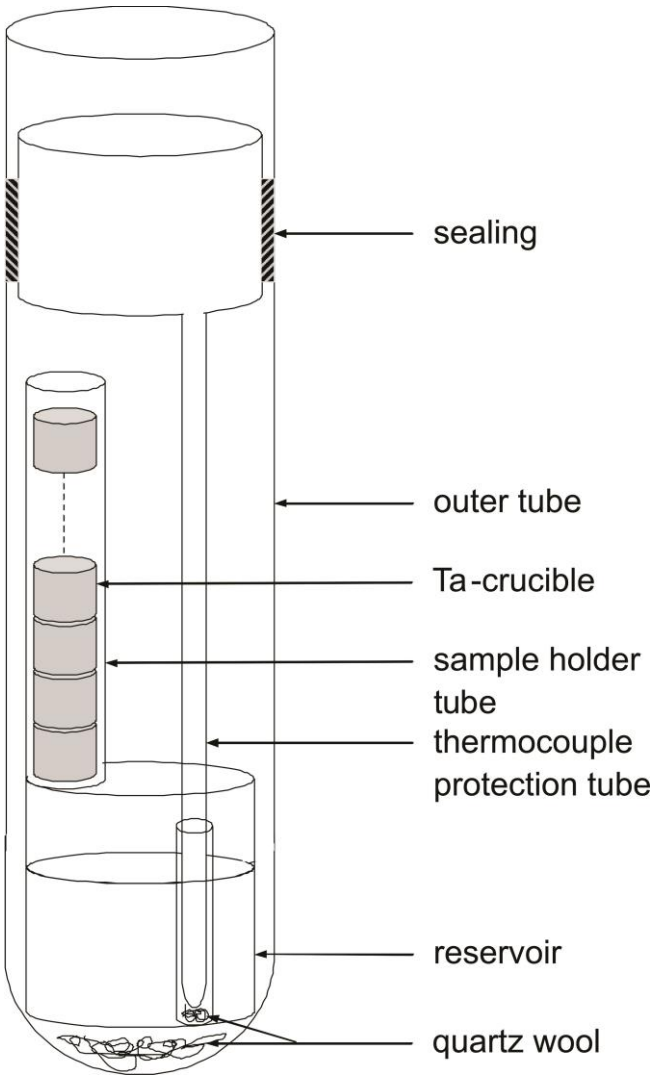

Fig. 1. The isopiestic quartz glass apparatus.

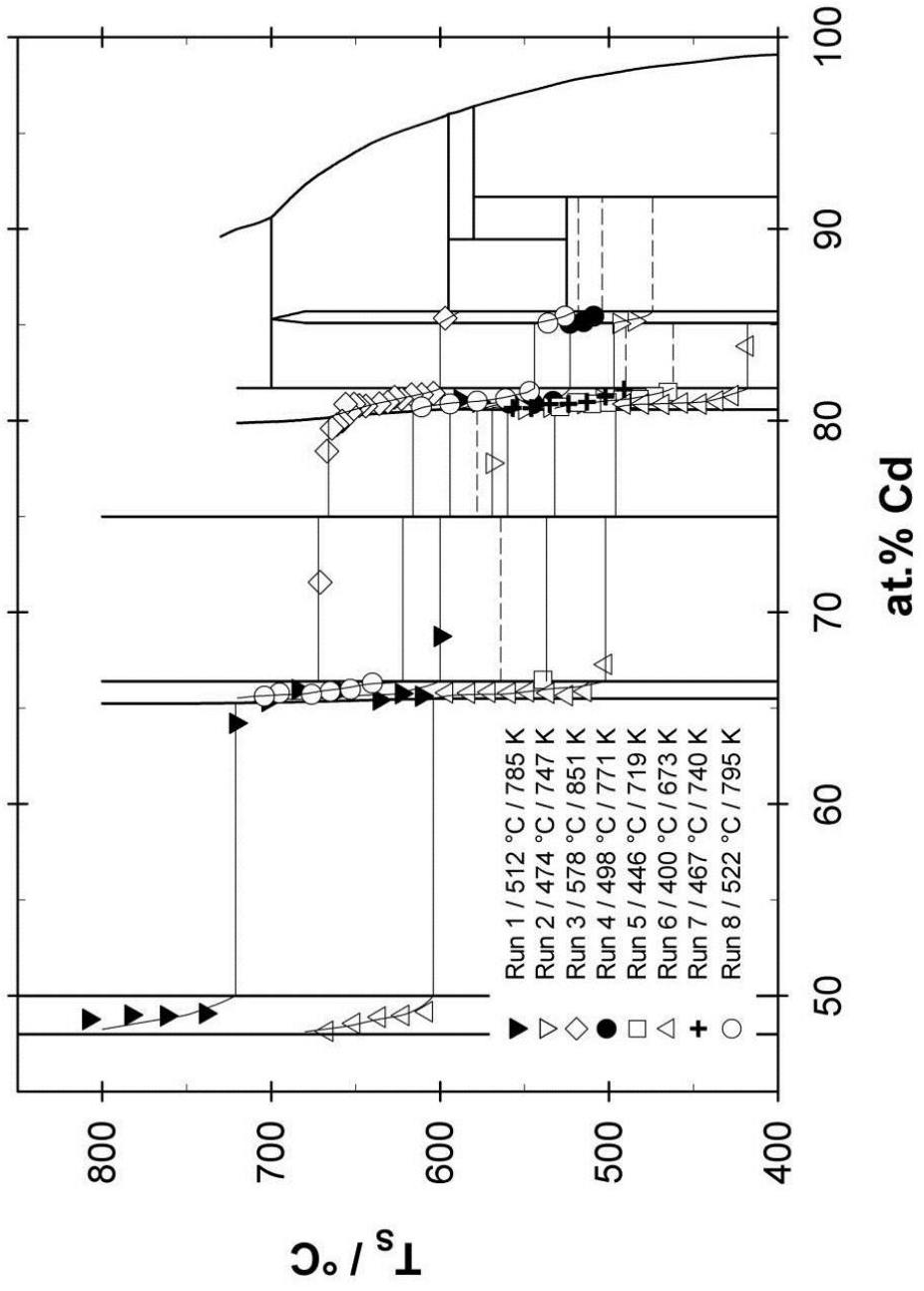

Fig. 2. Sample temperature vs. sample composition superimposed on the partial Ce-Cd phase diagram (dashed lines in two-phase fields are estimated and not supported directly by data points).

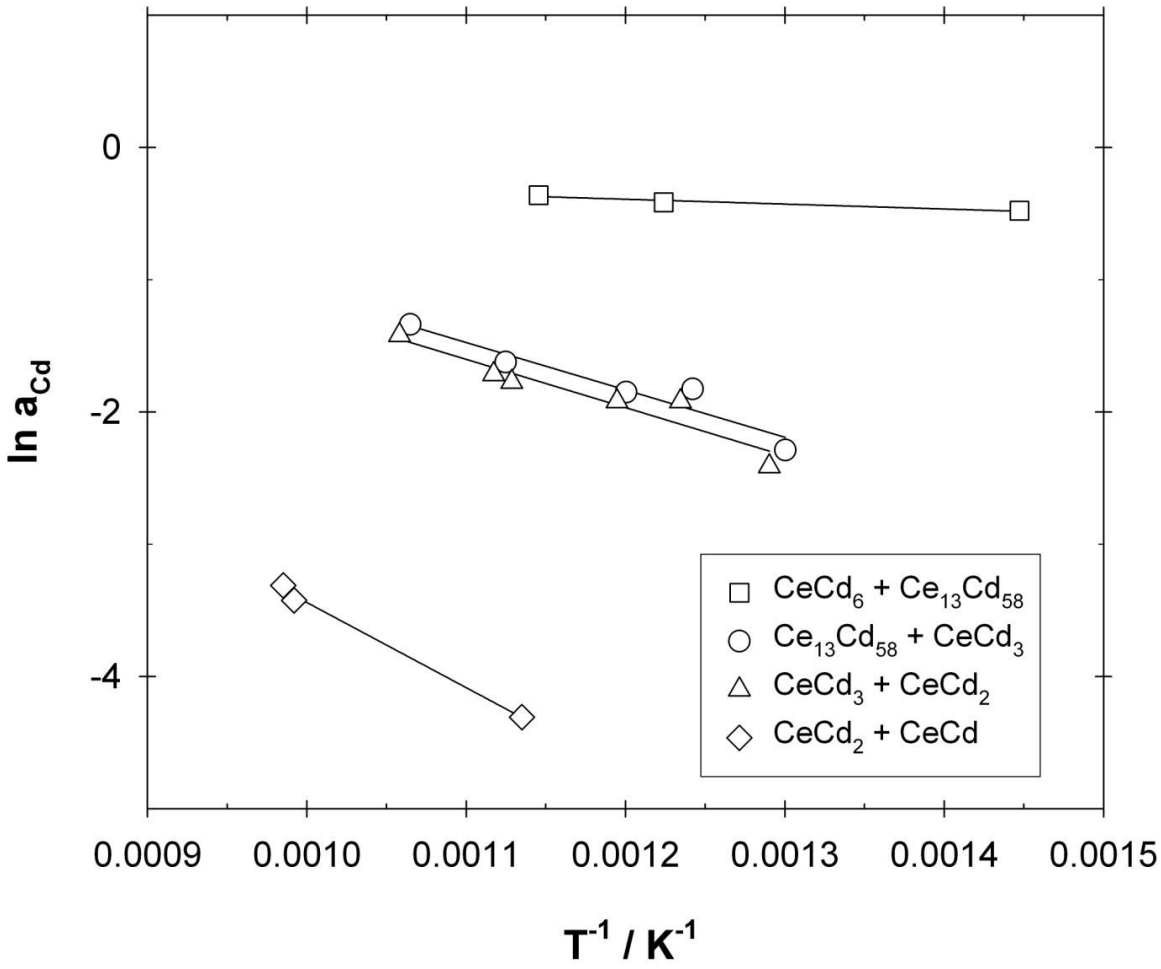

Fig. 3. Natural logarithm of the Cd activity vs. reciprocal temperature in four two-phase fields.

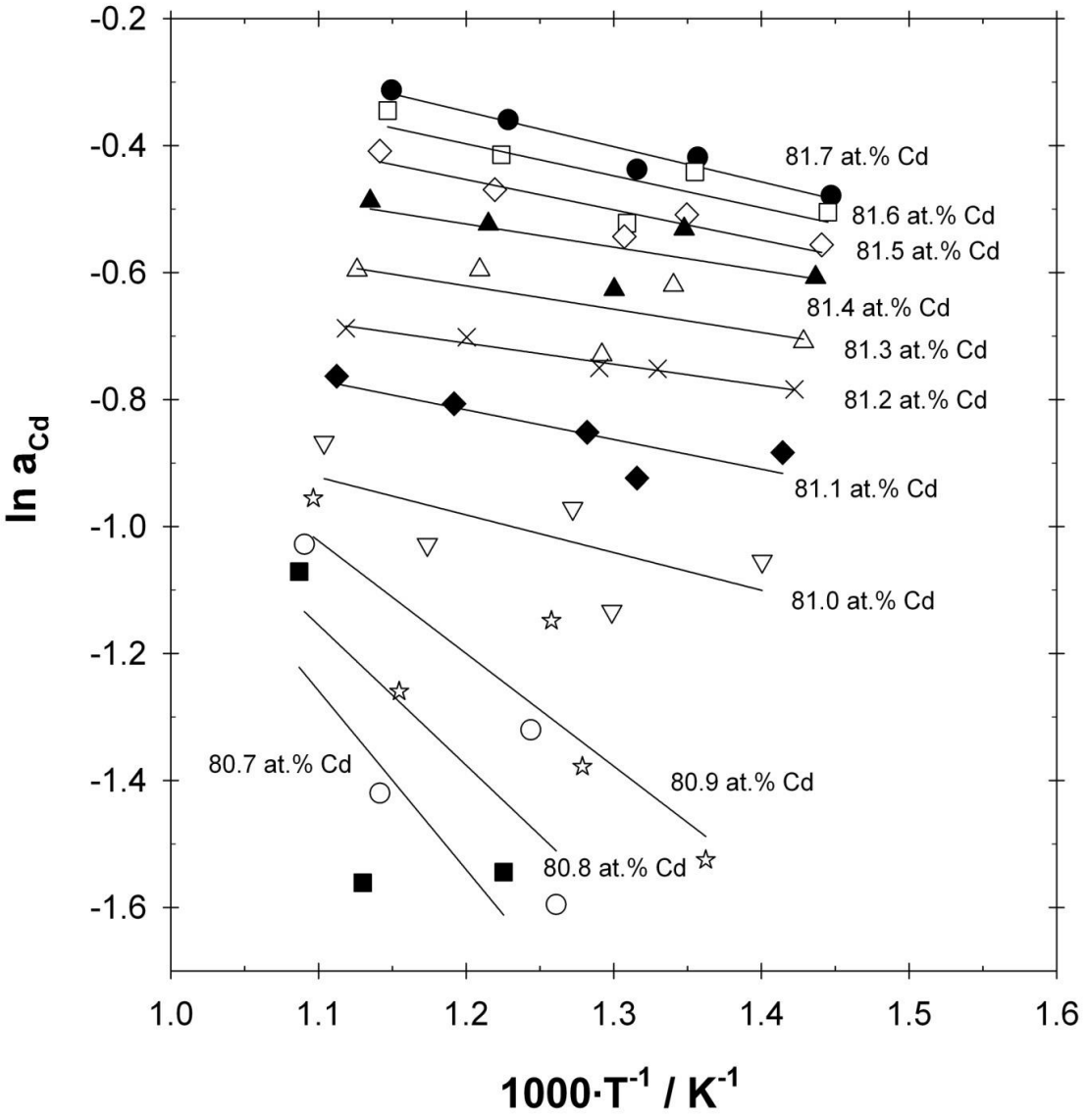

Fig. 4. Natural logarithm of the Cd activity vs. reciprocal temperature for selected compositions in the $Ce_{13}Cd_{58}$ phase.

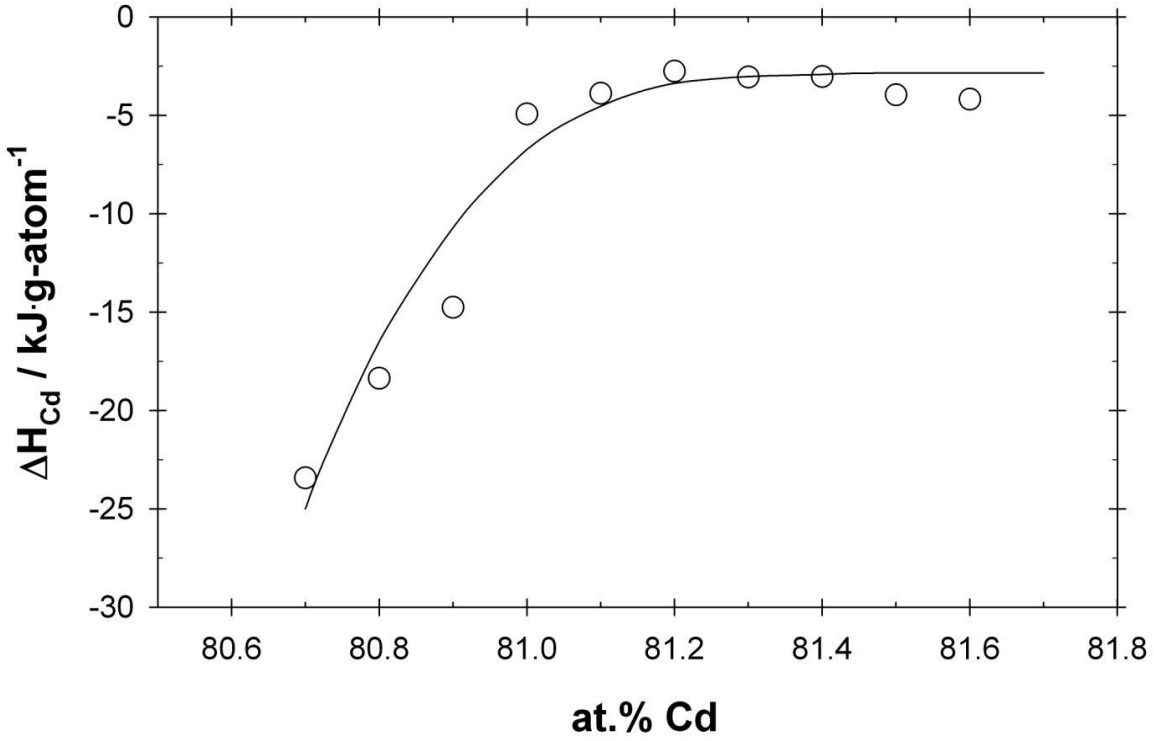

Fig. 5. Partial molar enthalpy of cadmium in $Ce_{13}Cd_{58}$ along the homogeneity range; standard state: Cd (l).

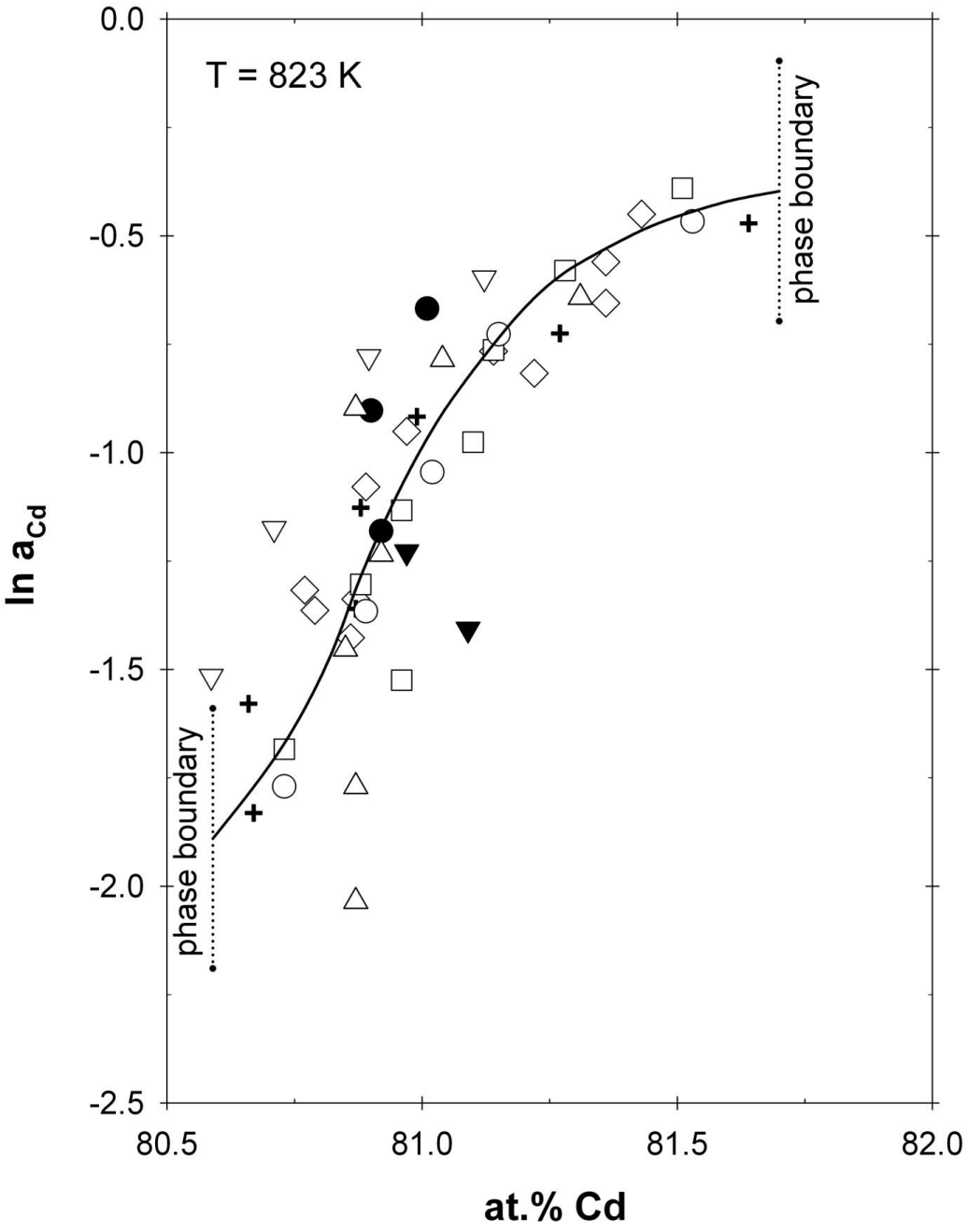

Fig. 6. Natural logarithm of the Cd activity in the $Ce_{13}Cd_{58}$ phase at 823 K; standard state: Cd(l); symbols equal to Fig. 2.

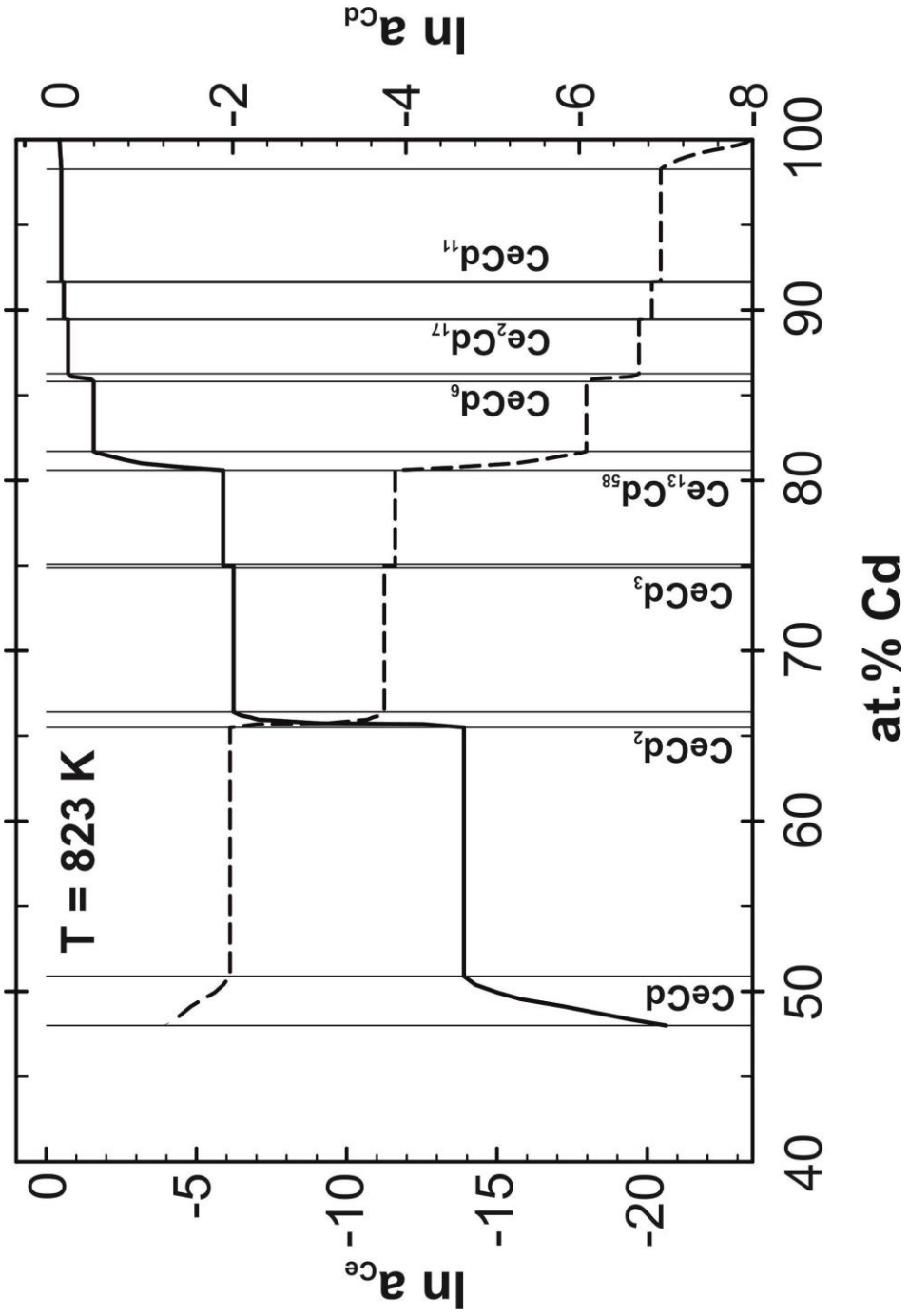

Fig. 7. Natural logarithm of the cadmium and cerium activities vs. composition at 823 K.

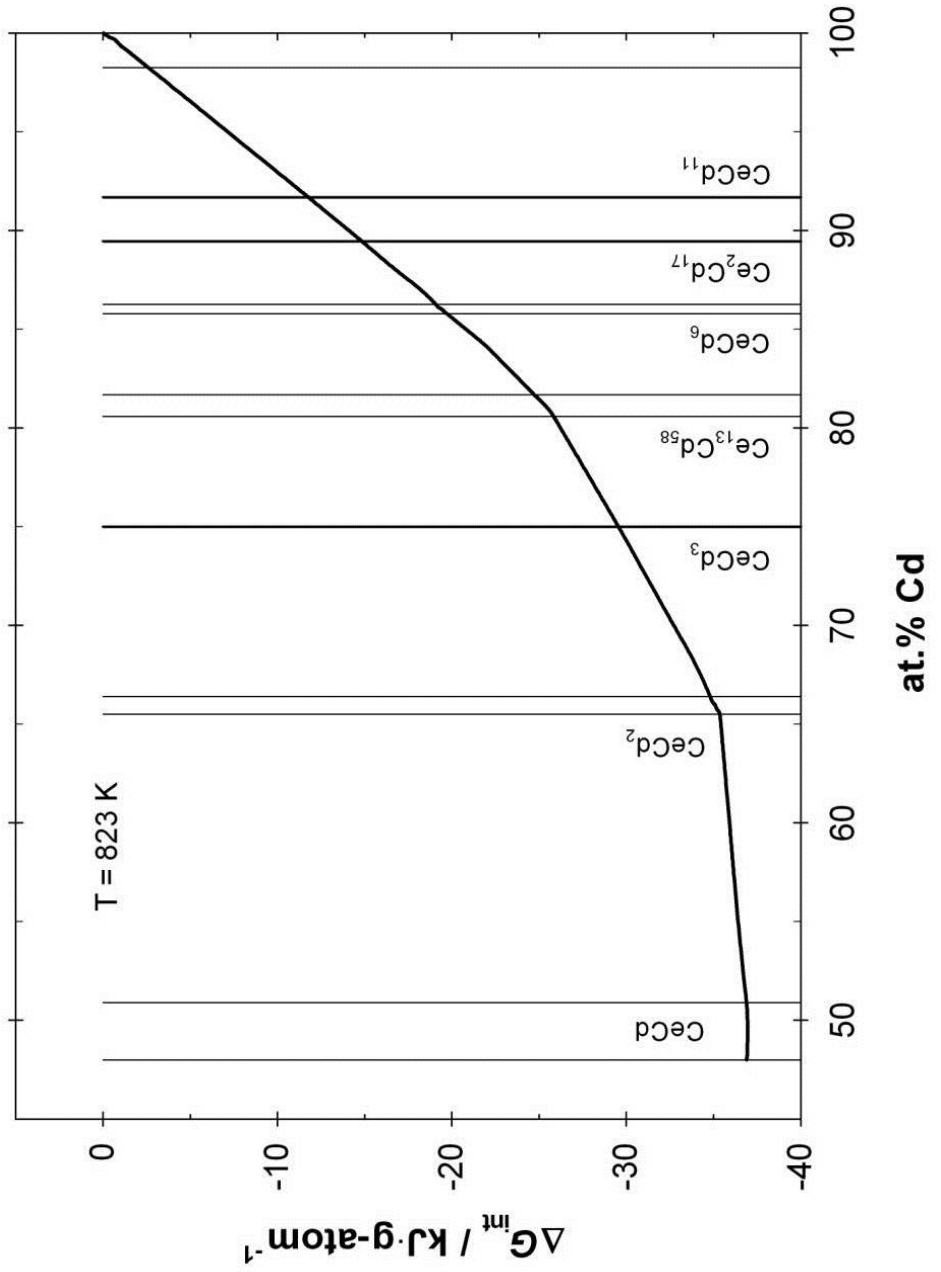

Fig. 8. Integral Gibbs energy of formation vs. composition at 823 K; standard states: Ce(s)

References

[1] Conocar O, Douyere N, Glatz J, Lacquement J, Malmbecke R, Serp J. Promising pyrochemical actinide/lanthanide separation processes using aluminum. Nucl Sci Eng 2006;153:253-261.

[2] Olander D. Nuclear fuels - Present and future. J Nucl Mater 2009;389:1-22.

[3] Kurata M, Sakamura Y, Hijikata T, Kinoshita K. Distribution behavior of uranium, neptunium, rare-earth elements (Y, La, Ce, Nd, Sm, Eu, Gd) and alkaline-rare metals (Sr, Ba) between molten LiCl-KCl eutectic salt and liquid cadmium or bismuth. J Nucl Mater 1995;227:110-121.

[4] Lukas H, Fries SG, Sundman B. Computational Thermodynamics: The Calphad Method. Cambridge: Cambridge University Press; 2007.

[5] Ipser H, Krachler R, Komarek KL. The isopiestic method and its application to a thermodynamic study to Au-Zn system. In: Brodowsky H, Schaller H-J, editors. Thermochemistry of Alloys, Dordrecht : Kulwer Academic Publisher; 1989,p. 293-306.

[6] Ipser H. Vapor pressure method: A source of experimental thermodynamic data. Ber Bunsenges Phys Chem 1998;102:1217-1223.

[7] Johnson I, Anderson KE, Blomquist RA. Partial constitutional diagram for the Cd-La, Cd-Ce, Cd-Pr, Cd-Nd, and Cd-Sm systems.Trans ASM 1966;59:352-355.

[8] Iandelli A, Ferro R. Sulle leghe del Cadmio col Lantanio, Cerio e Praeseodimio. Gazz Chim Ital 1954;84:463-478.

[9] Canepa F, Costa GA, Franceschi EA. The phase diagram of the Ce-Cd system. Lanthanide Actinide Res 1985;1:41-47.

[10] Okamoto H. Cd-Ce (cadmium-cerium). J Phase Equilibria 1999;20:636.

[11] Massalski TB. Binary Alloy Phase Diagrams. 2nd ed.Ohio: ASM International, Materials Park; 1990.

[12] Gschneidner Jr KA, Calderwood FW. The cadmium-rare earth systems. Bull Alloy Phase Diagrams1988;9:16-21.

[13] Piao SY, Palatinus L, Lidin S. All the disorder mechanisms in the 13:58 phases come together. Out of the modulated confusion rises the remarkable phase Ce12.60Cd58.68(2). Inorg Chem 2008;47:1079-1086.

[14] Elliot GRB, Lemons JF. A balanced isopiestic apparatus. Application to CeCd~6 solid solution systems. J Phys Chem 1960;64:137-145.

[15] Bayanov AP, Serebrennikov VV. E.M.F. study of the thermodynamic properties of cerium and erbium in some metallic melts. Zhurnal Fizicheskoi Khimii1965;39:717-721.

[16] Johnson I, Yonco RM. Thermodynamics of cadmium- and zinc-rich alloys in the Cd-La, Cd-Ce, Cd-Pr, Zn-La, Zn-Ce and Zn-Pr systems. Met Trans 1970;1:905-910.

[17] Colinet C, Pasturel A. Thermodynamic properties of metallic systems. In: Gschneidner Jr KA, Eyring L, Lander GH, Choppin GR, editors. Handbook on the Physics and Chemistry of Rare Earths - Lanthanides/Actinides: Physics – II, Amsterdam: Elsevier Science B.V.; 1994, p. 479-631.

[18] Kurata M, Sakamura Y. Thermodynamic assessment of system of actinide or rare earth with Cd. J Phase Equilibria 2001;22:232-240.

[19] Binnewies M, Milke E. Thermodynamical Data of Elements and Compounds, Weinheim: Wiley–VCH; 1999, p. 295.

[20] Darken LS,Gurry RW. Physical Chemistry of Metals, New York: McGraw-Hill; 1953, p. 264-265.

3.3. Phase equilibria in the neodymium-cadmium binary system

Barbara Skołyszewska-Kühberger, Thomas L. Reichmann, Herbert Ipser[*]

Department of Inorganic Chemistry (Materials Chemistry),
University of Vienna, A-1090 Wien, Austria

*Corresponding author:
E-mail address: Herbert.ipser@univie.ac.at

Published: *Journal of Alloys and Compounds* 606C (2014) 242–248

Contributions to this paper:
B.S-K.: sample preparation, analysis and interpretation, wrote the paper
T.L.R: advice in interpretation, proofreading
H.I.: proofreading, general advice and helpful comments

Contribution of B. Skołyszewska-Kühberger to this article: 85%

Abstract

The equilibrium phase diagram of the neodymium-cadmium system has been established by thermal, metallographic and X-ray analysis based on a study of 70 alloys. The system contains three congruently melting intermetallic compounds, i.e. NdCd (1040 °C), $NdCd_2$ (995 °C), $Nd_{11}Cd_{45}$ (855 °C), and four incongruently melting compounds $NdCd_3$ (860 °C), $Nd_{13}Cd_{58}$ (740°C), $NdCd_6$ (655 °C) and $NdCd_{11}$ (520 °C). Four eutectic reactions are found in this binary system, i.e. at ~25 at.% Cd and 770 °C, at 58 at.% Cd and 955 °C, at 79 at.% Cd and 850 °C, and very close to pure Cd at 318 °C, as well as one eutectoid reaction at ~15 at.% Cd and 500 °C. The solid solubility of Nd in Cd is negligible. Dilatometric curves were recorded for three Nd-Cd composition up to 4 at.% Cd, to accurately determine phase transitions between the solid solutions of Cd in the low- and high-temperature modification of Nd.

Introduction

Pyrochemical reprocessing techniques for high burn-up nuclear fuels promise more efficiency than traditional aqueous methods [1] and [2]. As described by Olander [2], pyrochemical reprocessing is based on an “electro-refining” process where a liquid metal cathode is applied for the selective recovery of Pu and minor actinides (MA). At least three different low-melting metals were investigated for this purpose: Kurata et al. [3] proposed Bi and Cd, and later on Conocar et al. obtained promising results using liquid Al [1]. As rare earth elements (RE) behave chemically in a similar way compared to minor actinides, optimal reprocessing conditions require also a detailed knowledge on the extractability of these elements, as described by Kurata et al. [3]. Accordingly, the formation of RE-Me intermetallic compounds affects the performance of the extraction process. For its optimization and better efficiency the knowledge on the existence and stability of the occurring compounds in the various binary phase diagrams RE-Me is important.

The present study has been carried out as part of a research project on the interaction of different RE elements (Ce, Pr, Nd and Gd) with Cd [4], [5], [6] and [7]. It presents the phase equilibria in the Nd–Cd system as a function of temperature and composition and specifies the existing Nd–Cd intermetallic compounds as well as all phase reactions among them.

A first partial Nd–Cd phase diagram was reported by Elliot [8] who presented the Cd-rich part for temperatures up to 600 °C. The first more detailed study of the Nd–Cd phase diagram was provided by Iandelli [9] and [10] who described the crystal structure of four intermetallic compounds, i.e. NdCd, $NdCd_2$, $NdCd_3$ and $NdCd_{11}$, applying X-ray diffraction (XRD). Nevertheless, no information concerning the melting temperatures of these compounds was given. It was later summarized by Gschneidner [11] with additional information about two allotropic modifications of Nd: α-Nd [12] and the high temperature modification β-Nd [13]. Further work in this system was done by Johnson et al. [14] and [15] who determined the solubility of Nd

in liquid Cd by chemical analysis of filtered samples of the equilibrium liquid phase in the temperature range 347–498 °C. The most Cd-rich compound in equilibrium with liquid Cd is $NdCd_{11}$. The peritectic decomposition of this phase at 530 °C was examined for a sample containing about 5 at.% Nd using differential thermal analysis (DTA). A maximum solubility of Nd at this peritectic was calculated as 2.6 at.% [15] and [16]. The existence of cubic $RECd_6$ was discussed by Johnson et al. [16], and later on the crystal structure of YCd_6, that shows close relationship with $NdCd_6$, was determined [17]. Bruzzone et al. [18] determined the existence and crystal structure of the following Nd–Cd compounds by use of metallographic and X-ray methods: $NdCd_4$ (γ-brass type) and $Nd_2Cd_{9\sim}$ ($Pu_{13}Zn_{58}$ type). The existence of a phase with the $Pu_{13}Zn_{58}$ type structure had been reported earlier by Iandelli and Ferro [19] but only for the La–Cd and Ce–Cd system. A rudimentary phase diagram of the Nd–Cd system can be found in Massalski's handbook [20], based mainly on the earlier work by Johnson et al. [15] and [16] and on the assessment of Gschneidner and Calderwood [21]. Seven intermetallic compounds are known which were also summarized by Colinet and Pasturel [22]. Table 1 compiles crystallographic data for all binary compounds and solid solutions that were determined in the Nd–Cd phase diagram.

Veleckis and van Deventer [23] listed temperatures for various "RE-RECd eutectics" obtained experimentally, among them a value of 486 °C for the Nd–Cd system. However, this value is obviously flawed due to the approximation of results derived from the Denbigh equation [21] and is far off the value proposed later in Ref. [20] (about 650 °C).

Literature review

Phase diagram

The Ce-Cd phase diagram appears to be reasonably well known. Johnson et al [7] determined a partial phase diagram in the Cd-rich part, i.e. they established the liquidus line in the composition range up to about 1 at.% Ce by measuring the solubility of Ce in liquid Cd by chemical analysis; they also examined the peritectic decomposition temperature of $CeCd_{11}$ by differential thermal analysis (DTA). Iandelli and Ferro [8] who applied micrography and X-ray diffraction (XRD), reported the existence of the six compounds CeCd, $CeCd_2$, $CeCd_3$, Ce_2Cd_9, $CeCd_6$ and $CeCd_{11}$. The complete phase diagram was experimentally investigated by Canepa et al [9] applying DTA, XRD and metallography. They found one additional high-temperature phase (Ce_2Cd_{17}). Their phase diagram version was the basis for the compilation by Okamoto [10] whereas Massalski et al. [11] still showed only a partial phase diagram. Systematic trends in the phase diagrams of the RE-Cd systems were discussed in a compilation by Gschneidner and Calderwood [12].

According to Okamoto [10] the system is characterized by seven intermetallic compounds, of which three (CeCd, $CeCd_2$, and $Ce_{13}Cd_{58}$) show a congruent melting behavior and the others ($CeCd_3$, $CeCd_6$, Ce_2Cd_{17}, and $CeCd_{11}$) are formed through peritectic reactions. All compounds are shown as line compounds without any significant homogeneity range. Only very recently Piao et al [13] discussed in detail the crystal structure of the compound $Ce_{13}Cd_{58}$ and its complicated disorder mechanism.

Thermochemical data

One of the earliest results on this system was given by Elliot and Lemons [14]. They used an isopiestic balance to determine the activity coefficient of Cd

over the $CeCd_{\sim 6}$ compound at two selected temperatures: 847 and 912 K. Bayanov and Serebrennikov [15] measured the activity of Ce in dilute solutions of Ce in Cd by a molten salt based emf technique in the temperature range 673-823 K and calculated the excess thermochemical properties. Johnson and Yonco[16] also used a molten salt based emf method to determine the Ce activity in the Cd-rich liquid phase in the temperature range 638-884 K and derived the molar Gibbs energy of formation of $CeCd_{11}$, using the solubility values of Ce in Cd reported by Johnson et al [7]. Colinet and Pasturel [17] compared the enthalpies and entropies of formation of $CeCd_{11}$measured by Bayanov and Serebrennikov[15] and Johnson and Yonko [16]. More recently Kurata and Sakamura [18] presented a thermodynamic assessment of RE-Cd systems although only limited information was provided for the Ce-Cd system.

Experimental

The starting materials used to prepare the Nd–Cd alloys were Cd shot (United Mineral & Chemical Corporation, U.S.A., and Alfa Aesar, Karlsruhe, Germany; both 99.9999%) and Nd in form of foil/rod (Alfa Aesar, Karlsruhe, Germany; 99.9%) and pieces (smart-elements, Vienna, Austria, 99.9%). Due to the high reactivity of Nd the preparation procedure was done in a glove box (MBraun Labmaster 130) under an Ar atmosphere (<1 ppm O_2, <1 ppm H_2O). Before use, the Nd pieces were cleaned with a file until a shiny surface was obtained. Calculated amounts of Nd and Cd were weighed on a semi-micro balance with an accuracy of at least ±0.5 mg.

The high reactivity of Nd with water and oxygen [24] as well as the high volatility of Cd restricts the number of materials that can be used for sample preparation. RE metals attack alumina and quartz glass largely at high temperature preventing their application. Tantalum had been found to be an ideal material. No intermetallic compounds are formed in the Nd–Ta system [20], and only a very slight pick-up of Ta by RE metals was reported by Spedding and Daane [25]. Dennison et al. [26] and [27] determined the very low solubility of Ta in liquid Nd only for high temperatures between 1547 and 2070 °C. The result of the assessment by Garg et al. [28] indicated a negligible (0.006 at.%) solubility of Nd in Ta at 1021 °C. In addition, a Ta crucible can be easily closed with a corresponding Ta lid by welding in a standard arc furnace [29] providing sufficient protection of the contained sample.

Therefore, all alloys were prepared in Ta crucibles (10 mm O.D., 15 mm height) which were closed by welding with a corresponding lid in a water-cooled arc furnace under an Ar pressure of 0.5 bar. The mass loss during the whole sample preparation procedure was usually below ±0.2 mg and did not significantly affect the sample composition. The total sample weight was usually 1 g, for dilatometric studies 2 g samples were prepared. The closed Ta crucibles were sealed separately in quartz glass tubes under 10^{-3} mbar and

placed into a muffle furnace for various durations ranging from 3 to 12 weeks. Initially, all samples were melted for proper homogenization for at least 3 days; for samples containing ⩽70 at.% Cd a temperature of 1050 °C was selected which is slightly above the melting point of pure Nd, all other samples were kept at 700 °C. Afterward, different heat treatment steps were applied in the temperature range between 200 and 850 °C (see Table 3). The annealed samples were quenched in cold water and characterized by X-ray diffraction (XRD), light optical microscopy (LOM), energy dispersive X-ray spectroscopy (EDS) and differential thermal analysis (DTA). Additional dilatometric measurements were carried out for three Nd-rich samples.

Phase identification was done by powder XRD using Cu Kα radiation on a Bruker D8 Advance Diffractometer with Bragg–Brentano focusing geometry. For this purpose, sample pieces were powdered inside the glove box and afterward glued to a carrier by use of Vaseline dissolved in n-hexane. Special sample holders with X-ray transparent lids were used to prevent sample powders from oxidation. The XRD patterns were analyzed and refined by means of the TOPAS 3 software (provided by Bruker), applying the fundamental parameter approach for peak profile modeling.

For metallographic studies, pieces of the quenched samples were first embedded in a resin/carbon mixture, ground under paraffin oil or kerosene, polished with an oil-based diamond suspension and finally cleaned in an ultrasonic bath with n-hexane. With increasing Nd content the surface oxidation rate increased, hence, the polishing of samples containing more than 50 at.% Nd was more laborious and required a rapid transfer into the glove box. The quality of the polished samples was checked in a LOM (Zeiss Axiotech 100). In order to investigate microstructures and chemical compositions of the samples, a scanning electron microscope (SEM: Zeiss Supra 55 VP) with directly coupled EDS was applied. The measurements were performed at an acceleration voltage in the range of 15–20 kV. Pure Co acted as a standard to control parameters of the measured beam.

Differential thermal analyses were carried out on a DTA 404 S and DSC 404 PC as well as on a SETARAM Setsys Evolution, using Pt/Pt10%Rh

thermocouples. The instruments were calibrated at the melting points of high purity metals: Ag, Cu, Ni and Zn. A sample mass of 100 mg was used for the experiments and high-purity γ-Al_2O_3 was employed as reference material. All samples, except pure Cd, underwent two heating and cooling cycles using a heating/cooling rate of 2 K min^{-1} (as-cast samples) and 5 K min^{-1} (annealed samples). They were contained in hermetically closed Ta-crucibles with plane bottoms (for better contact) which were formed using a hydraulic press. A constant Ar flow of 50 ml min^{-1} was applied in the DTA furnace chamber. The accuracy of the temperatures determined from the DTA curves is estimated to be better than ±2 °C.

Samples containing 1, 2, and 4 at.% Cd were also studied on heating and cooling by dilatometry using a horizontal dilatometer (Netzsch 402E) with inner tube diameter of 35 mm. The samples were prepared in closed Ta tubes (12 mm O.D., 35 mm long) and annealed at 200 °C. After an equilibration time of 12 weeks, the alloys were cut and precisely machined into the form of cuboids. In order to compare the DTA results with those from dilatometry, similar experimental conditions like heating and cooling rate (5 K min^{-1}) as well as an Ar flow of 50 ml min^{-1} were used.

Results and discussion

The equilibrium phase diagram

A total number of 70 samples were annealed and characterized by powder-XRD, SEM and DTA to obtain a complete description of the Nd–Cd phase diagram. Equilibrated samples and as-cast alloys were consulted to define homogeneity ranges, phase equilibria and crystallization behavior. Relevant samples, examined with isothermal methods, are listed in Table 2. Moreover, dilatometric measurements were performed to determine phase boundaries in the Nd-rich part (compare chapter *Dilatometic study*).

Based on the combined results from isothermal and dynamic methods as well as dilatometric measurements, a complete version of the Nd–Cd phase diagram was drawn, which is given in Fig. 1. All seven intermetallic compounds which were found in literature (Table 1) could be obtained in equilibrated samples. Lattice parameters and phase compositions of phases in relevant samples are listed along the complete composition range in Table 2. The corresponding phase boundaries of all intermetallic compounds as well as solid solutions are listed in Table 3 together with estimated homogeneity ranges from isopiestic vapor pressure measurements [30]. It is striking that the homogeneity ranges of all phases appear to be shifted toward the Nd-rich side of the nominal stoichiometry, something that had already been observed in other RE-Cd systems [4], [5], [6] and [7].

All experiments to obtain single-phase samples of the solid solutions of Nd by quenching failed. Although the solid solution of Cd in α-Nd could be clearly identified from the present EDX results, minor amounts of unreacted Nd were always present. Similarly, the high-temperature modification β-Nd could be observed in quenched samples but most of the corresponding microstructures showed inhomogeneities.

Besides, XRD investigations showed the presence of unreacted Cd in some quenched samples with nominal compositions between 0 and 90 at.%

Cd (cf. the pattern of sample $Nd_{37}Cd_{63}$ in Fig. 2). It has to be assumed that, due to rapid quenching of the sample, evaporated Cd condensed on the surface of the specimen. Therefore, the XRD pattern shows traces of Cd while the SEM micrograph does not. In fact, these relatively small amounts of Cd which had been evaporated and re-condensed on the sample surface on quenching did not significantly change the nominal compositions of the samples. Thus, the expected phase equilibria were reached in most of the samples which had been prepared with nominal compositions located in two-phase fields (see Table 2).

While most of the samples which contained intermetallic compounds turned out to be rather brittle, powdering of alloys containing the phases NdCd and $NdCd_2$ was very difficult due to their rather significant ductility. This is in agreement with observations in the related Gd–Cd system [31] where Vickers hardness measurements showed that the phases $GdCd_2$ and GdCd exhibited the lowest hardness values. Since $GdCd_2$ and GdCd are isotypic with the present compounds $NdCd_2$ and NdCd a similar mechanical behavior was to be expected and, in fact, observed. Consequently, the XRD-powder patterns of $NdCd_2$ and NdCd showed rather broad peak shapes. Additionally, absorption phenomena of these Nd-rich phases lowered also the intensities and made it altogether difficult to derive accurate lattice parameters.

Evaluation of isothermal and dynamic measurements

Samples studied by DTA are listed in Table 4, together with their thermal effects from two heating and cooling cycles, respectively. The temperatures for invariant effects in Fig. 1 are given as the average values from several independent measurements indicating error limits of ±5 °C or less. Generally, the results obtained for the as-cast samples are in good agreement with those for the annealed ones.

For each sample two heating and cooling cycles were performed at a heating rate of 2 K min^{-1} (as-cast samples) and 5 K min^{-1} (annealed

samples) in order to check if equilibrium conditions can be restored after the first melting of the sample. Liquidus effects were evaluated both on heating and cooling if possible; all other effects were taken from the heating curves only. All invariant reactions, evaluated from the present results, are listed in Table 5 together with the respective reaction temperatures and types and the phase compositions. As can be seen, the intermetallic compounds $NdCd_{11}$, $NdCd_6$, $Nd_{13}Cd_{58}$ and $NdCd_3$ are formed incongruently whereas $Nd_{11}Cd_{45}$, $NdCd_2$ and NdCd show congruent melting behavior.

According to literature [11], the transition between α-Nd and β-Nd occurs at 862 °C, and the melting point of Nd is at 1024 °C [11] or 1021 °C [21], respectively. Attempts to reproduce these values gave inconclusive results: the α to β transition appeared to be at lower temperature, and the melting point was indicated at higher temperature; however the corresponding melting effect in the DTA resembled more a typical non-invariant effect than a clear DTA signal which one might expect from an invariant melting point of a pure substance. From this it must be concluded that the impurity content (probably most of it oxygen) of the Nd was still high enough to prevent the determination of a reliable melting point. Thus we kept the literature values for the α-Nd to β-Nd transition (862 °C) and the melting point of β-Nd (1021 °C) for the present phase diagram.

Extended solid solutions of Cd in both α-Nd and β-Nd were reported earlier [12] and [13] and could be confirmed in the present study. The respective solubility limits of Cd within Nd were determined at about 3 (α-Nd) and 19 at.% (β-Nd) in the present study (cf. Table 1). It was observed that Cd stabilizes β-Nd down to 500 °C were it decomposes in a eutectoid reaction forming α-Nd and NdCd. At 770 °C β-Nd is formed according to the eutectic reaction L = β-Nd + NdCd. The recorded DTA curve for the sample $Nd_{60}Cd_{40}$, annealed at 400 °C for 6 weeks, is given in Fig. 3. Both, the eutectoid and the eutectic reaction as well as the melting effect can be clearly distinguished. Nevertheless, the eutectoid reaction could not be observed in the heating and cooling curves of the sample $Nd_{55}Cd_{45}$. Most probably, the effect is already too weak due to an insignificant amount of α-Nd in the sample.

The compound NdCd melts congruently at 1040 °C and forms a eutectic (58 at.% Cd) with $NdCd_2$ at 960 °C: L = NdCd + $NdCd_2$. The microstructure of the sample $Nd_{46}Cd_{54}$, representing the structure of the eutectic between NdCd and $NdCd_2$, is shown in Fig. 4. NdCd shows a relatively broad homogeneity range. Its limiting compositions were determined as 47 and 50.6 at.% Cd at 850 °C (cf. Table 3).

For compositions between 54 and 77 at.% Cd some additional thermal effects were noticed in the temperature range 860–960 °C, most probably corresponding to the transformation of $NdCd_2$ into a high temperature modification (shown as β-$NdCd_2$ in Fig. 1). Such a polymorphic modification of $RECd_2$ intermetallic phases was already found in other RE-Cd systems, for example in the systems Gd–Cd [31] and Pr–Cd [4]. Unfortunately, all attempts to synthesize the high temperature modification β-$NdCd_2$ and retain it by quenching were unsuccessful. The intermetallic compound $NdCd_2$ has a congruent melting point at 995 °C and takes part in the peritectic formation reaction of $NdCd_3$ at 860 °C which is clearly observed by DTA for samples between 70 and 78 at.% Cd. For example, for the sample $Nd_{22}Cd_{78}$ two sharp DTA peaks were registered: the peritectic decomposition of $NdCd_3$ as well as the eutectic reaction between $NdCd_3$ and $Nd_{11}Cd_{45}$ at 850 °C and 79 at.% Cd. No separate liquidus effect could be recognized in this sample, neither on heating nor on cooling, which indicates that it must be very close to the peritectic reaction temperature.

The intermetallic compound $Nd_{11}Cd_{45}$ with a nominal composition of 80.4 at.% Cd melts congruently at 855 °C which is an average value of several independent DTA measurements. Metallographic examination of the sample $Nd_{22}Cd_{78}$, annealed at 600 °C for 4 weeks, showed the presence of both phases, $NdCd_3$ and $Nd_{11}Cd_{45}$ (Fig. 5). At this temperature $Nd_{11}Cd_{45}$ dissolves about 1 at.% Nd (cf. Table 3). This solubility was also indicated by isopiestic vapor pressure measurements [30].

It can be recognized that the liquidus curve decreases rather steeply between 80.4 and 100 at.% Cd. In this composition range, three consecutive peritectic reactions occur: at 740 °C the phase $Nd_{13}Cd_{58}$ is formed, followed by

the peritectic formation of $NdCd_6$ and $NdCd_{11}$ at 655 and 520 °C, respectively. $NdCd_6$ showed a slight variation of the solubility of Nd with temperature and its homogeneity range is limited on the Nd-rich side at 84.6 at.% Cd at 600 °C. No significant solid solubility was determined for $NdCd_{11}$ which seems to be a line compound.

Similarly as reported by Johnson et al. [15], the liquidus temperature of an annealed sample with 5 at.% Nd could not be determined from the heating curve, however, it was observed during cooling. Nevertheless, for the as-cast sample Nd_4Cd_{96} it was clearly registered also on heating using a rate of 2 K min^{-1}.

In other RE-Cd systems, Bruzzone and Merlo [32] and Canepa et al. [33] indicated the tendency to supercooling for compositions between 3 and 15 at.% La or Ce, respectively. A similar tendency was also observed in this work, especially for sample compositions up to approximately 35 at.% Nd (see Table 4).

The shape of the liquidus curve between 97.4 and 100 at.% Cd was drawn following the extrapolation of the data listed in Ref. [15]. A strong invariant effect was noticed at 318 °C, which corresponds to the eutectic $L = NdCd_{11} + Cd$. When extrapolating the equation, given by Johnson et al. [14], to the eutectic temperature, the eutectic point itself would be at 0.017 at.%. No significant solid solubility of Nd in Cd was detected by SEM in the present study.

For the Cd-rich part of the phase diagram, the detected reaction temperatures were roughly comparable with values given in Ref. [20]: the peritectic decomposition of $NdCd_{11}$, reported at 530 °C in Ref. [20], was found here at 520 °C, and the eutectic between $NdCd_{11}$ and Cd was found at 318 °C instead of 321 °C in Ref. [20]. The value of 318 °C seems to be reasonable if compared with the published experimental data for the analogous eutectics in the Ce–Cd [33] as well as the Gd–Cd [31] systems, i.e. 315 and 316 °C, respectively.

For the annealed DTA samples, oxidation of the Ta-crucibles was observed after DTA measurements in cases when samples where heated

above 1000 °C. Apparently, Ta behaved as a getter material for oxygen traces in the DTA furnace chamber. Selected Ta crucibles were sectioned and both surface and cross-section were analyzed by SEM. Only minor amounts of Ta (up to 0.3 at.%) were observed in the corresponding samples, mostly in the part directly sticking to the crucible walls. It is assumed that this arises rather from a contamination during sample polishing than from a reaction of the sample with the crucible material itself.

Dilatometric study

Dilatometric curves display several effects observed upon heating of solid Nd–Cd samples. Although the signals of the recorded dimensional changes were weak, they nevertheless provided some additional information. Due to the high volatility of Cd only the following Nd-rich samples were investigated: $Nd_{99}Cd_1$, $Nd_{98}Cd_2$ and $Nd_{96}Cd_4$. The observed curve for the sample with 2 at.% Cd shows a similarity to the recorded DTA curve. It is presented in Fig. 6a, and the results can be summarized as follows:

(a) a sharp initial contraction (curve A–B);

(b) an expansion during heating with a slight maximum at about 440 °C (B′) corresponding to the phase boundary crossing α-Nd + NdCd → α-Nd (curve B–C);

(c) a decrease of the expansion rate between about 750 and 815 °C representing probably the transition into the two-phase field α-Nd + β-Nd (curve C–D);

(d) an increased expansion in the range between 815 °C and 950 °C (curve D–E);

(e) a shrinkage during the isothermal holding at 950 °C (curve E–F);

(f) a further contraction during cooling with a small effect (G) at about 810 °C which is probably connected to the phase boundary crossing β-Nd → α-Nd + β-Nd (curve F–G);

(g) a final contraction.

For the $Nd_{96}Cd_4$ sample the eutectoid reaction at 500 °C was indicated in the dilatometric curve during heating (A in Fig. 6b). DTA measurements of the latter sample did not show an effect which could be ascribed to the eutectoid reaction, probably because of the low sensitivity. A rather implausible contraction can be observed after point A in the dilatometric curve which was probably caused by a contraction of the sample during the eutectoid reaction which caused it to slip out of the specimen holder inside the dilatometer.

Fig. 7 shows the Nd-rich part of the Nd–Cd phase diagram with the effects recorded DTA and dilatometry (with a heating rate of 5 K min^{-1}). Obviously, these experimental data agree very well.

Summary

The Nd–Cd phase diagram was constructed using a combination of DTA, SEM, XRD and dilatometry data (Fig. 1). Cd solubilities in both α-Nd and β-Nd were determined and are listed in Table 1. Seven intermetallic compounds, described previously in literature, were confirmed and their phase boundaries were estimated by a combination of all available results. A congruent formation of NdCd, $NdCd_2$ and $Nd_{11}Cd_{45}$ was found whereas $NdCd_3$, $Nd_{13}Cd_{58}$, $NdCd_6$ and $NdCd_{11}$ decompose incongruently. The temperature values of the peritectic formation of $NdCd_{11}$ and of the eutectic between $NdCd_{11}$ and Cd were comparable with those given in Ref. [20], other invariant reaction temperatures had to be modified with respect to the literature values. Due to DTA results a polymorphic transition of $NdCd_2$ is proposed although the high temperature form β-NdCd could not be quenched. X-ray diffraction was used to confirm the crystal structure of all intermetallic compounds.

A dilatometric study was performed for Nd–Cd samples up to 4 at.% Cd. The results fit well with DTA data. α-Nd seems to have a higher thermal expansion than β-Nd.

Acknowledgements

This work was financially supported by the Austrian Science Fund (FWF) under Project No. P 23270-N19 as well as by the Scientific-Technical Cooperation Austria-India under Project No. IN 05/2011. The authors are grateful to Dr. Stephan Puchegger of the Faculty of Physics of the University of Vienna for his help and suggestions with the SEM measurements. The authors wish to thank Dr. Tadeusz Pieczonka from the AGH University of Science and Technology, Kraków, Poland, for his help with the dilatometric measurements.

Tables

Table 1. Crystal structure data (from literature) of phases in the Nd-Cd system.

Phase	Composition (at.% Cd)	Structure type	Pearson symbol	Space group	Ref.
α-Nd	0 – 3.0 [a]	α-La	*hP4*	*P6$_3$/mmc*	[12]
β-Nd	0 – 19.0 [a]	W	*cI2*	*Im3m*	[13]
NdCd	50.0 [b]	CsCl	*cP2*	*Pm$\bar{3}$m*	[9, 10]
$NdCd_2$	66.7 [b]	CdI_2	*hP3*	*P$\bar{3}$m1*	[9, 10]
$NdCd_3$	75.0 [b]	BiF_3	*cF16*	*Fm$\bar{3}$m*	[9, 10]
$Nd_{11}Cd_{45}$	80.4 [b]	γ-brass	*cF448*	*F$\bar{4}$3m*	[18]
$Nd_{13}Cd_{58}$	81.7 [b]	$Pu_{13}Zn_{58}$	*hP142*	*P6$_3$/mmc*	[18]
$NdCd_6$	85.7 [b]	YCd_6	*cI168*	*Im$\bar{3}$*	[17]
$NdCd_{11}$	91.7 [b]	$BaHg_{11}$	*cP36*	*Pm$\bar{3}$m*	[9,10]

[a] derived from the present results
[b] given by Massalski [20]

Table 2. Experimental phase compositions and lattice parameters of equilibrium phases in selected Nd-Cd samples.

Sample / nom. comp. (at.%)	Annealing Temp. (°C)	Phase analysis		SEM	
		Phases	Lattice parameters (Å)	Cd (at.%)	Nd (at.%)
1 Nd_3Cd_{97}	300	Cd	a = 2.9794(5), c = 5.6194(1)	100	0.0
		$NdCd_{11}$	a = 9.3011(5)	91.6	8.4
2 $Nd_{11}Cd_{89}$	300	$NdCd_{11}$	a = 9.2957(9)	91.3	8.7
		$NdCd_6$	a = 15.6285(2)	85.7	14.3
3 $Nd_{16}Cd_{84}$	300	$NdCd_6$	a = 15.6318(1)	85.0	15.0
		$Nd_{13}Cd_{58}$	a = 15.6152(1), c = 15.4661(1)	81.6	18.4
4 $Nd_{19}Cd_{81}$	600	$Nd_{13}Cd_{58}$	a = 15.6250(3), c = 15.4316(4)	-*	-*
		$Nd_{11}Cd_{45}$	low intensity	80.5	19.5
5 $Nd_{23}Cd_{77}$	600	$Nd_{11}Cd_{45}$	a = 21.7817(2)	79.2	20.8
		$NdCd_3$	a = 7.1692(3)	75.0	25.0
6 $Nd_{30}Cd_{70}$	600	$NdCd_3$	a = 7.1792(4)	74.5	25.5
		$NdCd_2$	a = 5.0232(2), c = 3.4489(2)	66.6	33.4
7 $Nd_{28}Cd_{72}$	850	$NdCd_3$	a = 7.1804(5)	76.3	23.7
		$NdCd_2$	a = 5.0231(4), c = 3.4474(4)	-*	-*
8 $Nd_{46}Cd_{54}$	600	$NdCd_2$	a = 5.0255(4), c = 3.4440(3)	65.0	35.0
		NdCd	a = 3.8198(2)	50.6	49.4
9 $Nd_{37}Cd_{63}$	850	$NdCd_2$	a = 5.0228(8), c = 3.4518(8)	65.5	34.5
		NdCd	a = 3.8204(5)	50.6	49.4
10 $Nd_{70}Cd_{30}$	600	NdCd	too ductile	47.4	52.6
		β-Nd	too ductile	16.5	83.5

* The microstructure of the respective phase was too fine for an accurate measurement by EDX

Table 3. Comparison of phase boundaries at different temperatures derived from SEM analyses and isopiestic vapor pressure measurements [30].

Compound	SEM		Isopiestic experiment	
	Temperature (°C)	**Phase boundaries at.% Cd**	**Temperature (°C)**	**Phase boundaries at.% Cd**
α-Nd	500	0 – 3.0	–	–
β-Nd	770	0 – 19.0	–	–
NdCd	300	47.8 – 50.0	550	48.7 – 50.1
	600	47.5 – 50.2		
	850	47.0 – 50.9		
$NdCd_2$	600	65.1 – 66.7	550	65.7 – 67.1
	850	65.5 – 66.7		
$NdCd_3$	600	74.4 – 74.8	–	–
	850	74.4 – 74.8		
$Nd_{11}Cd_{45}$	600	79.2 – 80.3	550	79.7 – 80.3
$Nd_{13}Cd_{58}$	300	81.4 – 81.7	550	81.2 – 81.7
	600	81.5 – 81.8		
$NdCd_6$	300	85.0 – 85.7	550	84.6 – 85.7
	600	84.6 – 85.6		
$NdCd_{11}$	300	91.3 – 91.8	–	–

Table 4. Experimental results of DTA in the Nd-Cd system.

Sample comp. (at.%)	Annealing T(°C)/ t(weeks)	Heating (°C)			Cooling (°C)	
		Invariant reaction*	Phase boundary	Liquidus	Liquidus
$Nd_{99}Cd_1$	250/12		325 705-777	n-o	n-o
$Nd_{98}Cd_2$	300/10		613-809	1016	1015
$Nd_{95}Cd_5$	as-cast	498	n-o	970	968[e]
$Nd_{95}Cd_5$	600/4	495	n-o	967	961
$Nd_{90}Cd_{10}$	as-cast	495	n-o	923	922
$Nd_{90}Cd_{10}$	800/3	502	n-o	914	913
$Nd_{88}Cd_{12}$	400/6	504	n-o	893	892
$Nd_{80}Cd_{20}$	as-cast	495 775		813	813
$Nd_{80}Cd_{20}$	400/6	498 773		804	803
$Nd_{78}Cd_{22}$	400/6	503 770		n-o	787
$Nd_{70}Cd_{30}$	as-cast	493 771		941	n-o
$Nd_{60}Cd_{40}$	400/6	504 769		1010	1004
$Nd_{55}Cd_{45}$	as-cast	n-o 765		1039	1033
		500±5 **770±5**		1018	1012
$Nd_{46}Cd_{54}$	as-cast	954 959		1030	1021
$Nd_{46}Cd_{54}$	400/6	950 957		1030	1023
$Nd_{37}Cd_{63}$	as-cast	955 961		991	990
$Nd_{37}Cd_{63}$	600/4	955 963		993	991
		955±5 **960±3**			
$Nd_{35}Cd_{65}$	600/4	n-o 866		992	965[sc]
$Nd_{30}Cd_{70}$	as-cast	864 n-o		964	950[sc]
$Nd_{26}Cd_{74}$	600/4	861 866		n-o	n-o
$Nd_{23}Cd_{77}$	as-cast	863 865	849	883	860[sc]

$Nd_{23}Cd_{77}$	600/4	860	**865±1**	853		n-o		n-o
$Nd_{22}Cd_{78}$	600/4	859		852		n-o		n-o
		860±4		**850±3**				
				n-o				
$Nd_{19}Cd_{81}$	as-cast					853		834^{sc}
$Nd_{16}Cd_{84}$	as-cast			738		843		812^{sc}
$Nd_{16}Cd_{84}$	600/4			740		834		834
$Nd_{12}Cd_{88}$	as-cast	515	653	744		775		750^{sc}
				740±4				
$Nd_{10}Cd_{90}$	400/6	520	n-o			744		724^{sc}
			655±2					
Nd_7Cd_{93}	as-cast	520			316	n-o		650^{sc}
Nd_5Cd_{95}	300/10	523			320	n-o		620^{sc}
Nd_4Cd_{96}	as-cast	521			316	622		577^{sc}
		520±3			**318±2**			

n-o not observed, sc supercooled effect.
a Average values of all invariant reaction temperatures are given together with estimated error limits in bold numbers.

Table 5. Invariant reactions in the system Nd-Cd derived from a combination of all present results.

Reaction	*T* (° C)	Phase compositions (at.% Cd)			Reaction type
L ⇄ Cd + $NdCd_{11}$	318 ±2	~100	~100	91.7	degenerate eutectic
L + $NdCd_6$ ⇄ $NdCd_{11}$	520 ±3	97.4	85.9	91.7	peritectic
L + $Nd_{13}Cd_{58}$ ⇄ $NdCd_6$	655 ±2	94.4	81.7	85.7	peritectic
L + $Nd_{11}Cd_{45}$ ⇄ $Nd_{13}Cd_{58}$	740 ±3	89.9	80.4	81.7	peritectic
$Nd_{11}Cd_{45}$ ⇄ L	855		80.4		congruent melting
L ⇄ $Nd_{11}Cd_{45}$ + $NdCd_3$	850 ±3	79.0	80.3	75.0	eutectic
L + α-$NdCd_2$ ⇄ $NdCd_3$	860 ±4	78.2	66.7	75.0	peritectic
α-$NdCd_2$ ⇄ β-$NdCd_2$	865 ±1		66.7		polymorphic transformation
	955 ±3		66.1		
β-$NdCd_2$ ⇄ L	995		66.7		congruent melting
L ⇄ β-$NdCd_2$ + NdCd	960 ±3	58.1	66.1	50.5	eutectic
NdCd ⇄ L	1040		50.0		congruent melting
L ⇄ NdCd + β-Nd	770 ±5	24.0	47.2	19.0	eutectic
β-Nd ⇄ NdCd + α-Nd	500 ±5	15.0	47.5	3.0	eutectoid

Figures

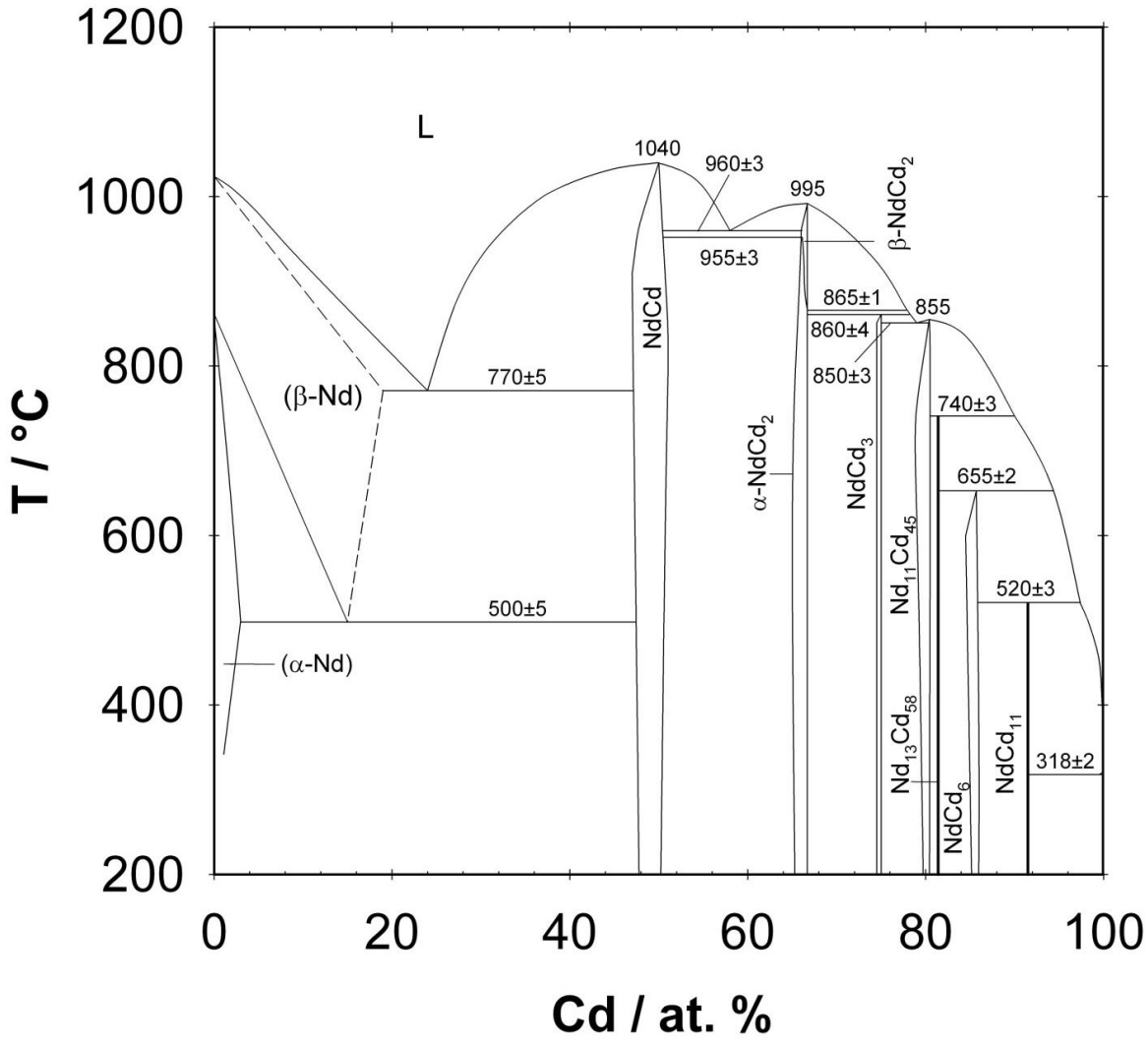

Fig. 1. The Nd-Cd phase diagram according to the present results.

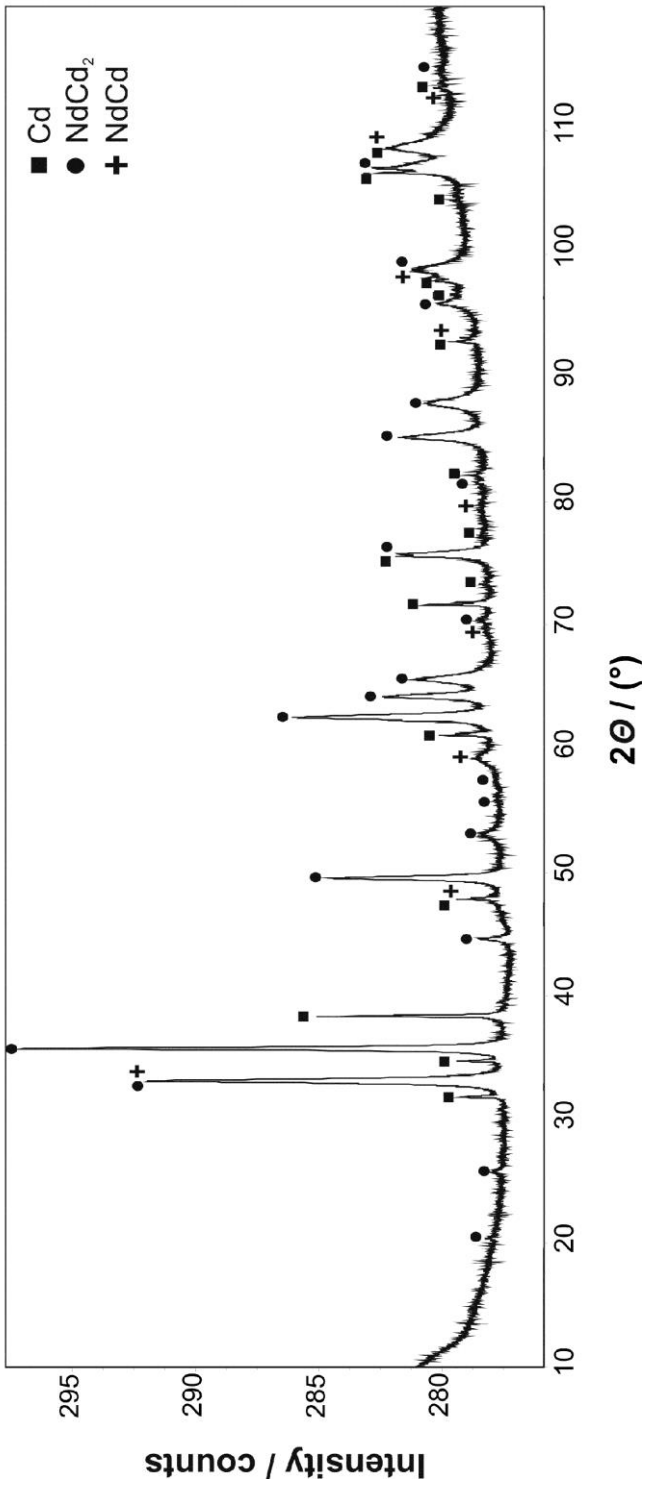

Fig. 2. The XRD pattern of the $Nd_{37}Cd_{63}$ sample annealed at 850°C for 3 weeks.

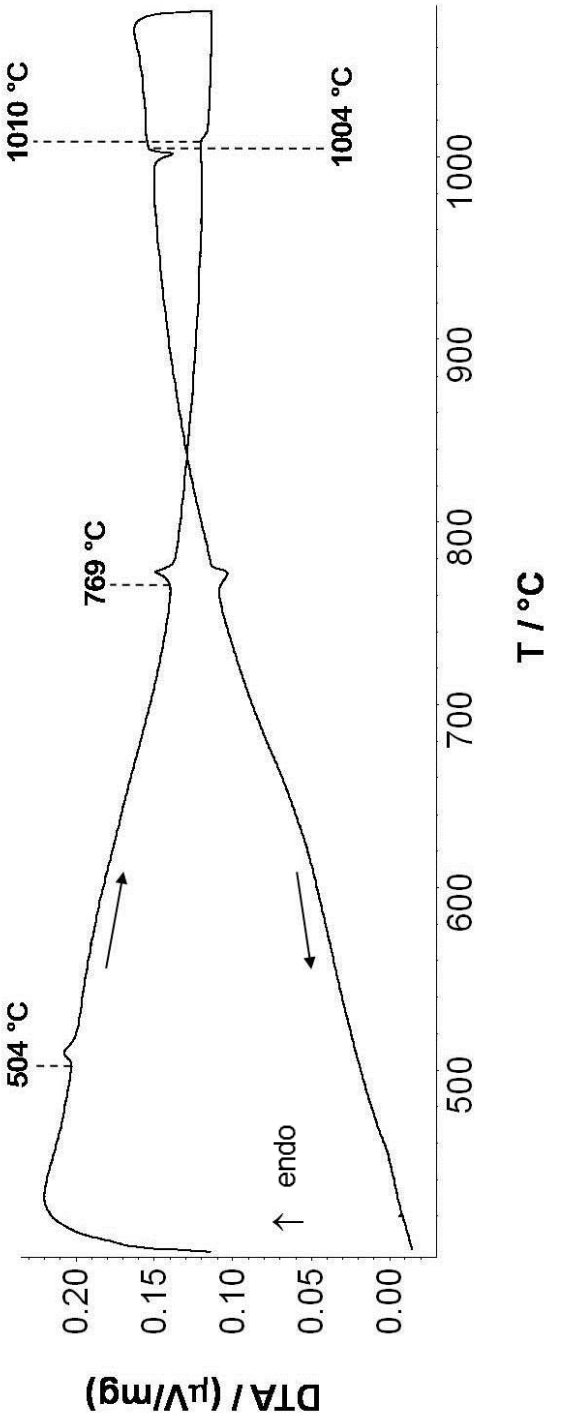

Fig. 3. DTA curves of the sample $Nd_{60}Cd_{40}$, annealed at 400 °C for 6 weeks, measured upon heating and cooling with 5 K min^{-1}.

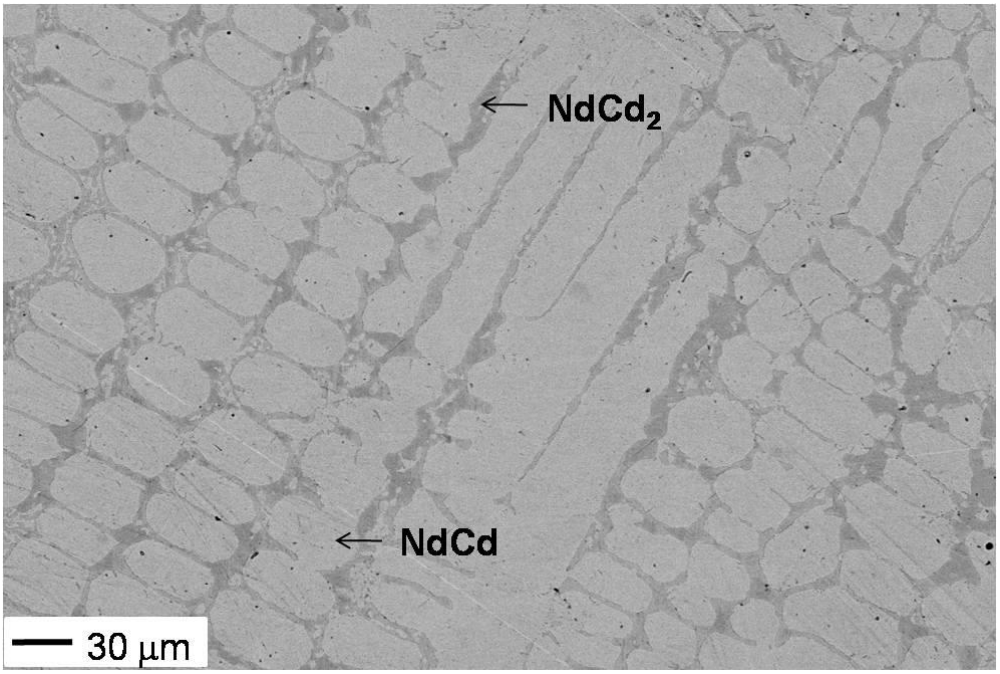

Fig. 4. Microstructure of the sample $Nd_{46}Cd_{54}$ annealed at 600 °C for 4 weeks.

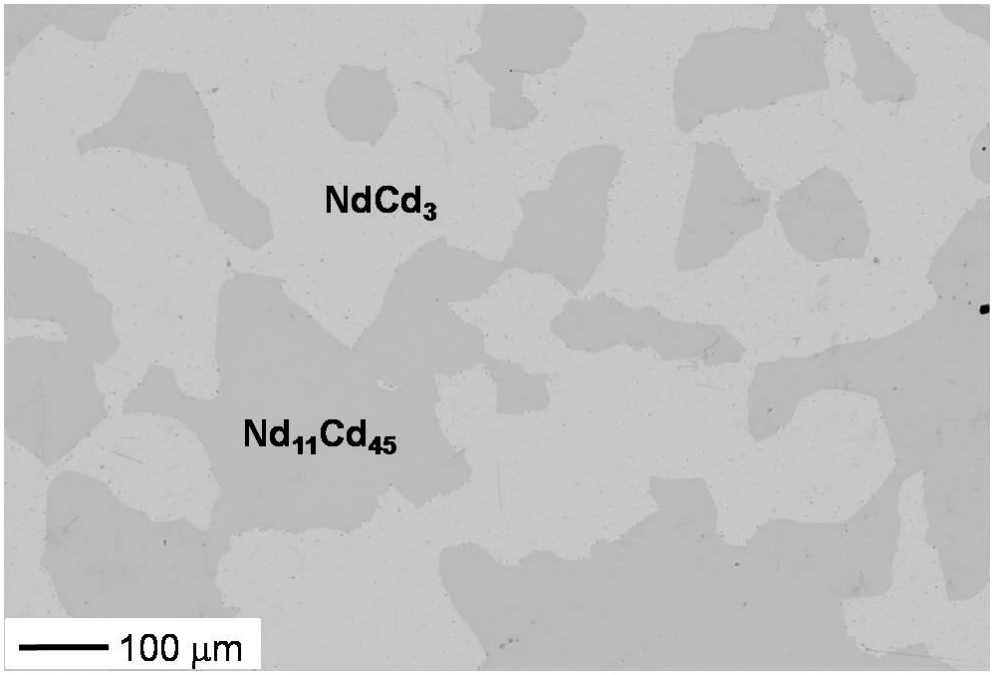

Fig. 5. Microstructure of the sample $Nd_{22}Cd_{78}$ annealed at 600 °C for 4 weeks.

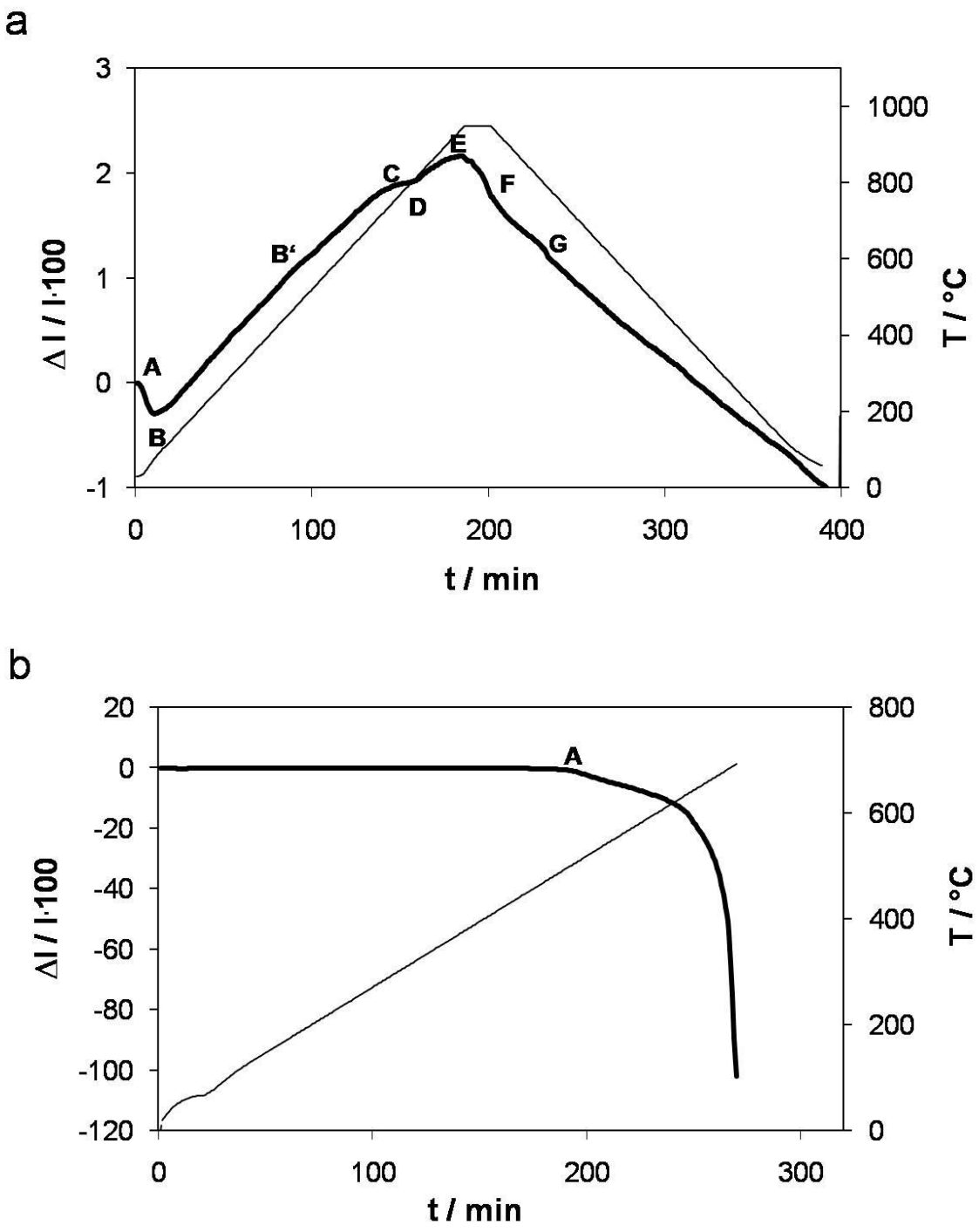

Fig. 6. Dilatometric curve (thick line) together with temperature curve (thin line) for the samples $Nd_{98}Cd_2$ (a) and $Nd_{96}Cd_4$ (b), recorded with a heating rate of 5 K min^{-1}.

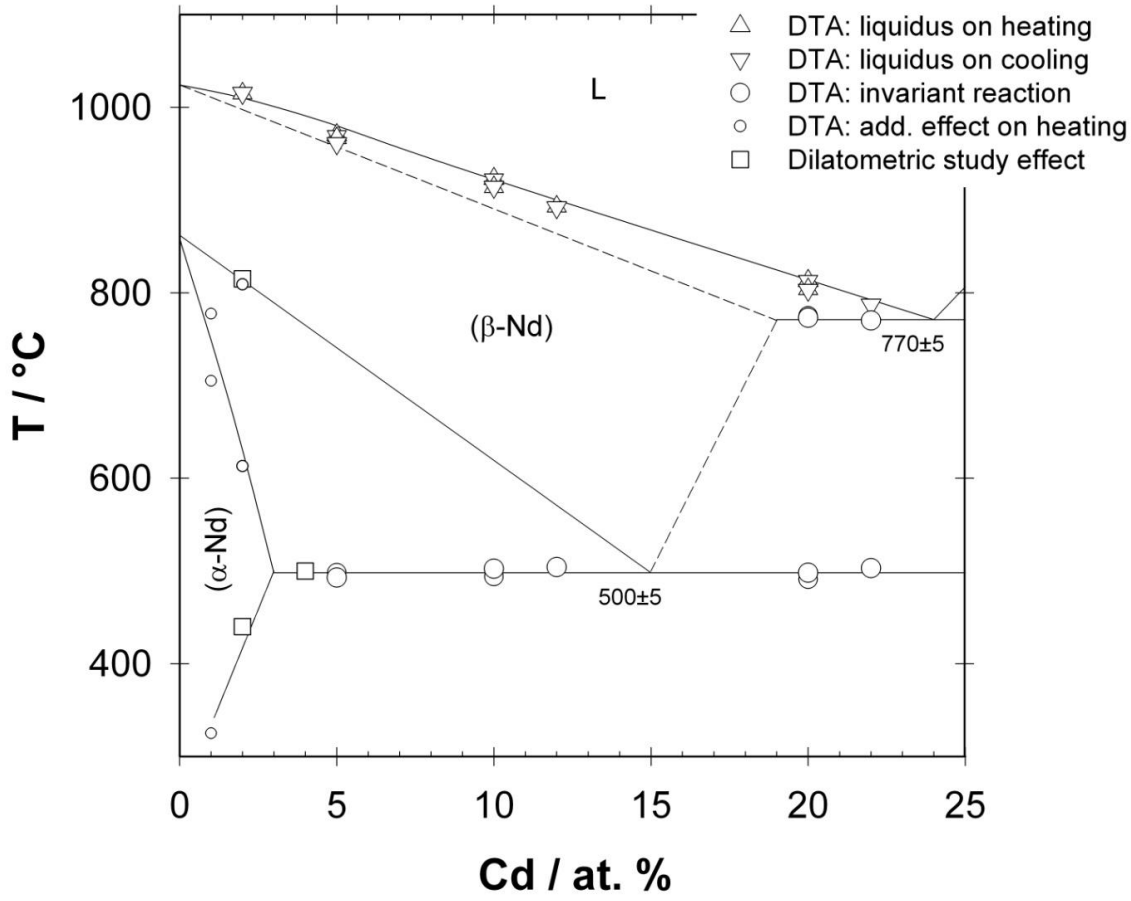

Fig. 7. Nd-rich part of the Nd-Cd phase diagram together with effects from DTA and dilatometry, recorded with a heating rate of 5 K min^{-1}.

References

[1] O. Conocar, N. Douyere, J. Glatz, J. Lacquement, R. Malmbecke, J. Serp, Promising pyrochemical actinide/lanthanide separation processes using aluminum, Nucl. Sci. Eng. 153(2006) 253-261.

[2] D. Olander, Nuclear fuels - Present and future, J. Nucl. Mater. 389 (2009) 1-22.

[3] M. Kurata, Y. Sakamura, T. Hijikata, K. Kinoshita, Distribution behavior of uranium, neptunium, rare-earth elements (Y, La, Ce, Nd, Sm, Eu, Gd) and alkaline-earth metals (Sr, Ba) between molten LiCl-KCl eutectic salt and liquid cadmium or bismuth, J. Nucl. Mater. 227 (1995) 110-121.

[4] T.L. Reichmann, H.S. Effenberger, H. Ipser, Experimental investigation of the Cd-Pr phase diagram. PLOS ONE (2014), submitted for publication.

[5] B. Skołyszewska-Kühberger, T.L. Reichmann, R. Ganesan, H. Ipser, Thermodynamic study of the cerium-cadmium system, CALPHAD (2014), in print.

[6] T.L. Reichmann, H. Ipser, Thermochemical investigations in the system cadmium-praseodymium relevant for pyro-metallurgical fuel reprocessing, Metall. Mater. Trans. A (2014), in print.

[7] K.W. Richter, S. Besana, G. Borzone, and H. Ipser, Thermodynamic investigations in the lanthanum-cadmium System, J. Alloys Comp. 365 (2004) 181-187.

[8] R.P. Elliott, Constitution of binary alloys, First supplement, McGraw-Hill Inc, New York, 1985.

[9] A. Iandelli, Congr. Intern. Chim. Pure Appl., 16, Paris, Mem. Sect. Chim. Minerale, 1958, 35-40.

[10] A. Iandelli, Atti. Accad. Nazl. Lincei, Rend., Classe Sci. Fis., Mat. e Nat. 29 (1960) 62-69.

[11] K.A. Gschneidner, Rare Earth Alloys, D. van Nostrand Company Ltd, Canada, 1961.

[12] F.H. Spedding, A.H. Daane, W. Herrmann, The Crystal Structures and Lattice Parameters of High-Purity Scandium, Yttrium and the Rare Earth Metals, Acta Cryst. 9 (1956) 559-563.

[13] F.H. Spedding, J.J. Hanak, A.H. Daane, High temperature allotropy and thermal expansion of the rare-earth metals, J. Less-Comm. Metals, 3 (2) (1961) 110-124.

[14] I. Johnson, in: J.F. Nachman, C.E. Lundin (Eds.), Rare Earth Research, Gordon and Breach Science Publishers Inc., New York, 1962, pp. 125-131.

[15] I. Johnson, K.E. Anderson, R.A. Blomquist, Partial constitutional diagram for the Cd-La, Cd-Ce, Cd-Pr, Cd-Nd, and Cd-Sm systems,Trans. ASM 59 (1966) 352-355.

[16] I. Johnson, R. Schablaske, B. Tani, K. Anderson, Trans. AIME 230 (1964) 1485.

[17] A.C. Larson, D.T. Cromer, Acta Cryst. B27 (1971) 1875-1879.

[18] G. Bruzzone, M.L. Fornasini, F. Merlo, Rare earth intermediate phases with cadmium, J. Less-Comm. Met. 30 (1973) 361-375.

[19] A. Iandelli, R. Ferro, Alloys of cadmium with lanthanum, cerium and praseodymium, Gazz. Chim. Ital. 84 (1954) 463-478.

[20] T.B. Massalski, Binary Alloy Phase Diagrams, second ed., ASM International, Materials Park, Ohio, 1990.

[21] K.A. Gschneidner Jr., F.W. Calderwood, The cadmium-rare earth systems, Bull. Alloy. Phase Diagrams 9 (1988) 16-21.

[22] C. Colinet, A. Pasturel, Thermodynamic properties of metallic systems, in: K.A. Gschneidner Jr., L.R. Eyring, G.H. Lander, G.R. Choppin (Eds.), Handbook on the Physics and Chemistry of Rare Earths - Lanthanides/Actinides: Physics – II, Elsevier Science B.V., Amsterdam 1994, pp. 479-631.

[23] E. Veleckis, E. van Deventer, Eutectic temperatures in the LnCd-Ln fields of the lanthanon-cadmium systems, ANL-6925, Semi-Annual Report, Jul-Dec 1964, Argonne National laboratory, Argonne, IL 1965.

[24] B.J. Beaudry, K.A. Gschneidner, Preparation and basic properties of the rare earth metals, in: K.A. Gschneidner Jr., L.R. Eyring (Eds.), Handbook on the Physics and Chemistry of Rare Earths - Metals – I, Elsevier Science B.V., Amsterdam, 1982, pp.173-233.

[25] F.H. Spedding, A.H. Daane, Preparation and properties of rare earth metals, in: Progress in Nuclear Energy, I (5) Metallurgy and Fuels, 1956.

[26] D.H. Dennison, M.J. Tschetter, K.A. Gschneidner Jr., The solubility of Ta in 8 liquid RE metals, J. Less-Comm. Met. 10 (1965) 108-115.

[27] D.H. Dennison, M.J. Tschetter, K.A. Gschneidner Jr., The solubility of Ta and W in liquid RE metals, J. Less-Comm. Met. 11 (1966) 423-435.

[28] S.P. Garg, M. Venkatraman, N. Krishnamurthy, S.J. Vijaykar, The RE-Ta system, J. Phase Equilibria, 19 (4) (1998) 385-394.

[29] Y. Janssen, M. Angst, P.C. Canfield, R.W. McCallum, Small sealed Ta crucibles for thermal analysis of volatile metallic samples, Rev. Sci. Instrum. 77 (2006) 056104_1-056104_3.

[30] B. Skołyszewska-Kühberger, T.L. Reichmann, H. Ipser, A. thermodynamic study of the neodymium-cadmium system, publication in preparation (2014).

[31] G. Bruzzone, M.L. Fornasini, F. Merlo, The gadolinium-cadmium system, J. Less-Comm. Met. 25 (1971) 295-301.

[32] G. Bruzzone, F. Merlo, The lanthanum-cadmium system, J. Less-Comm. Met. 30 (1975) 303-305.

[33] F. Canepa, G.A. Costa, E.A. Franceschi, The phase diagram of the Ce-Cd system, Lanthanide Actinide Research 1 (1985) 41-47.

4. Summary

4.1 Summary (English)

Intermetallic compounds of the RE-Cd systems are of interest of the pyroprocessing technology of spent nuclear fuel. For better understanding and design of this recovery method the comprehensive knowledge of RE-Cd alloys and their thermodynamical properties are significant. The current work is an evaluation of existing literature data on the constitution of the cerium-cadmium and the neodymium-cadmium systems supplemented by new experimental data filling the literature gaps.

The scope of the thesis is providing a detailed investigation of the cerium-cadmium and the neodymium-cadmium phase diagrams. Phase equilibria as well as structural characterization of the Ce-Cd and Nd-Cd alloys were studied. The both systems were investigated using light optical microscopy (LOM), scanning electron microscopy (SEM) in combination with EDS, powder X-Ray diffraction (XRD), differential thermal analysis (DTA) and dilatometric study. The isopiestic equilibration method was applied here to obtain a thermodynamical data.

The binary Ce-Cd phase diagram was re-evaluated over the whole composition range. Seven intermetallic compounds (CeCd, $CeCd_2$, $CeCd_3$, $Ce_{13}Cd_{58}$, $CeCd_6$, Ce_2Cd_{17} and $CeCd_{11}$) and two solid solutions of Cd in the low- and high-temperature modification of Ce, γ-Ce and δ-Ce respectively, were confirmed. The phase boundaries of all phases were investigated at different temperatures. By means of DTA results the invariant reactions were determined. Moreover the melting and decomposition temperatures of the Ce-Cd phases were verified. Here some discrepancies with the existing literature data were recognized and the new temperatures were suggested. In addition, it was possible to analyze structure of the high temperature phase

$Cd_{17+2x}Ce_{2-x}$ (x ~ 0.02) (the hexagonal Th_2Ni_{17} structure). A homogeneous single-phase sample was prepared what enables proposing the temperature range of existence of this intermetallic compound between 530 and 610 °C.

Thermodynamic activities of Cd were estimated for the Ce-Cd system in the temperature range between 690 and 1080 K and the composition range between 48 and 85 at.% Cd based on an isopiestic vapor pressure experiment. The activity values were converted to a common temperature of 823 K and are given for the composition range 48 to 100 at.% Cd. Using a literature value of ln aCe as integration constant, it was possible to calculate Ce activities and integral Gibbs energies of formation for the same temperature and composition range. A minimum of $\Delta_f G_{Cd}$ = -37 kJ·g-atom^{-1} was calculated in the phase CeCd. A relatively high stability of $Ce_{13}Cd_{58}$ phase was noticed.

The complete Nd-Cd phase diagram was studied with a combination of thermal, metallographic and X-ray analysis over the whole composition range. The compounds are very similar to those found in the Ce-Cd system. Anyhow in the Cd-rich part some differences were noticed: the existence of the intermetallic compound $Nd_{11}Cd_{45}$ was confirmed but no high temperature phase was found. The crystal structure of following phases was investigated NdCd, $NdCd_2$, $NdCd_3$, $Nd_{11}Cd_{45}$, $Nd_{13}Cd_{58}$, $NdCd_6$ and $NdCd_{11}$. Additionally, melting or decomposition temperatures of all intermetallic compounds were recorded by DTA. The homogenity ranges of the both allotropic modification of Nd (α-Nd and β-Nd) were determined. Based on the DTA and dilatometric results, the Nd-rich part of the binary diagram could be constructed. Similar to $CeCd_2$ phase, a polymorphic modification of $NdCd_2$ intermetallic compound was noticed.

At the moment the paper '*A thermodynamic study of the cadmium-neodymium system*' is under construction. The measurements were carried out in the temperature range from about 690 to 1200 K and over a composition range between 48 and 92 at% Cd. A minimum value of $\Delta_f G \approx$ -38 kJ·g-atom^{-1} at 873 K was obtained for the phase CdNd, a value that compares well with other CdRE compounds.

4.2 Zusammenfassung (Deutsch)

Legierungen des RE-Cd Systems sind von besonderem Interesse im Bereich der pyrotechnischen Aufarbeitung von verbrauchten Brennstäben aus Atomkraftwerken. Zum besseren Verständnis und künftigem Design von Aufarbeitungsmethoden sind die vergleichenden thermodynamischen Eigenschaften der RE-Cd Legierungen signifikant.

Ziel der vorliegenden Arbeit ist es, die existierenden Literaturdaten für die Systeme Cerium-Cadmium und Neodymium-Cadmium zu evaluieren und fehlende Daten experimentell zu bestimmen.

Die Systeme wurden mit Hilfe von optischer Mikroskopie (LOM), Elektronenstrahlmikroskopie (SEM) in Kombination mit energiedispersiver Analyse (EDS), Pulverröntgendiffraktometrie (XRD), Differentialthermoanalyse (DTA) und Thermodilatometrie untersucht. Die thermodynamischen Daten wurden mittels isopiestischer Gleichgewichtsmessungen bestimmt.

Das binäre Phasendiagramm Ce-Cd wurde über den gesamten Zusammensetzungsbereich re-evaluiert. Sieben intermetallische Verbindungen (CeCd, $CeCd_2$, $CeCd_3$, $Ce_{13}Cd_{58}$, $CeCd_6$, Ce_2Cd_{17} und $CeCd_{11}$) sowie zwei feste Lösungen von Cd in der Hoch- und Nieder-Temperaturmodifikation des Ce, γ-Ce and δ-Ce, wurden gefunden. Die Ausbildung der Phasengrenzflächen wurde bei unterschiedlichen Temperaturen untersucht; die Bestimmung der irreversiblen Reaktionen erfolgte mittels DTA.

Darüber hinaus wurden die Schmelz- und Zersetzungstemperaturen der Ce-Cd Phasen verifiziert. Dabei wurden einige Abweichungen zur Literatur festgestellt und Änderungen vorgeschlagen. Im Zuge dieser Arbeit gelang es außerdem, die Struktur der Hochtemperaturphase $Cd_{17+2x}Ce_{2-x}$ ($x \sim 0.02$) (hexagonale Th_2Ni_{17} Struktur) zu bestimmen.

Die thermodynamischen Aktivitäten von Cd im System Ce-Cd wurden in einem Temperaturbereich von 690 K bis 1080 K und einer Zusammensetzung von 48 % bis 85 % Cd untersucht. Ein Minimum von $\Delta_f G_{Cd}$ = -37 kJ·g-atom^{-1} wurde für die Phase CeCd ermittelt, sowie eine relativ hohe Stabilität der Phase $Ce_{13}Cd_{58}$.

Das Nd-Cd Phasendiagramm wurde über den gesamten Zusammensetzungsbereich bestimmt. Die gefundenen Phasen ähneln sehr stark jenen im System Ce-Cd; im Cd-reichen Teil wurden allerdings einige Abweichungen festgestellt. Die Existenz der Phase $Nd_{11}Cd_{45}$ konnte bestätigt werden, jedoch keine Hochtemperaturphase davon.

Die Kristallstruktur folgender Phasen wurde untersucht: NdCd, $NdCd_2$, $NdCd_3$, $Nd_{11}Cd_{45}$, $Nd_{13}Cd_{58}$, $NdCd_6$ and $NdCd_{11}$. Die homogenen Bereiche der beiden allotropen Modifikationen von Nd (α-Nd und β-Nd) wurden ermittelt. Basierend auf den Ergebnissen der DTA und Dilatometrie konnte der Nd-reiche Teil des Phasendiagramms konstruiert werden. Entsprechend der $CeCd_2$ Phase wurde auch hier eine polymorphe Modifikation von $NdCd_2$ gefunden.

Zur Zeit ist ein Artikel '*A thermodynamic study of the cadmium-neodymium system*' in Arbeit. Die Messungen wurden in einem Temperaturbereich von 690 K bis 1200 K und einem Zusammensetzungsbereich von 48 % bis 92 % Cd durchgeführt. Ein Minimum für $\Delta_f G \approx$ -38 kJ·g-atom^{-1} wurde bei 873 K für die Phase CdNd bestimmt, ein Wert, der sehr gut mit anderen Cd-RE Verbindungen korreliert.

Appendix: *Curriculum vitae*

First name	**BARBARA**
Last name	**SKOŁYSZEWSKA-KÜHBERGER**
Degree	D.I.
Date/place of birth	March 22nd, 1979; Kraków, Poland
E-Mail	barbara.kuehberger@omv.com

EDUCATION

9/1994 – 6/1998	Maria Skłodowska-Curie High School, Skawina, Poland Secondary studies examination (Matura) (May 1998)
10/1998 – 06/2003	Diploma Study: University of Science and Technology (AGH), Cracow, Poland
Focus	Solid state chemistry, materials science
Title of the diploma thesis	Physicochemical properties of Mg-Zn and Mn-Zn (with co-operation with LG.Philips Displays Ltd.)
Award	*Europrimus 2003* – The Best Student of Poland
9/2002 – 10/2002	Advanced Materials Science through Electron Microscopy Humboldt University, Berlin, Germany
07/2003	Advanced Studies on Superconducting Engineering Budapest University, Hungary

02/2011 – 10/2015	Doctoral Study: University of Vienna
Focus	Chemistry, materials chemistry
8/2011	Poly'tech Grenoble, France
07/2012	University of Science and Technology Faculty of Metals Engineering and Industrial Computer Science Cracow, Poland
02/2013	Indira Gandhi Centre for Atomic Research Kalpakkam, Tamil Nadu, India
7/2013	Ivan Franko National University Department of Metal Physics, Lviv, Ukraine

Additional qualifications:

Languages:

Polish	nativ
English	fluent
German	fluent

Courses:

03/2012: First Aid course, Wiener Rotes Kreuz, Austria

WORK EXPERIENCE

10/2014 – current	**Materials and corrosion Engineer** OMV Refining & Marketing GmbH, Austria
03/2014 – 05/2014	**Business Development Engineer** WERBA-Chem GmbH, Vienna, Austria
02/2011 – 02/2014	**Project Assistant** University of Vienna, Faculty of Chemistry, Austria
11/2010 – 01/2011	**Intern** UNIDO, Vienna. Austria
02/2010 – 10/2010	**Project Assistant** Vienna University, Faculty of Chemistry, Austria
10/2009 – 12/2009	**Intern** Permanent Mission of Poland to the UN Office Vienna, Austria
09/2003 – 10/2004	**Project Assistant** Vienna University of Technology, Austria
03/2003 – 06/2003	**University Assistant** University of Science and Technology, Cracow, Poland
07/2001 – 06/2003	**Project Assistant** LG.Philips Displays Poland Ltd., Skierniewice, Poland

Teaching activity:

Tutor:

Solid state chemistry; University of Science and Technology, Cracow, Poland

Assistant:

Chemistry II (BA12) (PI) – Geoscience; University of Vienna

LIST OF PUBLICATIONS:

B. Skołyszewska, K. Przybylski:
Kinetics and reaction mechanism in the mullite-Ferrite (Mg-Zn and Mn-Zn) systems at high temperatures.
Polish Ceramic Bulletin, Ceramics, 66 (2001) 867-874. (in Polish)

B. Skołyszewska, W. Tokarz, K. Przybylski, Z. Kakol:
Preparation and magnetic properties of MgZn and MnZn ferrites.
PHYSICA C 387 (2003) 290-294.

K. Przybylski, B. Skołyszewska:
Synthesis and physicochemical properties of MgZn and MnZn ferrites.
ANNALES DE CHIMIE - *science des matériaux* 28 (2003) 107-113.

B. Skołyszewska:
Synthesis and physicochemical properties of MgZn and MnZn ferrites.
Bulletin of the Cracow University of Science and Technology Students' Society, 1 (2002) 144-153. (in Polish)

M.C.J. Marker, B. Skołyszewska-Kühberger, H. S. Effenberger, C. Schmeterer,
K. Richter:
Phase equilibria and structural investigations in the system Al–Fe–Si.
Intermetalics 19 (12) (2011) 1919-1929.

B. Skołyszewska-Kühberger, T.L. Reichmann, R. Ganesan, H. Ipser:
Thermodynamic study of the cerium-cadmium system.
CALPHAD 44 (2014) 14-20.

B. Skołyszewska-Kühberger, T.L. Reichman, H. Ipser:
Phase equilibria in the neodymium-cadmium binary system.
Journal of Alloys and Compounds 606C (2014) 242–248.
B. Skołyszewska-Kühberger, T.L. Reichman, M. Marker, H.S. Effenberger, H. Ipser:
Re-investigation of the Cd-Ce phase diagram and structural characterization of the high-temperature phase $Cd_{17+2x}Ce_{2-x}$ (x ~ 0.02).
Submitted to Journal of Phase Equilibria and Diffusion, JPED-15-09-1719

PARTICIPATIONS IN INTERNATIONAL WORKSHOPS/CONFERENCES:

1. The 3rd Ceramic Conference, "Progress in Ceramic, Glass and Binding Building Materials Technology", September 2001, Zakopane, Poland.
B. Skołyszewska, K. Przybylski: '*Kinetics and reaction mechanism in the mullite-Ferrite (Mg-Zn and Mn-Zn) systems at high temperatures.'* (Poster)

2. The XXXIX Workshop of the Students' Society (AGH), May 2002, Kraków, Poland.
B. Skołyszewska: *'Synthesis and physicochemical properties of MgZn and MnZn ferrites'* (Oral presentation)

3. Third International Workshop on Magnetism and Superconductivity of Advanced Materials, July 2002, Ladek Zdrój, Poland.
B. Skołyszewska, W. Tokarz, K. Przybylski, Z. Kakol: *'Preparation and magnetic properties of MgZn and MnZn ferrites'* (Poster)

4. 13th French-Polish Seminar on the Reactivity of Solids, September 2002, Cluny, France.
K. Przybylski, B. Skołyszewska: '*Synthesis and physicochemical properties of MgZn and MnZn ferrites'* (Oral presentation)

5. The XVII Polish School of Chemistry, November 2002, Straszęcin, Poland.
B. Skołyszewska: *'Influence of chemical composition on magnetic properties of MgZn and MnZn ferrites'* (Oral presentation)

6. The XL Workshop of the Students' Society (AGH), May 2003, Kraków, Poland.
B. Skołyszewska: *'The corrosion of the Al-Fe-Si alloys'* (Oral presentation)

7. Energy Efficiency Forum, October 2009, Vienna, Austria.

8. Least Development Countries Ministerial Conference, December 2009, UNO Vienna, Austria.

9. UNIDO *General Conference* - Green Industry for Global Recovery and Growth December 2009, Vienna, Austria.

10. ENMAT 2010: 1st International Conference on Materials for Energy, DECHEMA, July 2010, Karlsruhe, Germany.

11. IAEA - *Technical Meeting,* September 2010, Cracow, Poland.

12. Chemie Tage 2011, September 2011, Linz, Austria.
B. Skołyszewska-Kühberger, H. Ipser: *,Investigation in the Nd-Cd phase diagram'* (Poster)

13. Nobel's Prize Lectures 2011, December 2011, Stockholm, Sweden.

14. WACÖ 2012, April 2012, Innsbruck, Austria.
B. Skołyszewska-Kühberger: *,Investigation in the systems Ce-Cd and Nd-Cd'* (Oral presentation)

15. HI Temp 2012 NETZSCH Conference, September 2012, Munich, Germany.
B. Skołyszewska-Kühberger, H. Ipser: *,The interaction of rare earth elements with cadmium: The systems Ce-Cd and Nd-Cd'* (Poster)

16. Indira Gandhi Centre for Atomic Research, February 2013, Kalpakkam, Tamil Nadu, India.
B. Skołyszewska-Kühberger, H. Ipser: *,The Ce-Cd and Nd-Cd binary phase diagrams'* (Oral presentation)

17. Nobel's Prize Lectures 2012, December 2012, Stockholm, Sweden.